

ABSTRACT

Title of Dissertation: ROLE OF FEED PROTOCOL IN ACHIEVING
CHAOTIC MIXING OF HIGHLY FILLED FLOW
SYSTEMS DURING FILLING THE EMPTY CAVITY

Yue Huang, Doctor of Philosophy, 2006

Dissertation directed by: Professor David Bigio
Department of Mechanical Engineering

Chaotic mixing of highly filled viscous fluids is desired but hardly achieved in the electronic packaging industries. The demand for high reliability found in electronic package attracts more and more researchers to study the properties and distribution of binders and filler particles. These will affect properties such as coefficient of thermal expansion and stiffness. Both of these contribute strongly to reliability. The filler concentration, size distribution and spatial distribution must be examined in a structured manner to understand their effects on final properties. However, most studies deal with filler concentration and size distribution, while very few studies have tied the particle spatial distribution to the properties. It is not enough to just properly control the filler concentration and size distribution. The more uniform filler distribution, the more uniform are local properties, and this can be achieved by well-designed mixing processes.

Mixing is very important and in many cases the goodness of the mixing of fillers will affect or determine the properties of the products. In this thesis, the local properties of electronic package and their relations with filler particle distribution are quantified. For the first time, a new feed protocol that can generate chaotic mixing during filling cavity by implementing periodic and aperiodic filling process is presented. Instead of using single gate in the molding process, we have developed a two-gate feeding protocol. A numerical simulation experiment is conducted on a 2-D square cavity to examine the mixing of polymer fluid in low *Reynolds* number flows. Since there are a vast number of geometries in electronic packages, only cavities with 46 and 49 bumps, which can be treated as solder balls or leadframe, is investigated. Periodic and aperiodic feed protocols resulted in exponential growth of the distance between two adjacent particles, an indication of chaotic mixing. Entropic study shows that the global mixing has been improved 858% compared to single gate feeding. The improved properties and reliability could be foreseen in electronic package.

ROLE OF FEED PROTOCOL IN ACHIEVING CHAOTIC MIXING OF HIGHLY
FILLED FLOW SYSTEMS DURING FILLING THE EMPTY CAVITY

by

Yue Huang

Dissertation submitted to the Faculty of the Graduate School of the
University of Maryland, College Park in partial fulfillment
of the requirements for the degree of
Doctor of Philosophy
2006

Dissertation Committee:

Professor David I. Bigio, Chair
Professor Bongtae Han
Professor F. Patrick McCluskey
Professor Michael Pecht
Professor Peter Kofinas

© Copyright by

[Yue Huang]

[2006]

Dedication

Dedicated to my wife Yamin.

Acknowledgments

I wish to thank my advisor Professor David I. Bigio, who supported my whole graduate studies at the University of Maryland. He made this long and hard working process an interesting and exciting journey. I learned not only how to work towards a Ph.D., but also lots of skills that can be used in professional work and daily life.

I would like to thank my dissertation committee members, Professor Michael Pecht, Professor F. Patrick McCluskey, Professor Bongtae Han, and Professor Peter Kofinas, for their invaluable suggestions to improve my dissertation.

I will never forget Dr. William Patten who guided my very first graduate studies and Dr. Stafford who encouraged me during my study at the University of Oklahoma.

I wish to acknowledge the support of Pentair-Hypro Corp., my director Jim Walsh who encouraged me to succeed.

I would like to thank all my family members, without their sacrifice, I will never fulfill this task.

Most importantly, I want to dedicate this dissertation to my lovely wife Yamin Li, who is living through the hard time and the happy time with me.

Table of Contents

Dedication.....	ii
Acknowledgments.....	iii
Table of Contents.....	iv
List of Tables.....	ix
List of Figures.....	x
Chapter 1: Introduction.....	1
1.1 Motivation.....	1
1.2 Concentration of research.....	3
1.2.1 Properties and filler particle distribution.....	3
1.2.2 Novel feed protocol.....	3
1.2.3 Flow model and numerical simulation.....	4
1.2.4 Measures of mixing.....	4
1.3 Organization of the thesis.....	5
Chapter 2: Background.....	6
2.1 Mixing Theory.....	6
2.2 Chaos theory.....	8
2.2.1 Introduction to chaotic flows.....	8
2.2.2 Periodic chaotic flow.....	8
2.2.3 Dimensionless time.....	10
2.2.4 Effect of different f or T on mixing.....	10
2.2.5 Periodic points.....	12
2.2.6 Aperiodic chaotic flow.....	12
2.3 Mixing Measures.....	13
2.3.1 Line growth.....	14
2.3.2 Interfacial area growth in a simple shear flow.....	14
2.3.3 Interfacial area and principal values and directions.....	15
2.4 Mixing in empty cavity.....	16

Chapter 3: Experimental work on electronic packages	17
3.1 Background on electronic package.....	17
3.1.1 Functions of electronic package.....	17
3.1.2 Structure of electronic package	17
3.1.3 Electronic packaging configurations	18
3.1.4 Role of molding compounds	20
3.1.4.1 Components of molding compounds	20
3.1.4.2 Properties of epoxy resin	20
3.1.4.3 Fillers	21
3.1.4.4 Filler and properties	22
3.1.4.5 Effective CTE of molding compounds	22
3.1.4.6 Filler content and properties of the molding compounds	23
3.1.4.7 Filler particle size and size distribution	23
3.1.4.8 Filler particle distribution	24
3.1.5 Molding process and failure modes electronic package.....	25
3.1.5.1 Molding process.....	25
3.1.5.2 Failure modes of the electronic packages	26
3.2 Experimental work on investigating of packaging properties as a function of filler microstructure in PQFPs	26
3.2.1 Introduction	26
3.2.2 Materials of chips	27
3.2.3 Experimental procedure	27
3.2.3.1 Image acquisition.....	27
3.2.3.2 Image processing software.....	28
3.2.3.3 Quantitative measures.....	31
3.2.4 Results and discussion.....	31
3.2.4.1 MQFPs	31
3.2.4.2 PQFP.....	35
3.2.5 Conclusions	40
3.3 Experimental work on distribution of a minor solid constituent in a transfer molded e – pad leadframe package.....	40

3.3.1 Introduction	41
3.3.2 Description of the packages and experimental technique	43
3.3.3 Results and discussion.....	45
3.3.3.1 Area fraction and size distribution results for the package with 7351UT.....	49
3.3.3.2 Area fraction and size distribution results for the package with 7351UL.....	53
3.3.4 Conclusions	56
Chapter 4: Modeling and Numerical Simulation	58
4.1 Governing Equations.....	59
4.1.1 Equations of motion	59
4.1.2 Boundary and initial conditions	60
4.1.3 Integration of the dynamical system	61
4.2 Modeling procedure	61
4.2.1 Flow geometry.....	62
4.2.2 MoldFlow®	62
4.2.3 Cavity construction.....	63
4.3 MoldFlow® simulation procedure	64
4.3.1 Mesh and gates locations.....	64
4.3.2 Material and molding conditions.....	64
4.3.3 Velocity field and streamline construction.....	67
4.3.4 Velocity field reconstruction	67
4.3.5 Velocity at nodes	68
4.3.6 Velocity interpolation.....	68
4.3.7 Streamline construction.....	73
Chapter 5: Model of mixing and measures of mixing.....	75
5.1 Model of mixing.....	75
5.1.1 Mixing Simulation - Particle tracking.....	75
5.1.2 Two important parameters.....	75
5.1.3 Design of experiment	77
5.1.3.1 One gate and two gates filling	77

5.1.3.2 Effects of f and ball pattern.....	78
5.2 Stretching.....	79
5.3 Entropic mixing characterization	80
5.3.1 Background on Shannon Entropy.....	80
5.3.2 Entropic Characterization of Mixing.....	81
5.4 Analysis of mixing and stretching in empty cavity without bumps.....	83
5.4.1 Mixing study.....	84
5.4.2 Stretching analysis.....	86
Chapter 6: Chaotic mixing analysis.....	90
6.1 Analysis of flow and mixing in cavity with stagger bumps	90
6.1.1 Particle distribution	90
6.1.1.1 $d1 = 5.4\text{mm}$ and $d2 = 5.4\text{mm}$	90
6.1.1.2 $d1 = 5.4\text{mm}$ and $d2 = 7.56\text{mm}$	93
6.1.1.3 $d1 = 7.56\text{mm}$ and $d2 = 7.56\text{mm}$	96
6.1.2 Entropy study	99
6.1.2.1 $d1 = 5.4\text{mm}$ and $d2 = 5.4\text{mm}$	100
6.1.2.2 $d1 = 5.4\text{mm}$ and $d2 = 7.56\text{mm}$	101
6.1.2.3 $d1 = 7.56\text{mm}$ and $d2 = 7.56\text{mm}$	103
6.1.2.4 Analysis of entropy.....	104
6.1.2.5 Entropy as a function of f	105
6.1.2.6 Effects of $d1$ and $d2$	109
6.1.2.7 Compare with one gate filling.....	111
6.1.3 Stretching analysis showing chaotic flow in two gates filling.....	111
6.1.4 Conclusion.....	114
6.2 Analysis of flow and mixing in cavity with regular bumps	115
6.2.1 Particle distribution	115
6.2.1.1 $d1 = 5.4\text{mm}$ and $d2 = 5.4\text{mm}$	115
6.2.1.2 $d1 = 5.4\text{mm}$ and $d2 = 7.56\text{mm}$	118
6.2.1.3 $d1 = 7.56\text{mm}$ and $d2 = 7.56\text{mm}$	118
6.2.2 Entropy	121
6.2.2.1 $d1 = 5.4\text{mm}$ and $d2 = 5.4\text{mm}$	122

6.2.2.2 $d_1 = 5.4\text{mm}$ and $d_2 = 7.56\text{mm}$	123
6.2.2.3 $d_1 = 7.56\text{mm}$ and $d_2 = 7.56\text{mm}$	125
6.2.2.4 Compare with stagger bump pattern.....	127
6.2.3 Stretching analysis.....	131
6.2.4 Improve CTE.....	134
Chapter 7: Conclusion.....	135
Appendix.....	138
References:.....	147

List of Tables

Table 3.1 Results from image analysis of 3 MQFPs	33
Table 3.2 ANOVA test results of MQFPs with 3 replicates.....	33
Table 3.3 Image analysis results of Visteon chip	36
Table 3.4. Results of ANOVA analysis	37
Table 3.5 Major constituents in typical molding compound formulations.....	42
Table 3.6 Area fraction (%) results with 6 replicates, L1 & L2 indicate level.....	51
Table 3.7 Area fraction (%) results with 6 replicates, L3 indicates level.....	51
Table 3.8 ANOVA test results	51
Table 3.9 Results of particle number and size for six cells of level 1	52
Table 3.10 Results of particle number and size for six cells of level 2	52
Table 3.11 Results of particle number and size for six cells of level 3	52
Table 3.12 Area fraction (%) results with 6 replicates, L1 & L2 indicate level.....	54
Table 3.13 Area fraction (%) results with 6 replicates, L3 indicates level.....	54
Table 3.14 ANOVA test results	54
Table 3.15 Results of particle number and size for six cells of level 1	56
Table 3.16 Results of particle number and size for six cells of level 2	56
Table 3.17 Results of particle number and size for six cells of level 3	56
Table 4.1 Process settings	66
Table 5.1 Periodic procedure	77
Table 5.2 Aperiodic procedure	77
Table 5.3 DOE study of f and ball pattern	79
Table 5.4 Simulation results for filling the clear cavity.....	89
Table 6.1 DOE result for irregular bump pattern.....	105
Table 6.2 DOE results for regular bump pattern.....	128

List of Figures

Figure 2.1 Idealized cavity flow is produced by moving the top and/or the bottom wall while keeping the vertical walls stationary [Muzzio 94]	9
Figure 2.2 Stretching field of periodic cavity flows with different T : (a) $T = 2.0, n = 50$; (b) $T = 7.0, n = 20$; (c) $T = 5.6, n = 20$ [Muzzio, 94]	12
Figure 2.3 Stretching field of aperiodic cavity flow [Muzzio 94]	13
Figure 3.1 Electronic package construction	18
Figure 3.2 PQFP – Plastic Quad Flat Package	19
Figure 3.3 Flip-chip with underfill	19
Figure 3.4 Relationship between filler type, volume percentage and the CTE of molding compounds [Pecht 95]	23
Figure 3.5 Transfer molding press [Calce 03]	25
Figure 3.6 Sample image position and fill direction	29
Figure 3.7 Image size $325\mu\text{m} \times 300\mu\text{m}$ (a) Image BLB (b) Image BLB after threshold and binary operation	30
Figure 3.8 Grouping method	32
Figure 3.9 Main effects plot – data means for AF	34
Figure 3.10 Main effects plot – data means for d_v	34
Figure 3.11 Main effects plot – data means for d_n	34
Figure 3.12. Main effects plot – data means for d_b	35
Figure 3.13 Main effects plot – data means for d_v	38
Figure 3.14 Main effects plot – data means for d_n	38
Figure 3.15 Main effects plot – data means for d_b	39
Figure 3.16 Schematic diagram of the e-pad package	43
Figure 3.17 (a) Schematically show the fill direction; (b) A-A view shows the locations of levels 1, 2, 3	44
Figure 3.18 Surface plot of area fraction of level 1, the gray scale shows the percentage of the red particulate	45
Figure 3.19 A sample image obtained from level 1	46

Figure 3.20 Image of level 3 showing the die and leadframe.....	46
Figure 3.21 3-D plot of area fraction of level 1	47
Figure 3.22 Surface plot of area fraction (%) of level 2	47
Figure 3.23 3-D plot of area fraction of level 2	48
Figure 3.24 Distance factor.....	49
Figure 3.25 Convergence study for area fraction.....	50
Figure 3.26 Plot of mean area fraction as a function of distance from the gate and level.....	55
Figure 4.1 Flow geometry.....	63
Figure 4.2 Stagger array bumps model and mesh.....	65
Figure 4.3 Regular array bumps model and mesh	66
Figure 4.4 Determine a point inside a triangle.....	69
Figure 4.5 Linear interpolation from triangle's vertices.....	72
Figure 4.6 Streamlines obtained from $d_1 = 5.4\text{mm}$ and $d_2 = 7.56\text{mm}$	74
Figure 5.1 Initial positions of two particle balls	78
Figure 5.2 Streamlines obtained from $d_1 = 7.56\text{mm}$ and $d_2 = 7.56\text{mm}$	84
Figure 5.3 Initial and final particles position with single gate filling.....	85
Figure 5.4 Initial and final particle positions with two gates filling.....	85
Figure 5.5 $S_{\text{locations}}(\text{species})/\ln(2)$ vs. time for left gate filling (blue) and two gates filling with $f = 1.125$ (cyan)	87
Figure 5.6 Entropy $S(\text{locations})$ for left gate filling (blue) and two gates periodic filling with $f = 1.125$ (cyan)	87
Figure 5.7 Entropy S for left gate filling (blue) and two gates periodic filling with $f = 1.125$ (cyan)	88
Figure 5.8 Mean $\log(\lambda)$ vs. time for left gate (red) and two gates $f = 1.125$ (blue), $d_1 = 7.56\text{mm}$, $d_2 = 7.56\text{mm}$	88
Figure 6.1 Distribution of particles at $t = 1.6\text{s}$ with left gate filling at $d_1 = 5.4\text{ mm}$..	91
Figure 6.2 Distribution of particles at $t = 1.6\text{s}$ for $f = 0.2813$	91
Figure 6.3 Distribution of particles at $t = 1.6\text{s}$ for $f = 1.125$	92
Figure 6.4 Distribution of particles at $t = 1.6\text{s}$ for $f = 1.9687$	92
Figure 6.5 Distribution of particles at $t = 1.6\text{s}$ for aperiodic filling.....	93

Figure 6.6 Distribution of particles at $t = 1.6s$ for $f = 0.2813$	94
Figure 6.7 Distribution of particles at $t = 1.6s$ for $f = 1.125$	94
Figure 6.8 Distribution of particles at $t = 1.6s$ for $f = 1.9687$	95
Figure 6.9 Distribution of particles at $t = 1.6s$ for aperiodic filling.....	95
Figure 6.10 Distribution of particles at $t = 1.6s$ with left gate filling at $d1 = 7.5$ mm	97
Figure 6.11 Distribution of particles at $t = 1.6s$ for $f = 0.2813$	97
Figure 6.12 Distribution of particles at $t = 1.6s$ for $f = 1.125$	98
Figure 6.13 Distribution of particles at $t = 1.6s$ for $f = 1.9687$	98
Figure 6.14 Distribution of particles at $t = 1.6s$ for aperiodic filling.....	99
Figure 6.15 $S_{\text{locations}}(\text{species})/\ln(2)$ vs. time for left gate filling (blue) and two gates filling with $f = 0.02813$ (green), $f = 1.125$ (cyan), $f = 1.9687$, (red), aperiodic (black)	100
Figure 6.16 $S(\text{locations})$ vs. time for left gate filling (blue) and two gates filling with f $= 0.02813$ (green), $f = 1.125$ (cyan), $f = 1.9687$, (red), aperiodic (black).....	100
Figure 6.17 S vs. time for left gate filling (blue) and two gates filling with $f = 0.02813$ (green), $f = 1.125$ (cyan), $f = 1.9687$ (red), and aperiodic (black)	101
Figure 6.18 $S_{\text{locations}}(\text{species})/\ln(2)$ vs. time for left gate filling (blue) and two gates filling with $f = 0.02813$ (green), $f = 1.125$ (cyan), $f = 1.9687$, (red), aperiodic (black)	101
Figure 6.19 $S(\text{locations})$ vs. time for left gate filling (blue) and two gates filling with f $= 0.02813$ (green), $f = 1.125$ (cyan), $f = 1.9687$, (red), aperiodic (black).....	102
Figure 6.20 S vs. time for left gate filling (blue) and two gates filling with $f = 0.02813$ (green), $f = 1.125$ (cyan), $f = 1.9687$ (red), and aperiodic (black)	102
Figure 6.21. $S_{\text{locations}}(\text{species})/\ln(2)$ vs. time for left gate filling (blue) and two gates filling with $f = 0.02813$ (green), $f = 1.125$ (cyan), $f = 1.9687$, (red), aperiodic (black)	103
Figure 6.22 $S(\text{locations})$ vs. time for left gate filling (blue) and two gates filling with f $= 0.02813$ (green), $f = 1.125$ (cyan), $f = 1.9687$, (red), aperiodic (black).....	103
Figure 6.23 S vs. time for left gate filling (blue) and two gates filling with $f = 0.02813$ (green), $f = 1.125$ (cyan), $f = 1.9687$ (red), and aperiodic (black)	104

Figure 6.24 $S_{\text{location}}(\text{species})$ vs. f , red: $d_1 = 5.4\text{mm}$, $d_2 = 5.4\text{mm}$; blue: $d_1 = 5.4\text{mm}$, $d_2 = 7.56\text{mm}$; green: $d_1 = 7.56\text{mm}$, $d_2 = 7.56\text{mm}$	107
Figure 6.25 $S(\text{locations})$ vs. f , red: $d_1 = 5.4\text{mm}$, $d_2 = 5.4\text{mm}$; blue: $d_1 = 5.4\text{mm}$, $d_2 = 7.56\text{mm}$; green: $d_1 = 7.56\text{mm}$, $d_2 = 7.56\text{mm}$	107
Figure 6.26 S vs. f , red: $d_1 = 5.4\text{mm}$, $d_2 = 5.4\text{mm}$; blue: $d_1 = 5.4\text{mm}$, $d_2 = 7.56\text{mm}$; green: $d_1 = 7.56\text{mm}$, $d_2 = 7.56\text{mm}$	108
Figure 6.27 $S_{\text{location}}(\text{species})$ vs. f , $d_1 = 5.4\text{mm}$, $d_2 = 7.56\text{mm}$	108
Figure 6.28 $S(\text{locations})$ (blue) and $S(\text{red})$ vs. f , $d_1 = 5.4\text{mm}$, $d_2 = 7.56\text{mm}$	109
Figure 6.29 $S_{\text{location}}(\text{species})$ vs. f , $d_1 = 7.56\text{mm}$, $d_2 = 7.56\text{mm}$	110
Figure 6.30 $S(\text{locations})$ (blue) and $S(\text{red})$ vs. f , $d_1 = 7.56\text{mm}$, $d_2 = 7.56\text{mm}$	110
Figure 6.31 Mean λ for Left gate (blue) and two gates $f = 0.02813$ (green), $f = 1.125$ cyan), $f = 1.9687$ (red), aperiodic (black); $d_1 = 5.4\text{mm}$, $d_2 = 5.4\text{mm}$	112
Figure 6.32 Mean λ for Left gate (blue) and two gates $f = 0.02813$ (green), $f = 1.125$ cyan), $f = 1.9687$, (red), aperiodic (black); $d_1 = 5.4\text{mm}$, $d_2 = 7.56\text{mm}$	113
Figure 6.33 Mean λ for Left gate (blue) and two gates $f = 0.0281$ (green), $f = 1.125$ cyan), $f = 1.9687$, (red), aperiodic (black); $d_1 = 7.56\text{mm}$, $d_2 = 7.56\text{mm}$	113
Figure 6.34 Stretching as a function of f , red: $d_1 = 5.4\text{mm}$, $d_2 = 5.4\text{mm}$; blue: $d_1 = 5.4\text{mm}$, $d_2 = 7.56\text{mm}$; green: $d_1 = 7.56\text{mm}$, $d_2 = 7.56\text{mm}$	114
Figure 6.35 Distribution of particles at $t = 1.6\text{s}$ with left gate filling at $d_1 = 5.4\text{ mm}$	116
Figure 6.36 Distribution of particles at $t = 1.6\text{s}$ for $f = 0.2813$	116
Figure 6.37 Distribution of particles at $t = 1.6\text{s}$ for $f = 1.125$	117
Figure 6.38 Distribution of particles at $t = 1.6\text{s}$ for $f = 1.9687$	117
Figure 6.39 Distribution of particles at $t = 1.6\text{s}$ for $f = 0.2813$	118
Figure 6.40 Distribution of particles at $t = 1.6\text{s}$ for $f = 1.125$	119
Figure 6.41 Distribution of particles at $t = 1.6\text{s}$ for $f = 1.9687$	119
Figure 6.42 Distribution of particles at $t = 1.6\text{s}$ for $f = 0.2813$	120
Figure 6.43 Distribution of particles at $t = 1.6\text{s}$ for $f = 1.125$	120
Figure 6.44 Distribution of particles at $t = 1.6\text{s}$ for $f = 1.9687$	121
Figure 6.45 $S_{\text{locations}}(\text{species})/\ln(2)$ vs. time for two gates filling with $f = 0.02813$	

(green), $f = 1.125$ (cyan), $f = 1.9687$ (red)	122
Figure 6.46 $S(\text{locations})$ vs. time for and two gates filling with $f = 0.02813$ (green), $f = 1.125$ (cyan), $f = 1.9687$ (red)	122
Figure 6.47 S vs. time for two gates filling with $f = 0.02813$ (green), $f = 1.125$ (cyan), $f = 1.9687$ (red)	123
Figure 6.48 $S_{\text{locations}}(\text{species})/\ln(2)$ vs. time for left gate filling (blue) and two gates filling with $f = 0.02813$ (green), $f = 1.125$ (cyan), $f = 1.9687$, (red), aperiodic (black)	123
Figure 6.49 $S(\text{locations})$ vs. time for left gate filling (blue) and two gates filling with $f = 0.02813$ (green), $f = 1.125$ (cyan), $f = 1.9687$, (red), aperiodic (black)	124
Figure 6.50 S vs. time for left gate filling (blue) and two gates filling with $f = 0.02813$ (green), $f = 1.125$ (cyan), $f = 1.9687$ (red), and aperiodic (black)	124
Figure 6.51 $S_{\text{locations}}(\text{species})/\ln(2)$ vs. time for two gates filling with $f = 0.02813$ (green), $f = 1.125$ (cyan), $f = 1.9687$ (red)	125
Figure 6.52 $S(\text{locations})$ vs. time for and two gates filling with $f = 0.02813$ (green), $f = 1.125$ (cyan), $f = 1.9687$ (red)	125
Figure 6.53 S vs. time for and two gates filling with $f = 0.02813$ (green), $f = 1.125$ (cyan), $f = 1.9687$ (red)	126
Figure 6.54 $S_{\text{location}}(\text{species})$ vs. f , $d1 = 5.4\text{mm}$, $d2 = 7.56\text{mm}$, $t = 1.6\text{s}$	126
Figure 6.55 $S_{\text{location}}(\text{species})$ vs. f , $d1 = 5.4\text{mm}$, $d2 = 7.56\text{mm}$, $n = 2$	127
Figure 6.56 $S(\text{locations})$ (blue) and S (red) vs. f , $d1 = 5.4\text{mm}$, $d2 = 7.56\text{mm}$	127
Figure 6.57 $S_{\text{location}}(\text{species})$ vs. f , red for $d1 = 5.4\text{mm}$ and $d2 = 5.4\text{mm}$, blue for $d1 = 5.4\text{mm}$ and $d2 = 7.56\text{mm}$, green for $d1 = 7.56\text{mm}$ and $d2 = 7.56\text{mm}$, stagger pattern – circle, regular pattern – star	129
Figure 6.58 $S(\text{locations})$ vs. f , red for $d1 = 5.4\text{mm}$ and $d2 = 5.4\text{mm}$, blue for $d1 = 5.4\text{mm}$ and $d2 = 7.56\text{mm}$, green for $d1 = 7.56\text{mm}$ and $d2 = 7.56\text{mm}$, stagger pattern – circle, regular pattern – star	130
Figure 6.59 S vs. f , red for $d1 = 5.4\text{mm}$ and $d2 = 5.4\text{mm}$, blue for $d1 = 5.4\text{mm}$ and $d2 = 7.56\text{mm}$, green for $d1 = 7.56\text{mm}$ and $d2 = 7.56\text{mm}$, stagger pattern – circle, regular pattern – star	130
Figure 6.60 Mean λ for two gates $f = 0.02813$ (green), $f = 1.125$ cyan), $f = 1.9687$	

(red); $d_1 = 5.4\text{mm}$, $d_2 = 5.4\text{mm}$	132
Figure 6.61 Mean λ for two gates $f = 0.02813$ (green), $f = 1.125$ cyan), $f = 1.9687$ (red); $d_1 = 5.4\text{mm}$, $d_2 = 7.56\text{mm}$	132
Figure 6.62 Mean λ for two gates $f = 0.02813$ (green), $f = 1.125$ cyan), $f = 1.9687$ (red); $d_1 = 7.56\text{mm}$, $d_2 = 7.56\text{mm}$	133
Figure 6.63 Stretching as a function of f , red for $d_1 = 5.4\text{mm}$ and $d_2 = 5.4\text{mm}$, blue for $d_1 = 5.4\text{mm}$ and $d_2 = 7.56\text{mm}$, green for $d_1 = 7.56\text{mm}$ and $d_2 = 7.56\text{mm}$, stagger pattern – circle, regular pattern – star	133

Chapter 1: Introduction

1.1 Motivation

Mixing of highly viscous fluids is well known by its importance in the plastic manufacturing industry. The mixing process is responsible for the final uniformity and in many cases, properties, of the polymer product. The recent fast growth in electronic packaging field with the use of highly filled filler particles and some of minor additives, raised a new area of study, which is how to produce uniformly distributed filler particles and what mixing measures are applicable to such systems.

With ever-finer area-array lead spacing, thinner packages, and smaller device feature size, control of highly filled mold compound's properties and processing parameters becomes more important to satisfy the needs of current and new technologies. This will be especially important to the electrical devices used in high temperature environment. The properties and distribution of binders and filler particles affect properties like coefficient of thermal expansion (CTE) and stiffness, both of which determine the stress index and thus contribute strongly to reliability [Pecht 95, Lantz 02]. The interplay between the chip size, pitch and the filler concentration, size distribution and spatial distribution must be examined in a structured manner to understand their effects on final properties. The study of the mixing of filler particles cannot be overemphasized. In our study the particle distribution resulting from mixing will play an important role and is to

be the focus of the research.

Mixing is very important to the molding process. In many cases it has been shown that the goodness of the mixing of fillers will affect or determine the properties of the products. An uneven mixed electronic package could cause stress concentration due to CTE mismatch during the thermal cycle and final product failure such as delamination of the die.

One goal in the molding process is to obtain uniform mixing. Unlike fully filled mixers, which can mix well the mold compound as long as the time is enough, the process of electronic packaging with molding machine requires fast mixing during the cavity filling process. This is foreseen to result in poor mixing and low reliability.

One of the main contributions of this work to the study of mixing and chaos is the generation of chaotic flow while filling the empty cavity. This thesis first investigates the properties of highly filled electronic package made using the traditional molding processes. The local property and their relationship with filler particle distribution are quantified. Then we investigate the minor solid constituent of the additives. A new feed protocol that can generate chaotic mixing by making use of periodic and aperiodic filling procedure is proposed. A square cavity model is constructed and the mixing of filler particles in this flow system is simulated by using a commercial software package.

Another contribution of this work is to develop unique measures of mixing, which are applicable to quantify the mixing of highly filled system and tell the difference in electronic packages.

This work is motivated by the role of mixing in the electronic packaging industry. This thesis represents the first effort to understand the chaotic mixing during the process

of filling empty cavity with certain geometries and quantity measures suitable to describe the mixing of highly filled systems. With more than half of failure of electronic packages are due to thermal problems, this study becomes important and gives us a new direction to solve the problem.

1.2 Concentration of research

This thesis will emphasize the following topics:

- Relations between properties of electronic package and filler particle distribution
- Uneven particle distribution problem within the highly filled flow system
- Novel feed protocol with mixing function embedded
- Flow model and simulation
- Measures of mixing

1.2.1 Properties and filler particle distribution

There is much information about the relationship between filler concentration, size distribution and properties [Deanin 89, Pecht 95, Sumitomo, Bae 00, and Lowry 01]. However, there is little known or published about the role of filler particle distribution.

In this study we investigate the effects of the filler particle distribution on the properties of electronic package and how this affects the product reliability. It is desirable to know if a change of filler distribution will change local properties like CTE.

1.2.2 Novel feed protocol

The goal of this study is to design a novel feed protocol with a mixing function

embedded. Previous studies have shown that at very low *Reynolds* number periodic flow can generate chaos in the laminar flow in fully filled cavities, and this chaos is essential to good mixing [Ottino 89, Muzzio 94]. Furthermore Muzzio [94] indicated that aperiodic flow could make more uniform mixing by deleting periodic points generated in periodic flow. Both of the works examined fully filled flows in channels; in our study we apply the principles to the mold filling process.

By generating chaotic flow regions during the molding process, we expect improved filler particle distribution, i.e. more uniform distribution, and thus improved reliability of electronic package.

1.2.3 Flow model and numerical simulation

The flow during molding process is a typical creeping flow since its *Reynolds* number is much less than 1. A 2-D square cavity model is constructed and the streamlines and the mixing of fillers are obtained by using a commercial mold-simulating package, Moldflow®.

Well-designed numerical simulation experiment is conducted. Filling the cavities is simulated with 46 and 49 bumps representing either solder balls or leadframe inside and two gates one on top edge and one on left edge. Velocity field obtained from Moldflow® is reconstructed by using Matlab® and interpolated by using triangular element method.

1.2.4 Measures of mixing

Both new and existing measures are carefully designed and selected to be used in this study. These measures include area fraction, number average and volume average diameters, interparticle distance, stretching and entropy. The first 4 measures are used for the analysis of actual electronic packages while the stretching and entropy are used

for the analysis of simulation results.

1.3 Organization of the thesis

Chapter 1 is the introduction and description of the main contributions of the study. Chapter 2 gives the background of mixing, chaos theory, chaotic mixing and measures of mixing. It also presents details about both periodic and aperiodic flows, and how a researcher might choose parameters, which could define the period. Chapter 3 provides the background on electronic package that includes the functions of molding compounds, effects of filler concentration, and of size distribution on properties. Then the experimental study on electronic packages and detailed study on filler distribution and minor additive distribution. Chapter 4 discusses the numerical modeling method and important parameters for this study. Chapter 5 describes the theory of mixing model and measures to be used in the analysis. The results from simulating a clear cavity without any bumps are presented. Chapter 6 presents simulation results from filling cavity with bumps inside. Single gate and two gates filling, periodic and aperiodic filling results are analyzed for stretching and entropy. Chapter 7 is the conclusion of the dissertation.

Chapter 2: Background

This chapter addresses mixing, chaos, and measures of mixing. Laminar mixing theory will be introduced through its evolution to processing examples. Then the development of the chaos theory will be discussed where detailed description is given to periodic and aperiodic chaotic flow, since these are the basis for this study.

2.1 Mixing Theory

In polymer processing, mixing significantly affects material properties, processability, and cost. Various reinforcing materials are mixed with polymers to increase moduli or impact toughness. Additives are mixed with polymers to improve flame retardance or reduce coefficient of thermal expansion. No engineers can accurately predict how efficiently a particular processor will mix from a quantitative theoretical basis, however.

To achieve better mixing, we need to understand why flow during mold filling process doesn't give good mixing, and why periodic and aperiodic flows generate chaotic flow and better mixing.

The flow of the mold compound in the filling process is a creeping flow with the *Reynolds* number much less than 1 [White 91]. The filler particles are conveyed along the streamlines of the flow. Since there are no crossing streamlines, mixing will be a minimum. This is true for all constant flows. Creeping flow in parallel plates and tubes are typical constant flows with parallel streamlines, and little mixing can be observed in

these flows.

Turbulent flow is associated with random fluid motion and is a very effective mechanism for mixing. The criterion for maintaining turbulent flow in any channel depends on the *Reynolds* number. With the channel size D , the average velocity of the flow V in the channel, the fluid density ρ , and fluid viscosity η , the following relationship is valid for the *Reynolds* number:

$$\text{Re} = \frac{DV\rho}{\eta} \quad (2.1)$$

The *Reynolds* number must exceed a value of 2000 to achieve turbulence. This means it is impossible to have turbulent flow in polymer melts, which have the extremely high viscosities and very low *Reynolds* number. So laminar flow is the only mechanism for mixing of high viscosity polymers.

Mixing is the intermingling by mechanical action of two or more initially segregated components. Two distinct physical phenomena are involved in mixing: dispersion and distributive mixing. Mixing in polymer melt processing is primarily the reduction of scales of segregation between fluids. The scale of a polymer mixture is typically described by either an average striation thickness or the amount of the interfacial area. Interfacial area generation was recognized by Brothman et al. [Brothman 45] as a primary mechanism for mixing.

2.2 Chaos theory

Chaos shows a system's sensibility to initial conditions. That is, the ability of two adjacent points to diverge in space over time. A chaotic system offers the potential for significantly better mixing than non-chaotic systems. Aref is commonly recognized as the first person to introduce chaotic flow in creeping flow [Aref 84]. He has studied stirring in a blinking vortex inside a closed circular geometry. Ottino and others extended the fundamental understanding of mixing with the use of chaos theories [Ottino 86, 89]. The research concentrated on the study of a cavity flow with alternate periodic motion of one or two boundaries.

2.2.1 Introduction to chaotic flows

One of our goals is to achieve uniform mixing in desired regions. Many studies have been conducted to find ways to generate chaos in laminar flow [Ottino 86, Leong 90, Muzzio 94, Anderson 00]. Almost all of them used periodic or aperiodic flow methods. These chaotic flows generally greatly enhanced the mixing. We will introduce the cavity flow only because it is similar to filling an electronic package. Bigg and Middleman simulated the circulating flow in a rectangular cavity based on the finite difference method [Bigg 74]. By plotting the distributions of advected particles at successive times, they simulated laminar mixing in a 2D rectangular cavity and showed excellent agreement with experiments results.

2.2.2 Periodic chaotic flow

Periodic cavity flow is defined in a rectangular domain with two moving walls and

fully filled fluid as shown in Figure 2.1 [Muzzio 94]. The aspect ratio is defined as H/L , where H is the height of the cavity and L is the length of the moving horizontal walls. Periodic flows are generated by alternatively moving the top and bottom walls with constant velocity each for a time $T/2$, where T , the period of the flow, is defined in dimensionless terms as the combined displacement of both walls during one period divided by the length of the cavity. In two dimensional flows, crossing streamlines are a prerequisite for periodic flow.

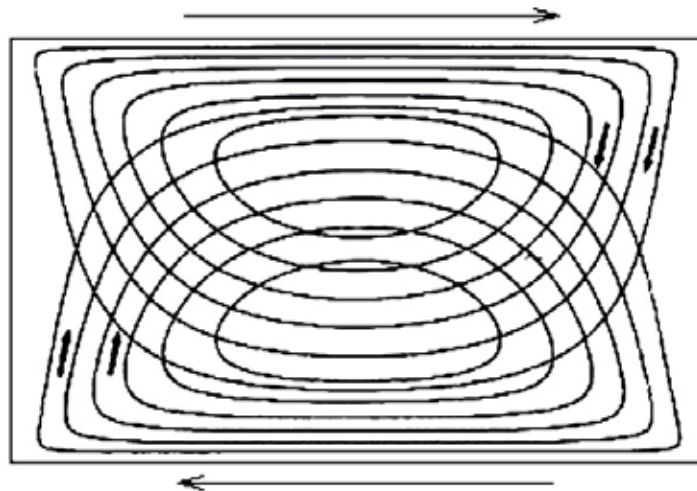
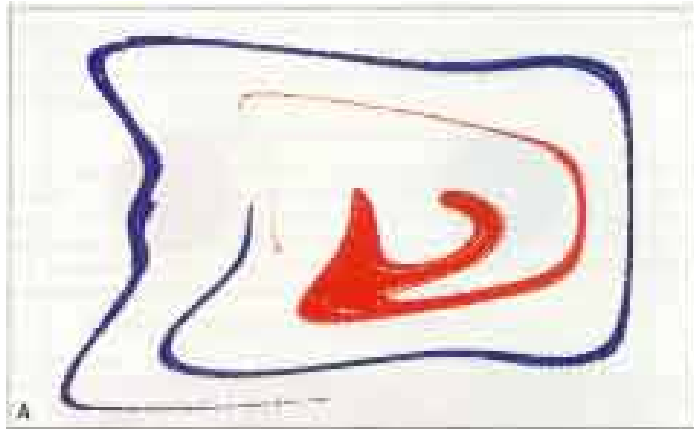


Figure 2.1 Idealized cavity flow is produced by moving the top and/or the bottom wall while keeping the vertical walls stationary [Muzzio 94]

Motions a and b to describe the cavity flow, where motions a and b are respectively driven by the displacement of the upper and lower walls. Then the time periodic flows are generated by the periodic sequence P ,

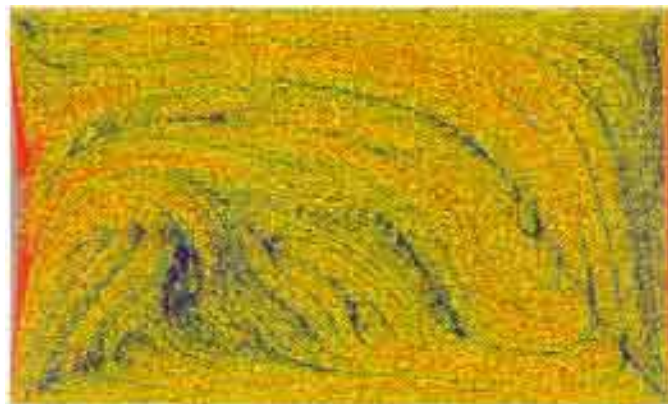
can be clearly seen. The flow is mostly chaotic when $T = 5.6$ (c). However, we can only find the optimal T for good mixing by experiment or simulation.



(a)



(b)



(c)

Figure 2.2 Stretching field of periodic cavity flows with different T : (a) $T = 2.0, n = 50$;
(b) $T = 7.0, n = 20$; (c) $T = 5.6, n = 20$ [Muzzio, 94]

Zerafati [Zerafati 94] studied f values from 0.58 to 3.49 and found that there is a threshold value for f (f_c), increasing f above the critical value will substantially increase the mixing performance. And this f_c occurs between 0.58 and 1.16.

2.2.5 Periodic points

Time-periodic flows contain periodic points; some of these are elliptic and give rise to islands. These islands must be removed if the flow is to achieve complete mixing.

There are two kinds of periodic points:

- 1) Elliptic (stable) periodic points: at the center of non-mixing rotating regions, called islands [Anderson 00]. In general, the lower the period, the larger the island. In a time-periodic flow, regions of regular motion are due to the periodicity [Muzzio 94].
- 2) Hyperbolic (unstable) periodic points: are centers of stretching in the flow, and these regions are favorable for mixing [Anderson 00].

2.2.6 Aperiodic chaotic flow

The islands in time-periodic flows will result in poor mixing zone and should be removed. Aperiodic flows are devoid of periodic points, and hence they are free of islands [Muzzio 94]. So we can expect more complete and efficient mixing in aperiodic flows. Aperiodic flows can be generated in several ways [Muzzio 94, Ottino 89]. For example, the restricted random period (RRP) introduced by Muzzio.

This aperiodic procedure is to impose a random perturbation of restricted magnitude

to the duration of a and b . Instead of $T/2$, the duration of each motion is given by $T(1+\varepsilon_i)/2$, where ε_i is a random number in the interval $(0, 1)$. The restricted random period prescription generated by this procedure can be represented as:

$$a(\varepsilon_1)b(\varepsilon_2)a(\varepsilon_3)b(\varepsilon_4) a(\varepsilon_5)b(\varepsilon_6)a(\varepsilon_7)b(\varepsilon_8)a(\varepsilon_9)b(\varepsilon_{10})a(\varepsilon_{11})\dots$$

In Figure 2.3, for the same T and n as in Figure 2.2 (a), a very different situation is generated by using the aperiodic flow, considerably better mixing is achieved.

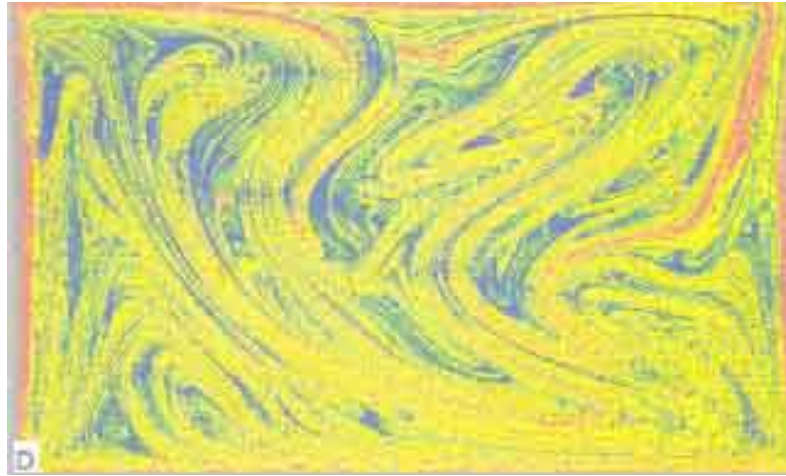


Figure 2.3 Stretching field of aperiodic cavity flow [Muzzio 94]

There are still many other aperiodic procedures that can be designed easily. In this thesis, we decided that the restricted random period procedure is more suitable for our study and is used in the simulation.

2.3 Mixing Measures

Numerous measures and indices have been proposed to characterize a mixture's state

of “mixedness.” In laminar mixing theory, the fundamental equations relate interfacial area growth as a function of the shear field. Direct measures determine the growth and reorientation of the interfacial area. Indirect measures, such as the mixture’s bulk electrical conductivity, offer little insight into the mechanisms of mixing. Most direct measures are simply related to interfacial area or striation thickness distributions.

A comprehensive description of mixing requires both local and global measures. Local and global measures are developed and applied to the cavity flow of interest.

2.3.1 Line growth

The aim in the mixing process is to increase efficiently the interface between different fluids. An interface should divide the bonding into two separate regions. For a 2-D analysis, a line interface will do the job. Line growth is a very basic measure for the mixing.

2.3.2 Interfacial area growth in a simple shear flow

For a 3-D analysis an interfacial area is required to perform the task. Spencer and Wiley [Spencer 51], in 1950, developed an equation for the growth of interfacial area in a simple shear flow:

$$\frac{A_f}{A_i} = s \cos \alpha \quad (2.5)$$

where A_i and A_f are the initial and final interfacial area, s is the magnitude of the shear strain, and α is the angle defining the initial orientation of the element relative to the

shearing plane. This is the first fundamental study of mixing in a laminar flow. It shows the growth of interface is linear.

In the late 1970's, Erwin showed that re-orienting the interfacial area, after substantial deformation, could improve the linear rate of mixing. In a simple shear flow, as the interfacial area deforms it orients itself toward an unfavorable direction, parallel to the direction of shear. If this area were re-oriented then the rate of growth of that area would be significantly larger. The final growth in area could be greater-than-linear and approaches an exponential rate of growth, which is also an indication of chaos. Therefore, the linear mixing process has been improved when a process of area re-orientation can be achieved [Conner 91]. This finding gave the ideas of how to generate chaotic mixing in a fully filled cavity to the other researchers.

2.3.3 Interfacial area and principal values and directions

A method which stands in continuum mechanics is developed to quantify the mixing process by relating interfacial area growth with the principal values and directions of the appropriate tensors [Zerafati 94]. This approach is good to find out which regions in the flow field will have efficient mixing. It shows that if the maximum instantaneous rate of mixing is determined by the magnitude of the largest eigenvalue of the \mathbf{D} tensor (rate-of-deformation tensor), then tracking the orientation of the line relative to that value as they both vary throughout the flow field would give insight into the mixing, rather than just quantify it.

If c_i ($i = 1, 2, 3$) are the principal values of \mathbf{C} (deformation tensor) and d_i ($i = 1, 2, 3$) the principal values of \mathbf{D} , one of the c_i 's quantifies the highest value for the stretch and

one of the d_i 's characterizes the highest rate of stretch. These eigenvalues, as well as the associated directions, are calculable. When these two directions happen to be the same orientation, the highest rate of stretch will occur and when the direction of smallest c_i and smallest d_i are the same, the stretch decreases at the highest rate. The approach of relating mixing to the principal directions of the appropriate tensors is a criterion for determining the rate of stretch, therefore the rate of mixing.

2.4 Mixing in empty cavity

One of the main objectives of this research project is to generate chaotic mixing during the filling process of any empty cavities. This is a unique contribution to the mixing study and it is one of the most difficult problems. The most important reason is that, unlike the fully filled systems the mixing process can be as long as we want, the mixing time is equal to the filling time, once the cavity is filled the mixing process is finished. Normally this filling time in a molding machine is on the order of seconds.

All of the previous studies of the nature of chaos theory and the application are on chaotic advection in filled cavities. None of them have touched filling of empty cavity. We are studying the case of filling an empty cavity where there is no steady flow and a moving flow front. In that case some of the descriptions of the flow no longer are rigorous, nor the measures of the chaos. While we are studying the filler distribution in electronic packages, it is more and more important to study the mixing during the filling process. With the development of a novel feed protocol, we are finally able to generate chaotic flow and dramatically improve the local and global mixing.

Chapter 3: Experimental work on electronic packages

This chapter provides basic knowledge of electronic package such as construction and functions of mold compound. The molding process and failure modes will also be included. Then experimental work on filler and minor additive distributions and their relations to properties will be reviewed.

3.1 Background on electronic package

3.1.1 Functions of electronic package

Electronic packaging is the technology dealing with the mechanical and electrical connections between a die and the surrounding components together with protection of the chip from the environment. Molded or underfilled electronic packages are used to protect silicon chips from harmful environmental conditions such as moisture, chemical agents, dust, and light, and to provide the chips with excellent mechanical strength.

3.1.2 Structure of electronic package

There are many kinds electronic packages. A typical cross section of an electronic package with leadframe is shown in Figure 3.1. An integrated circuit chip is physically attached to a leadframe, with bond wires as interconnections, and then it is molded in the specially prepared molding compound.

The leadframe is the carrier for package assembly. It acts as the mechanical support of the die for handling, wire bonding, and assembly. The die attach is used as mechanical

attachment of the die to the leadframe paddle and provides heat dissipation from the die to the leadframe. Bond wires are used as electrical contacts from the die bond pads to the leadframe [Pecht 95]. We will discuss the details of molding compounds in the next section.

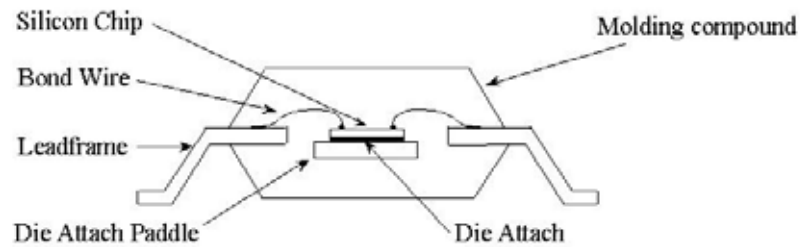


Figure 3.1 Electronic package construction

3.1.3 Electronic packaging configurations

There are many styles of configurations of electronic packages. From the view of polymer processing they all have one common characteristic, which is filling a cavity with certain geometry. So we have chosen to study some typical electronic packages such as plastic quad flat package (PQFP) and transfer molded exposed die paddle (e-pad) leadframe microcircuit package. The schematic illustration of a PQFP is shown in Figure 3.2.

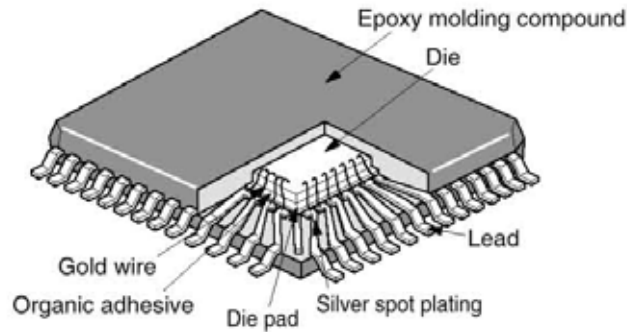


Figure 3.2 PQFP – Plastic Quad Flat Package

The flip-chip technology is a relatively newer technology intended to meet ever-increasing demand of high I/O requirements. Unlike conventional packages, by using flip chip connections, the chip is placed face downward and the connection between chip and chip carrier is achieved by solder bumps rather than bond wires. Since the solder bumps can be placed anywhere on the chip face, the I/O number can be increased. This technique also has many other advantages such as better heat transfer, reduced capacitance, and reduced inductance, both are due to small size of the solder bumps. The underfill technique has been developed and implemented for the flip-chip technology to enhance solder bump reliability. The specially formulated epoxy encapsulant is commonly used as underfill material. Figure 3.3 shows the structure of a flip-chip.

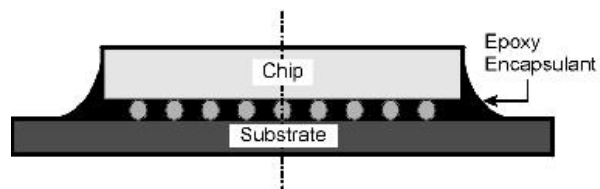


Figure 3.3 Flip-chip with underfill

To be noted is that the gap between chip and substrate for a flip-chip is very small compared that for a PQFP. The gap for a flip-chip is on the order of tens of microns, and that for a PQFP is a few millimeters. Our simulation on filling empty cavity with bumps is more similar to a flip-chip.

3.1.4 Role of molding compounds

3.1.4.1 Components of molding compounds

The electronic packages provide mechanical strength and protection of environmental hazards to the silicon die. Epoxy resins are generally used as matrix for molding compounds; other resins include biphenyl resins and silicone resins. Epoxy is a thermosetting polymeric material and need to be modified by the additives, such as inorganic fillers, in order to be used in plastic packaging of integrated circuit devices. These additives include: curing agents or hardeners, accelerators, inert fillers, coupling agents, flame retardants, stress-relief additives, coloring agents, and mold-release agents.

3.1.4.2 Properties of epoxy resin

The properties of epoxy resins depend on temperature, time and shear rate. The epoxy resins are kept below their frozen point and can flow at a low initial viscosity after being thawed. The gel time of a thermoset resin indicates polymerization rates. After gel and cure, epoxy resins cannot flow as a true liquid, and their viscosity will go to infinity. The glass transition temperature T_g , which is characterized by a step drop in modulus, is an important parameter of epoxy resins. Below the glass transition temperature, the material will be brittle. Above the glass transition temperature, the material will behave

like a crosslinked rubber.

The epoxy resins are non-Newtonian fluids with shear thinning viscosity and will show Newtonian behavior at a very low shear rate. So in this study we will use the Carreau model, which attempts to describe a wide range of fluids for both Newtonian and shear-thinning non-Newtonian laws.

The epoxy resins have a CTE much higher than that of the silicon die. Below the glass transition temperature (T_g), the CTE of the most commonly used epoxy resins are in the range of 50-90 ppm/°C, while the CTE of the silicon die is around 2.3-2.6 ppm/°C. To minimize the thermal stress, it is necessary to reduce the CTE of the epoxy resins so as to reduce the CTE mismatch. There are many ways to reduce the CTE and one effective way is to add fillers such as silica (SiO₂). Highly filled epoxy resins have reduced CTE and increased reliability.

3.1.4.3 Fillers

Fillers are used in the molding compounds to minimize the stress of electronic packaging by reducing the CTE mismatch between the silicon die and the molding compounds. The weight percentage of the fillers is normally around 70% while the epoxy resins have a weight percentage around 20%. Thus the volume percentage of the fillers is around 50%. It is desirable to increase the filler content, but at a too high level (when it exceeds 90%) the properties of the molding compounds will decrease to an extent that it will no longer be useful [Bae 00].

Other functions of the fillers include:

- Reduce the shrinkage (and thus reduce residual thermo-mechanical stress)

- Raise the elastic modulus and toughness
- Prevent resin bleed at the molding tool parting line
- Increase the viscosity, which is a disadvantage since it reduces the flowability

Our study is to find how fillers distribution will affect product properties and reliability, and then propose a way toward improvements.

3.1.4.4 Filler and properties

Filler will affect the properties of the molding compounds by its content, shape, size and size distribution. However, there is little known or published about the role of the filler particle distribution. We will show how some important physical properties vary as a function of compositional variations.

3.1.4.5 Effective CTE of molding compounds

Many models have been developed to predict the effective CTE of the polymeric composite materials [Kwon 98, Shin 98, Vo 01]. Kwon also mentioned about inhomogeneous thermal properties due to uneven particle distribution. One widely employed model for calculating the effective CTE of the composite is Kerner's equation:

$$\alpha_C = \phi_F \alpha_F + (1 - \phi_F) \alpha_M - (\alpha_F - \alpha_M) \frac{\frac{\phi_F}{K_F} + \frac{(1 - \phi_F)}{K_M} - \frac{1}{K^*}}{\frac{1}{K_F} - \frac{1}{K_M}} \quad (3.1)$$

where α is CTE, ϕ is volume fraction, K is bulk modulus, and K^* is effective bulk modulus. The subscripts C, F, and M denote composite, filler, and matrix respectively.

Though this model is dealing with CTE of the bulk material, we are going to use it to estimate the local CTE as well, once we found the filler particle spatial distribution.

3.1.4.6 Filler content and properties of the molding compounds

Figure 3.4 shows the effect of lowering the CTE of the molding compounds as a function of the crystalline silica, α -alumina, and fused silica volume percentage.

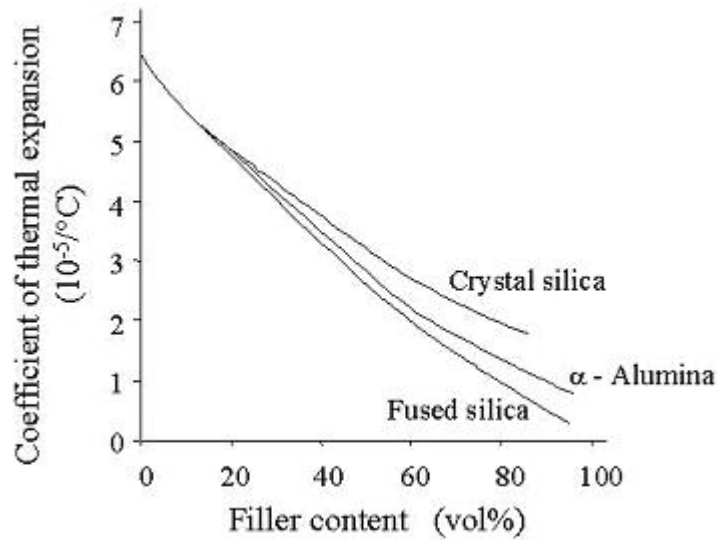


Figure 3.4 Relationship between filler type, volume percentage and the CTE of molding compounds [Pecht 95]

3.1.4.7 Filler particle size and size distribution

Previous studies show that increasing the filler content will decrease the CTE. The epoxy resins filled with large-size particles have slightly higher values of CTE than that filled with small-size particles [Bae 00, Vo 01]. Vo explained that for a given volume fraction of filler, a smaller particle size has a larger fraction of interphase volume; i.e. the

region between the filler and the matrix. Also they found that the CTE value decreased as the portion of smaller particle increased. These factors will be ultimately related to the filler's microstructure. However, the effects of filler spatial distribution on material properties are not often addressed particularly in the area of electronic packaging.

In an underfill reliability test, 1 μm filler showed improved yield compared to 5 μm filler [Dory 00]. This is consistent with its reduced CTE.

3.1.4.8 Filler particle distribution

From the above we have shown that the properties of epoxy molding compounds (EMC) will be affected by filler content, particle size, and particle size distribution. These factors presumably will be ultimately related to the filler's microstructure. But little information has been found in previous works that address this issue (particularly in the area of electronic packaging). We will propose a method to quantify the filler particle distribution, and find the relations between the properties of EMC and the interparticle distance (IPD).

To be noted is that increasing filler content and decrease the filler size would always decrease the IPD, and the IPD is an important parameter, in most cases the smaller IPD will result in better properties [Bigio 01, Wu 85]. However, little study has been done on relations of IPD and CTE and most studies regard macroscopically the molding compounds as homogeneous materials, which is not appropriate when the mixing is poor. The relations of IPD and CTE would be worth investigating in the future research. The more uniform mixing of filler particles the more uniform and better properties, since the IPD or variance of IPD is smaller.

3.1.5 Molding process and failure modes electronic package

3.1.5.1 Molding process

We will simulate a modified transfer molding press to mold chips. We will describe the molding process below and discuss how we expect to design the new control system and the mold in order to achieve the periodic and aperiodic chaotic mixing.

The molding facilities are used to mold the package assemblies [Manzione 90]. The molding equipment includes a transfer molding press, the mold and a dielectric preheater.

Figure 3.5 shows the features of a transfer molding press and a mold.

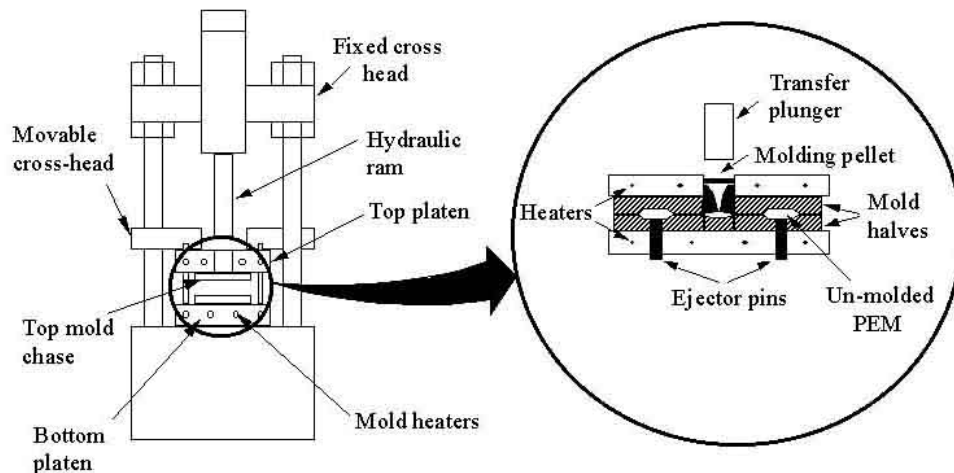


Figure 3.5 Transfer molding press [Calce 03]

The pre-shaped molding compound is dielectrically preheated first. Then it is placed into the pot of the mold. The plunger (hydraulic ram) is then activated and it pushes the molding compound into the cavities via the gates through the runner system. Thus the chip is encapsulated. After curing for 1-3 minutes, the molded package assemblies are

removed for the next process operation.

3.1.5.2 Failure modes of the electronic packages

While the goal of our research is to achieve uniform mixing and better properties, the way to judge the result is to see if it will reduce or delay the failure of electronic packages.

There are many failure modes for electronic packages. The failure modes related to the molding compounds include crack and delamination. Crack can be brittle or ductile, or through fatigue crack propagation. The most important reason of these kinds of failure is CTE mismatch. CTE mismatch causes stress concentrations and since the flaws, like voids, are unavoidable, the cracks initiate from flaws.

We expect to improve the reliability of electronic packages by reducing CTE mismatch through our feed protocol research.

3.2 Experimental work on investigating of packaging properties as a function of filler microstructure in PQFPs

3.2.1 Introduction

In this section, we present experimental work on electronic packages. These electronic packages were made by using conventional methods. No chaotic mixing was performed. This study concentrates on the effect of filler particle spatial distribution. Quantitative measures of the particle distribution were experimental determined, including area fraction, size and IPD.

3.2.2 Materials of chips

An 80 leads PQFP with the dimension of 20mm × 13mm has been analyzed. The molding compound is Sumitomo EME - 6300H. The filler materials are a silica flake and sphere and a silicone rubber as a part of low stress modifier. The filler concentration is about 70 wt% or 56 vol% and the effective CTE of 17 ppm/°C.

To gain statistical significance another 3 molded quad flat packages (MQFPs) with the dimension of 27mm × 27mm have been studied. The molding compound is EME - G700 and the filler is silica sphere. The filler concentration is about 84 wt% or 72 vol%. The average filler size is between 10 ~ 20 μ m. The effective CTE is 12 ppm/°C. For both the molding compounds, $K_f = 34.8$ GPa, $K_m = 3.01$ GPa and for PQFP $K^* = 8.57$ GPa, for MQFPs $K^* = 12.55$ GPa.

3.2.3 Experimental procedure

The chips were received from the provider without further treatment. X-rays were taken to locate the die position for the cutting purpose. Since the chips are rectangular, the cutting planes were chosen to be parallel to one pair of the edges.

3.2.3.1 Image acquisition

The fill direction and cutting planes are shown in Figure 3.6 and we used F (Front), M (Middle), and B (Back) to denote three cutting planes. Only M cut goes through the die. Three pieces of each chip were encapsulated for better polish result. We used several grades of polishing papers, i.e. from 600, 800, to 1200. Then we changed to finer polisher with 1 μ m, 0.3 μ m and 0.05 μ m diamond powders to finish the polish process.

For particles bigger than $1\mu\text{m}$, Optical Microscopy is capable to catch them with sufficient clearness and is used for our study. As shown in Figure 3.6, images were obtained at six places within one cross section. There are 3 positions, which are L (Left), M (Middle), and R (Right) and two die positions, which are B (Below die) and U (Above die). Thus each image will be denoted such as BLU, MLU etc. There are total 18 images for one chip.

3.2.3.2 Image processing software

The images were modified by using common image tool and were analyzed by using ‘Scion Image’, a shareware programmable image analysis package. Since the fillers have a wide range of particle size, a $20\times$ magnification which gives the viewing area of $325\mu\text{m} \times 300\mu\text{m}$ was used. If smaller particles are of interest, we can use $50\times$ magnification.

Macros, which can be incorporated into ‘Scion Image’, were developed to locate the particles, calculate the average particle diameter, and obtain the area fraction. In addition one short macro was added to calculate the interparticle distance. These measures will be introduced later.

By employing a threshold criterion, which removes all of the particles smaller than $9\mu\text{m}$ for Visteon chip and $8\mu\text{m}$ for MQFPs, the distribution of the larger silica particles can be examined. These bigger particles account for more than 90% of the fillers, which means the significance will not be lost. Figure 3.7 shows one of MQFP images – BLB (a) and the image after threshold and binary operation (b).

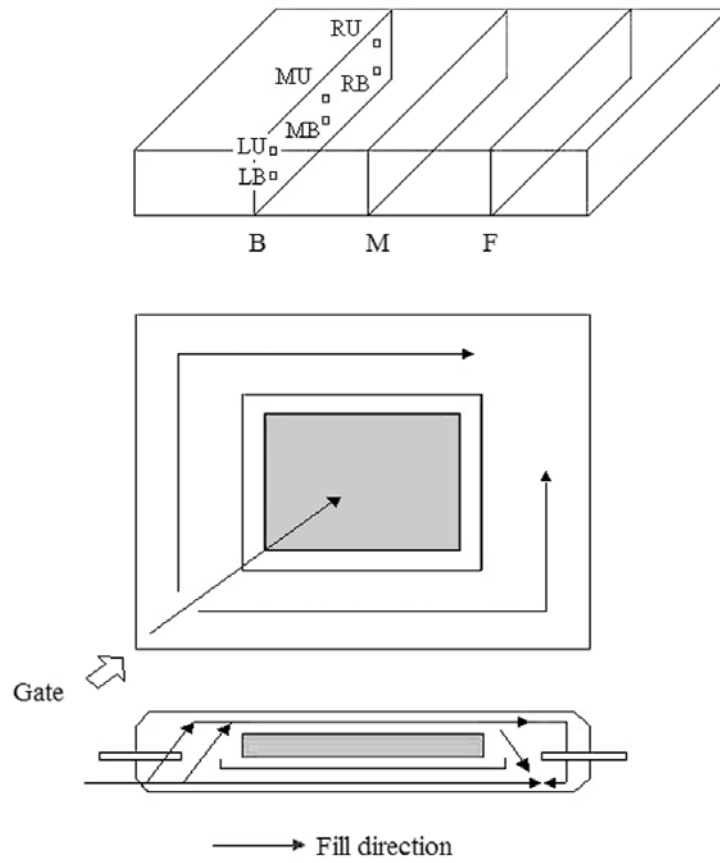
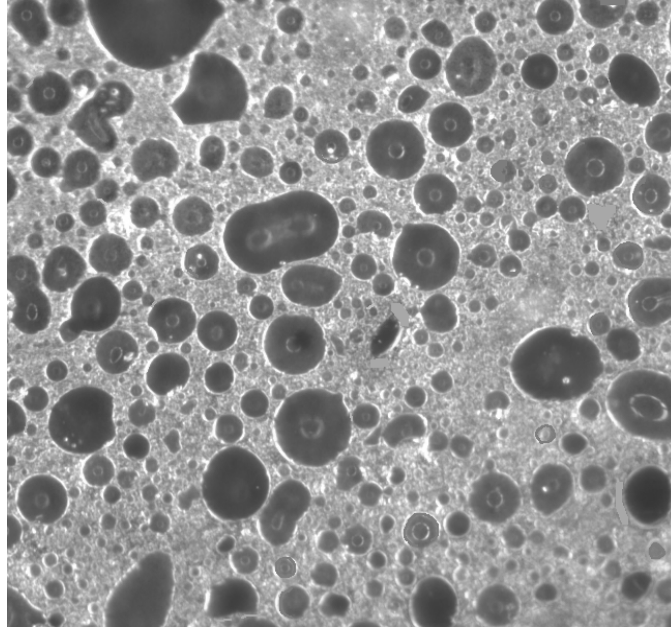
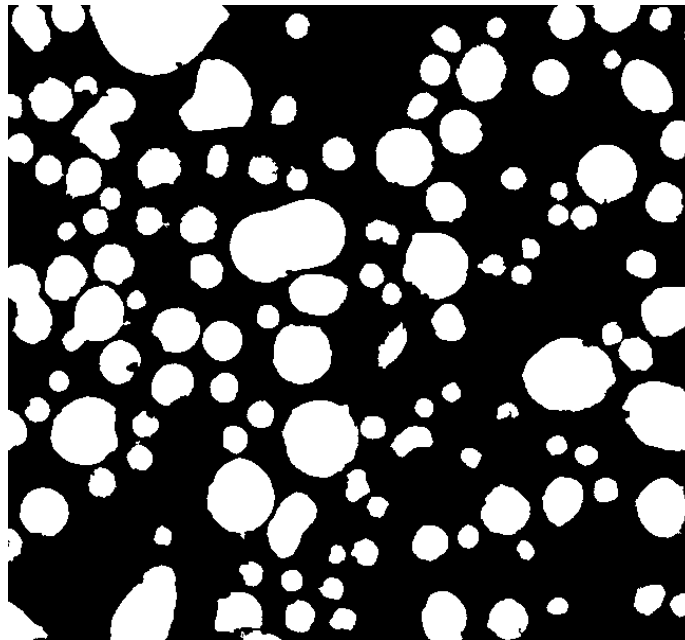


Figure 3.6 Sample image position and fill direction



(a)



(b)

Figure 3.7 Image size $325\mu\text{m} \times 300\mu\text{m}$ (a) Image BLB (b) Image BLB after threshold and binary operation

3.2.3.3 Quantitative measures

The size distribution and spatial distribution of the particles are of interest. The measures that we are employing include: Diameter-volume d_v , Diameter-number d_n , Area fraction (AF), and Average IPD d_b . Equations (3.2) and (3.3) are used for calculating d_v and d_n :

$$d_v = \frac{\sum d_i^4}{\sum d_i^3} \quad (3.2)$$

$$d_n = \frac{\sum d_i}{N} \quad (3.3)$$

where d_i is the Feret's diameter of the i^{th} particle. N is the particle count.

AF can approximate the volume fraction, and normally will be less than the volume fraction. The closest IPD from border to border can be found by using dilation method. We can then deduce the distribution of IPD. The average IPD to the nearest neighbor was thus calculated.

3.2.4 Results and discussion

3.2.4.1 MQFPs

For MQFPs, since the chip is a square, to reflect the actual flow process, new grouping method is used as shown in Figure 3.8, and the figure is symmetric. Three factors to be used are distance, position, and die position. For distance, '-1' is close to the gate and for position, '-1' is on the left side. Die position includes below '-1' and

above the die '1'. Thus a 2×3×3 ANOVA test was conducted to see if there has any effect of the distances from the gate and if the results are symmetric by position.

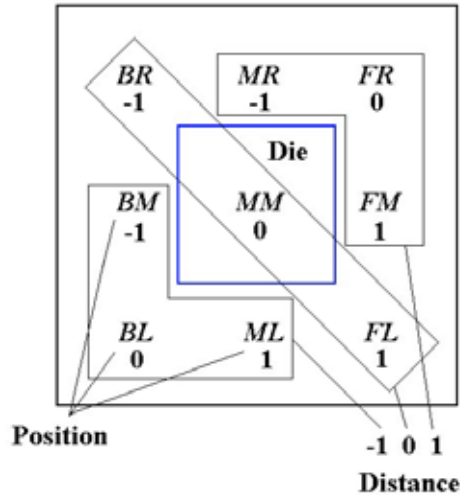


Figure 3.8 Grouping method

The image analysis results of MQFPs are shown in Table 3.1. The statistical results with 3 replicates including ANOVA, main effect plots and interaction plots are obtained by using MINITAB. The ANOVA results with all P values less than 30% are bolded and shown in Table 3.2. The results are summarized below:

Over 83% confidence that d_v varies with position;

Over 95% confidence that d_n varies with distance;

Over 97% confidence that d_b varies with distance.

All the measures show the symmetric trend by position but not distance or die position. This is clear by looking at Figure 3.9 – 3.12.

	Chip 1					Chip 2					Chip 3				
	AF	d_v	d_n	d_b	N	AF	d_v	d_n	d_b	N	AF	d_v	d_n	d_b	N
FRB	32.94	27.15	15.67	8	105	37.73	41.21	16.63	6.99	107	36.74	35.09	16.98	7.6	91
MRB	40.58	52.62	16.54	6.92	100	39.94	36.83	16.95	7.4	94	39.75	40.73	17.02	7.39	92
BRB	40.97	42.38	18.18	7.06	87	38.99	40.76	18.15	7.37	89	43.24	49.49	18.34	7.39	85
FRU	38.79	34.63	16.24	6.85	104	41.88	37.38	17.89	6.43	92	41.7	35.51	16.95	6.1	103
MRU	40.06	46.93	17.96	7.84	87	38.19	41	18.17	7.2	85	35.67	40.26	17.85	8.03	80
BRU	32.97	26.5	15.74	8.19	96	37.82	42.11	17.7	7.93	86	41.29	43.97	17.16	6.32	95
FMB	36.58	34.42	16.87	7.37	95	42.89	40.22	18.37	6.57	91	34.58	35.85	15.47	8.68	109
MMB	43.08	51.68	17.09	6.57	98	38.11	35.39	16.71	7.85	92	34.09	30.97	16.11	7.61	103
BMB	37.42	35.11	16.35	7.43	98	35.14	32.04	16.98	8.89	94	46.1	53.59	22.37	7.47	68
FMU	33.97	45.14	15.57	8.06	105	34.55	42.01	16.17	8.06	100	37.77	34.84	16.78	8.09	90
MMU	39.39	38.93	17.36	5.69	90	40.18	44.83	17.5	7.73	96	42.43	42.34	18.95	7.45	84
BMU	40.47	37.71	18.25	7.81	94	41.01	39.62	17.23	7.05	95	41.55	40.45	17.11	7.24	98
FLB	31.7	35.8	16.29	9.17	92	43.07	42.82	18.3	5.56	90	39.33	37.43	16.26	7.21	96
MLB	40.54	42.87	16.32	7.3	91	43.95	42.19	17.67	6.37	92	38.4	47.01	18.81	9.44	68
BLB	38.35	35.82	17.28	8.17	93	37.2	43.71	18.25	8.47	81	35.19	36.34	17.63	8.83	87
FLU	42.91	35.81	18.58	5.67	86	46.37	43.11	18.45	5.91	87	45.79	44.9	20.48	7.19	72
MLU	35.86	35.53	16.2	8.72	103	46.78	47.8	20.33	7.1	71	36.71	39.02	20.34	9.25	69
BLU	39.28	37.65	18.53	7.64	90	32.9	31.67	17.44	9.15	92	38.85	36.44	17.19	6.92	98

Table 3.1 Results from image analysis of 3 MQFPs

ANOVA: Area Fraction, d_v , d_n , d_b versus Distance, Position, DiePosition					
Factor	Type	Levels	Values		
Distance	fixed	3	-1	0	1
Position	fixed	3	-1	0	1
DiePosition	fixed	2	-1	1	
Analysis of Variance for AF					
Source	DF	SS	MS	F	P
Distance	2	39.16	19.58	1.46	0.244
Position*DiePos	2	35.18	17.59	1.31	0.281
Analysis of Variance for d_v					
Source	DF	SS	MS	F	P
Position	2	129.81	64.91	1.86	0.169
Analysis of Variance for d_n					
Source	DF	SS	MS	F	P
Distance	2	11.707	5.853	3.42	0.043
DiePos	1	2.053	2.053	1.2	0.28
Position*DiePos	2	4.568	2.284	1.33	0.275
Analysis of Variance for d_b					
Source	DF	SS	MS	F	P
Distance	2	6.7159	3.3579	4.13	0.023

Table 3.2 ANOVA test results of MQFPs with 3 replicates

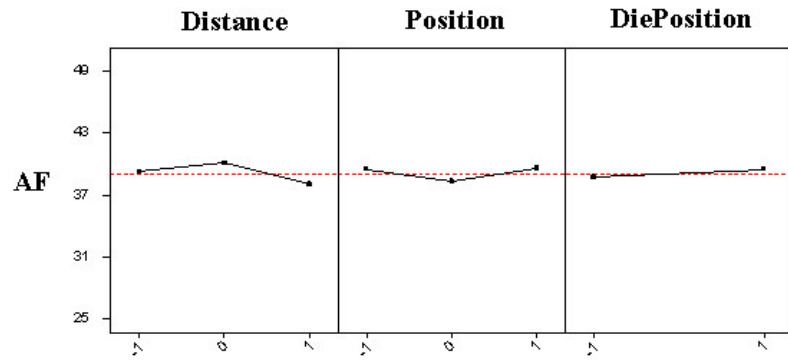


Figure 3.9 Main effects plot – data means for AF

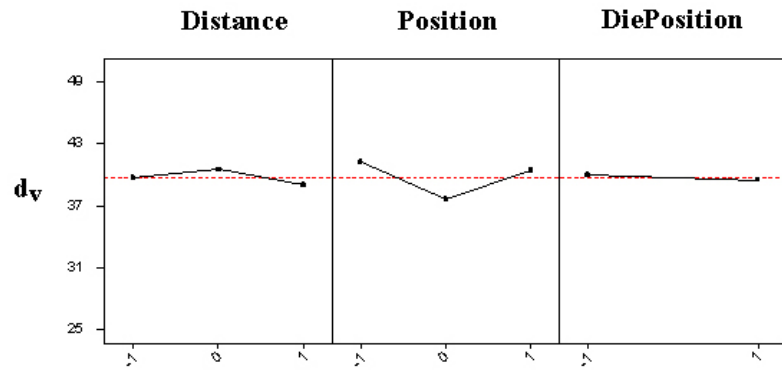


Figure 3.10 Main effects plot – data means for d_v

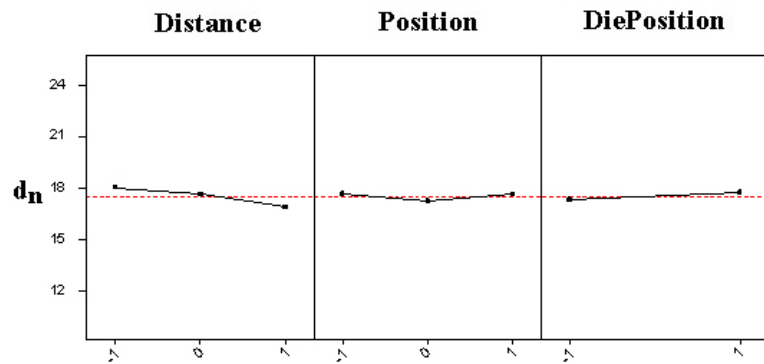


Figure 3.11 Main effects plot – data means for d_n

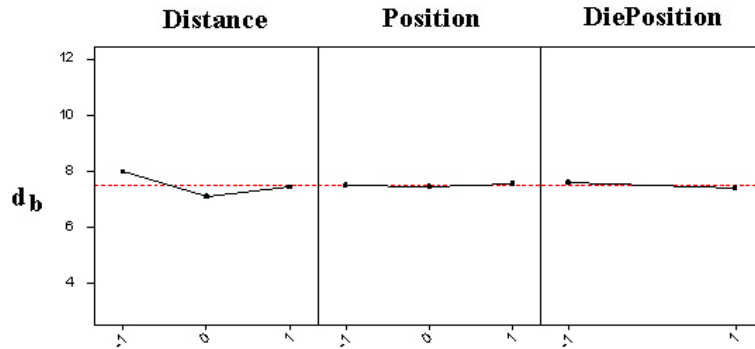


Figure 3.12. Main effects plot – data means for d_b

AF values can be used to predict the local CTE difference by using Equation (3.1). The minimum AF is 31.7% and the maximum AF is 43.1% for chip 1. If $\alpha_F = 0.6$ ppm/ $^{\circ}$ C, $\alpha_M = 68$ ppm/ $^{\circ}$ C, then $\Delta\alpha_C = 5.3$ ppm/ $^{\circ}$ C. Since AF is not equal to actual volume fraction due to that only the large particles are considered, the volume fraction, which is 72%, of the molding compound is used as the mid point to get the minimum and maximum volume fraction, then $\Delta\alpha_C$ is calculated. So the difference of CTE can be as big as 5.3 ppm/ $^{\circ}$ C at different locations within one chip. This value is about 44% of the effective CTE, which is about 12 ppm/ $^{\circ}$ C. This value cannot be neglected when we study the reliability of the PEM. The prediction provided here could be useful for the future work of experimental verification.

3.2.4.2 PQFP

The results of image analysis are shown in Table 3.3. Since the PQFP is rectangular other than square, three factors have been used are the plane, position and die position, as shown in Figure 3.6. By using MINITAB's ANOVA, the statistical differences between different planes, positions or above and below the die can be found. It will be shown that

the different measures each have a statistical variation in some direction in the part. What is interesting, and worth interpretation, is that the variations are in different directions for different measures. Table 3.4 shows the ANOVA results of AF, d_v , d_n , and d_b vs. die position, plane, and position and their two-factor interactions.

	AF	d_v	d_n	d_b	N
BLB	0.3235	31.561	16.085	7.98	97
MLB	0.3608	30.49	16.462	6.96	112
FLB	0.3068	30.181	16.765	9.27	88
BLU	0.3218	36.925	17.661	8.55	94
MLU	0.3496	32.014	16.161	6.35	110
FLU	0.3672	33.189	16.951	6.37	98
BMB	0.324	28.386	15.857	6.58	107
MMB	0.3503	29.887	16.509	6.61	109
FMB	0.2858	26.677	16.338	7.76	101
BMU	0.3536	30.164	16.336	6.07	122
MMU	0.3182	26.958	16.468	7.23	107
FMU	0.3072	22.951	15.667	6.67	108
BRB	0.2909	22.735	14.432	7.79	113
MRB	0.3217	33.213	15.602	8.77	101
FRB	0.3111	23.665	15.314	8.14	118
BRU	0.3325	26.802	16.018	6.49	118
MRU	0.3838	28.249	17.078	6.07	107
FRU	0.2945	26.52	15.846	8.14	116

Table 3.3 Image analysis results of Visteon chip

1. AF:

- No significant effect of any of the three factors or their two-factor interactions

2. d_v :

- Over 99% confidence that d_v varies with position
- Over 90% confidence that d_v varies with plane

- Over 90% confidence that d_v varies with interaction of die position and plane, plane and position

The response curves are shown in Figure 3.13. It shows that d_v decreases with plane and position away from the feeding gate. This could be caused by the less flowability of the large particles.

ANOVA: Area Fraction, d_v , d_n , d_b vs. Die Position, Plane, Position					
Factor			Levels	Values	
DiePos			2	1-Jan	
Plane			3	0	1 -1
Position			3	0	1 -1
Analysis of Variance for AF					
Source	DF	SS	MS	F	P
Plane	2	0.003853	0.001927	1.91	0.262
Analysis of Variance for d_v					
Source	DF	SS	MS	F	P
Plane	2	28.222	14.111	5.19	0.077
DiePos*Plane	2	25.758	12.879	4.74	0.088
Position	2	109.78	54.89	20.2	0.008
DiePos*Position	2	18.221	9.11	3.35	0.14
Plane*Position	4	49.628	12.407	4.57	0.085
Analysis of Variance for d_n					
Source	DF	SS	MS	F	P
DiePos	1	1.2918	1.2918	10.68	0.031
DiePos*Plane	2	1.1324	0.5662	4.68	0.09
Position	2	2.7985	1.3993	11.57	0.022
DiePos*Position	2	1.2258	0.6129	5.07	0.08
Plane*Position	4	1.6523	0.4131	3.42	0.131
Analysis of Variance for d_b					
Source	DF	SS	MS	F	P
DiePos	1	3.485	3.485	2.75	0.172

Table 3.4. Results of ANOVA analysis

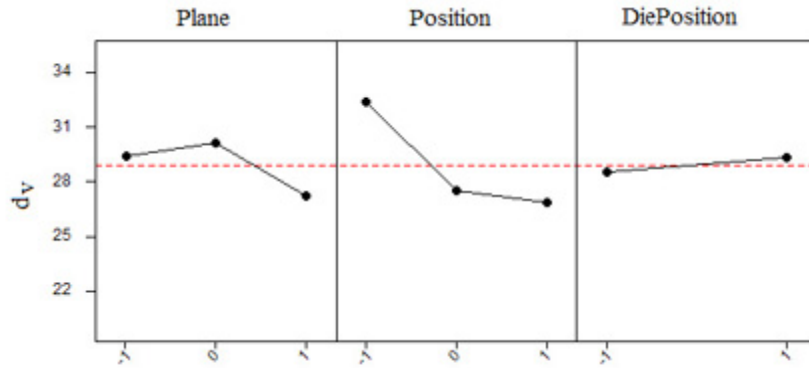


Figure 3.13 Main effects plot – data means for d_v

3. d_n :

- Over 95% confidence that d_n varies with die position and position
- Over 90% confidence that d_n varies with interaction of die position and plane, die position and position

The response curves are shown in Figure 3.14 with d_n vs. position has the same trend as d_v .

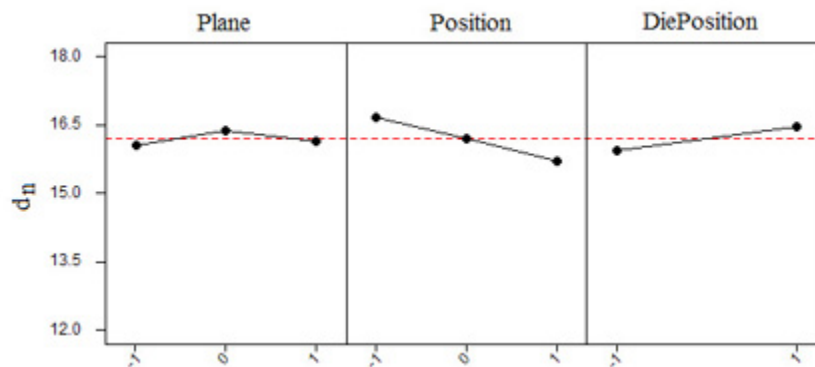


Figure 3.14 Main effects plot – data means for d_n

4. d_b :

- Over 80% confidence that d_b varies with die position.
- No significant effect of other two factors or any of the two-factor interactions.

The response curves are shown in Figure 3.15. The d_b will be smaller below the die.

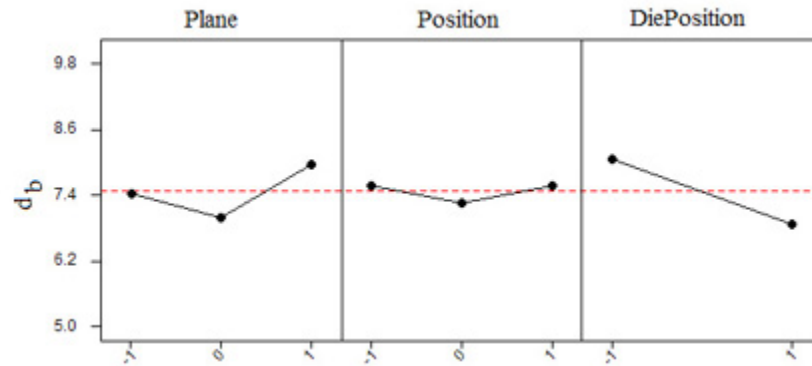


Figure 3.15 Main effects plot – data means for d_b

The above results clearly indicate that the different places within the chip will greatly affect the distribution of filler particles by its size. This could also be related to the flow conditions and package geometry, and more study is needed to understand its effect. We know that the particle size can affect CTE and thermal conductivity of the molding compounds, so the non-uniform particle size distribution is undesirable because it will cause different properties within the molding compounds. By implementing our new feed protocol we would expect this variance be minimized.

By using Equation (3.1), we can estimate the CTE difference. The minimum AF is 28.6% and the maximum AF is 38.4%. Using the similar method for MQFPs, for $\alpha_F = 0.6 \text{ ppm}/^\circ\text{C}$, $\alpha_M = 58 \text{ ppm}/^\circ\text{C}$, we have $\Delta\alpha_C = 5.5 \text{ ppm}/^\circ\text{C}$. This value is about 27% of

the effective CTE, which is about 17 ppm/°C.

3.2.5 Conclusions

Two kinds packages with different geometry are studied, one is square, and the other is rectangular. Images obtained from cross sections at various places are analyzed for the particle distribution. A set of measures include d_v , d_n , AF and d_b have been created to assess the particle distribution. These measures are supposed to tie to different properties, and more general work need to be done to determine which measures are the key factors for which property.

The statistical results show that the filler particles are not uniformly distributed within the package. It can be found that different measures vary in different directions. For MQFPs, over 83% confidence that d_v varies with position, over 95% confidence that d_n varies with distance, and over 97% confidence that IPD varies with distance. For Visteon chip, d_v is affected by plane, position and interactions of die position and plane, plane and position; d_n affected by die position, position and interactions of die position and plane, die position and position.

The uneven distribution has a big influence on local CTE property, and could affect the reliability. In this study the CTE is tied to AF. The maximum AF variation is found about 10% and makes a local CTE difference more than 5 ppm/°C. This value is about 44% of the effective CTE for MQFPs and 27% of the effective CTE for PQFPs. These differences could be harmful to the reliability of the packages.

3.3 Experimental work on distribution of a minor solid constituent in a

transfer molded e – pad leadframe package

This study investigates the spatial distribution of a minor particulate constituent in a transfer molded exposed die paddle (e-pad) leadframe microcircuit package. Packages were polished at three depths parallel to its top surface. Levels 1 and 2 are above the die and leadframe while level 3 is just below the top surface of the die and leadframe. The distribution of area fraction and size of the particulate was analyzed for each level and with respect to the distance from the gate using micro-photographic image analysis. A non-uniform distribution of the particulate material for both particle size and location is evident, and its relations with gate, die and leadframe are interpreted. ANOVA tests were conducted to assess the statistical significance of the variations.

3.3.1 Introduction

Encapsulation using a transfer molding process is the most common packaging method for integrated circuits. There may be eight or more major constituent in a molding compound used for encapsulation and the physical and chemical compositions may vary with purpose of use and by manufacturer. Table 3.5 summarizes some of the typical constituents and their concentration in mold compound formulations. The molding compound constituents are mixed and formed into a pellet. In the transfer molding process, the pellet is heated and forced by pressure, usually at a temperature around 175°C, into a mold to encapsulate microcircuits. Generally, the molding process takes a few minutes and the encapsulant is sufficiently cured for the part to be removed from the mold. Then the encapsulated parts are further cured, usually for approximately 2 to 6 hours [Tummala, 88, Wright 92, Manzione 90].

Constituent	Concentration (wt. %)
Inert fillers	75 – 90 %
Epoxy resin	8 – 20 %
Curing agents (Hardeners)	3 – 10 %
Stress-relief additives	1 – 5 %
Flame retardants	0.3 – 5 %
Mold-release agents	0.1 – 1.0 %
Coloring agents	0.2 – 0.4 %
Accelerators	0.2 – 0.3 %

Table 3.5 Major constituents in typical molding compound formulations

In our study we selected devices, which use a red phosphorous flame retardant material added to the molding compound as a minor solid constituent. Because this material is red, it offers a unique opportunity to optically study distribution characteristics. The particulate material has only a small volume percentage, which is approximately up to 0.64 vol%, and thus the spatial distribution of the particles can provide information on the area fraction and size of the particles, and their relation with the gate, die and lead frame.

There is much literature on the particle size distribution in mold compounds [Nguyen 93, Baikerikar 00, Iwasaki 97, Garrett 98], but negligible studies have been conducted on the particle spatial distribution, or the spatial particle size distribution. Experiments have previously been performed on plastic packages to investigate the silica filler distribution by studying the cross sections of the packages [Huang 03]. The disadvantage of studying the filler is that its volume fraction is too high to assess flow characteristics. In this study, a minor constituent is investigated and assessed in terms of the particle distribution

along the filling direction at different planar levels.

3.3.2 Description of the packages and experimental technique

The e-pad package (shown in Figure. 3.16) has an exposed die paddle and thus the flow of mold compound can be uniquely assessed. Two Philips 80-lead transfer molded e-pad leadframe microcircuit package, with dimensions of 14mm × 14mm and thickness of 0.9mm, were studied. One package contained the mold compound Sumitomo EME-7351UT and the other Sumitomo EME-7351UL. Both contained the same resin, spherical silica filler, and particulated red phosphorous flame retardant.

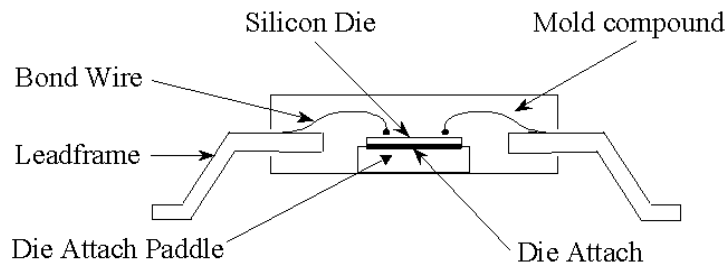
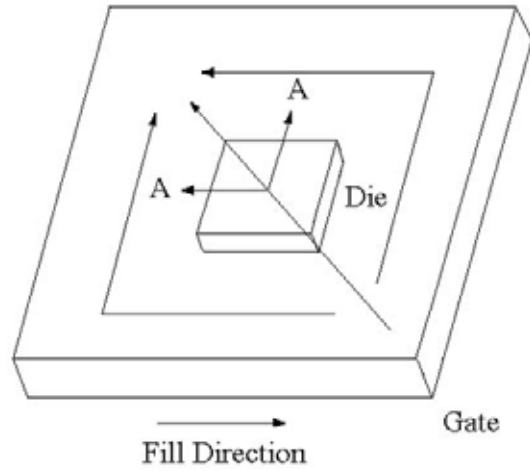


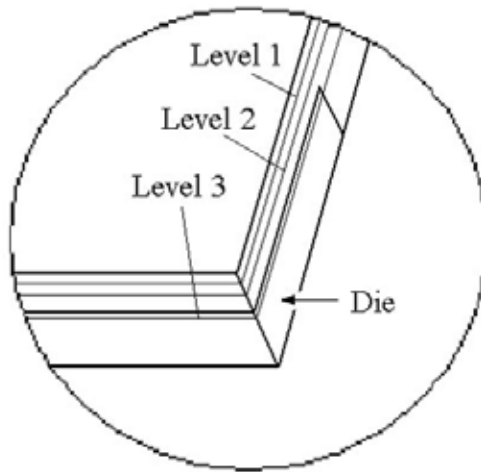
Figure 3.16 Schematic diagram of the e-pad package

The packages were polished using 3 grades of polishing papers, i.e. from 600, 800, to 1200. The packages were polished to three levels: 0.1 mm, 0.2 mm and 0.4 mm below the top surface; defined as level 1, level 2, and level 3 respectively. The fill direction and locations of levels 1, 2, 3 are shown in Figures 3.17 (a) and (b). A 26 × 21 grid was then formed over the surface and images of the cells were obtained. Each cell in the grid was 658 μ m × 517 μ m, and the scan resolution per cell was 1315 pixels × 1033 pixels, or 0.5 μ m per pixel length. In total, 273 alternating cells were studied per layer for layers 1

and 2. A schematic of the surface is shown in Figure 3.18.



(a)



(b)

Figure 3.17 (a) Schematically show the fill direction; (b) A-A view shows the locations of levels 1, 2, 3

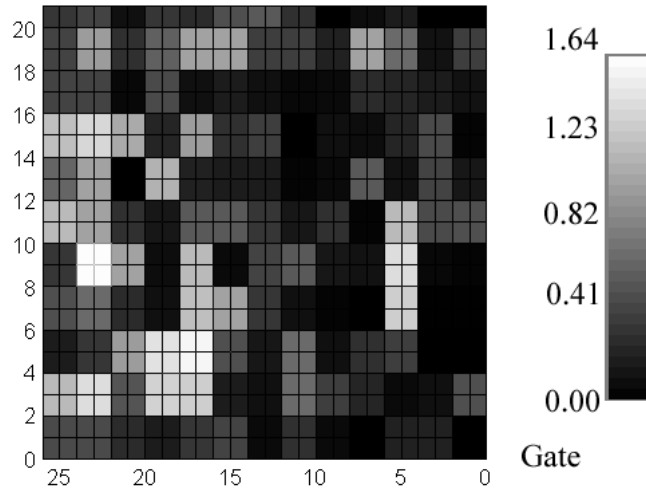


Figure 3.18 Surface plot of area fraction of level 1, the gray scale shows the percentage of the red particulate

Figure 3.19 shows one of the images obtained from level 1 for the 7351UL package. It represents the size and shape of a single cell. The white areas in this grayscale photograph are the red particulate. The other regions include the silica filler resin and other constituents. There were no visibly significant differences in the two mold compound types.

A different method was used for level 3 since it contains the leadframe and die. In this case, the regions between the lead frames and the die were analyzed first. Figure 3.20 shows the polished surface of level 3. At this level, selected positions between the leads were analyzed with a smaller cell size, which is $300\mu\text{m} \times 200\mu\text{m}$.

3.3.3 Results and discussion

Each image of the cell in the grid was analyzed using ‘Image Pro-plus[®]’ to assess constituent area fractions. The agglomerates were treated as single particles. Particles

intersecting the cell boundaries were ignored. Figures 3.18 and 3.21 – 3.23 show 2-D and 3-D plots of the area fraction for levels 1 and 2 for the 7351UT mold compound. These figures show distributions from a single replicate.

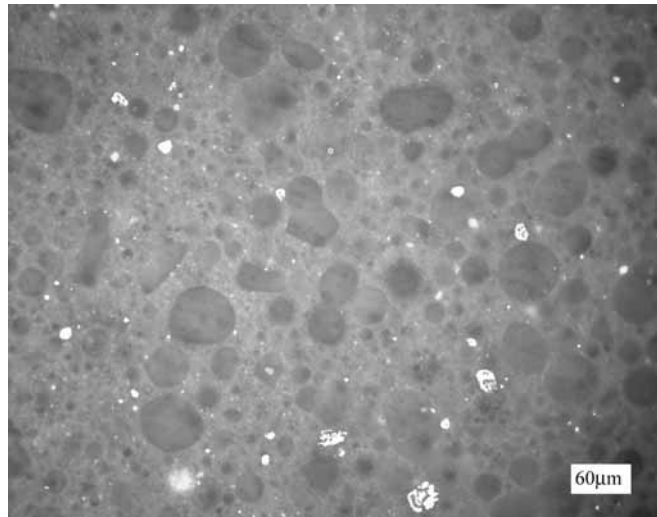


Figure 3.19 A sample image obtained from level 1

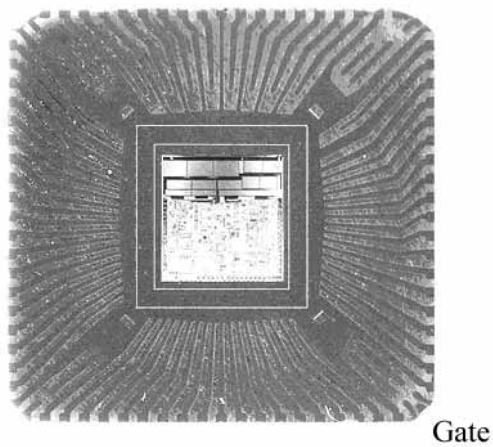


Figure 3.20 Image of level 3 showing the die and leadframe

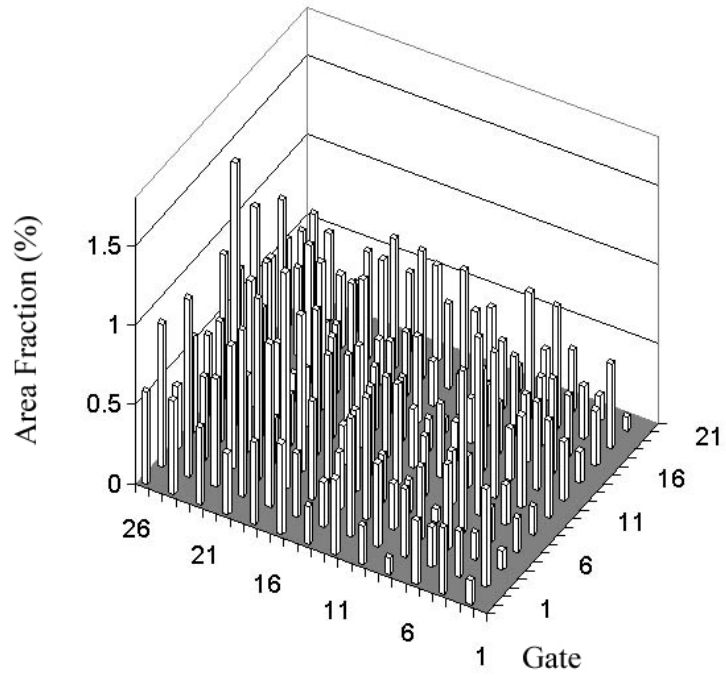


Figure 3.21 3-D plot of area fraction of level 1

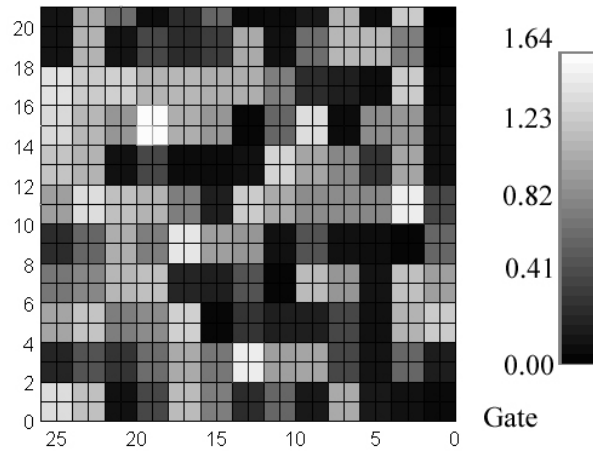


Figure 3.22 Surface plot of area fraction (%) of level 2

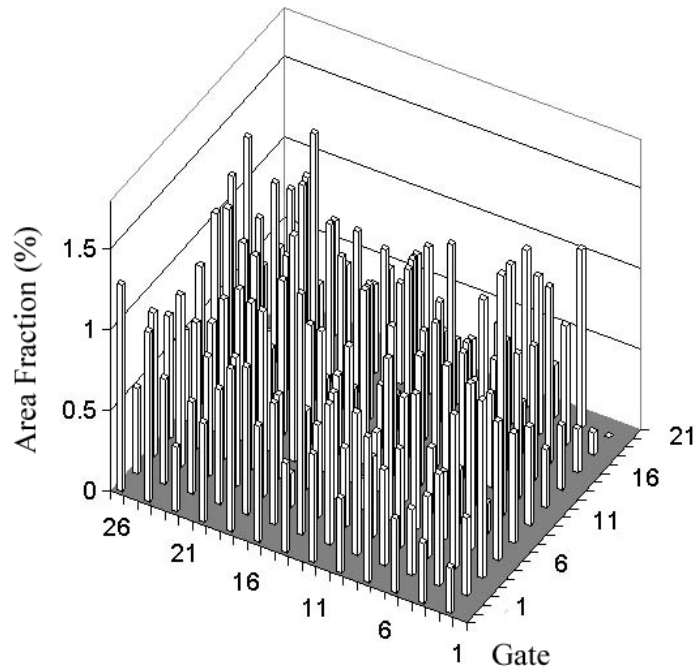


Figure 3.23 3-D plot of area fraction of level 2

Statistical analysis, using Minitab[®], was performed to assess two factors which could affect the particle distribution: one is the distance from the gate, and the other is the level. The distance factor is sketched in Figure 3.24 with -1 , 0 and 1 indicating near to gate, center and far from gate respectively. Also 1 is assigned to level 1 and -1 is assigned to level 2. Level 3 is not compatible with levels 1 and 2, because of the existence of the die and leadframe. As a result level 3 could not be included in the ANOVA. Then a 2×3 ANOVA test was performed. A total of 6 replicates have been used for each factor in the study. All other cells outside the selected locations were not analyzed. Another possible factor, e.g., left, middle and right of the gate location was not significant and is not included.

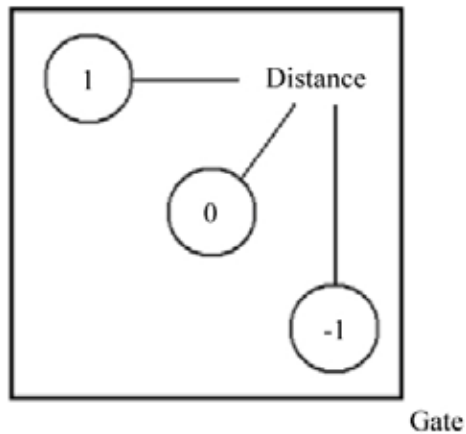


Figure 3.24 Distance factor

Before performing the actual ANOVA test, a convergence study was conducted. A series of replicates from 2 to 7, which were chosen from the same location of the package, have been analyzed for area fraction with distance and level factors. Figure 3.25 shows that the P-value converges as the number of replicates increases, where the P-value is the probability that the variation between factors may not have occurred by chance [Ostle, 96]. The conclusion is that sufficient accuracy can be obtained if the number of replicates is greater than 5. Therefore, for this study 6 replicates were analyzed for each factor for each of the three levels.

3.3.3.1 Area fraction and size distribution results for the package with 7351UT

Table 3.6 and 3.7 show area fraction data for each factor from each level. The ANOVA test results in Table 3.8, show that the effects of distance and level are significant, and the interaction between distance and level is also significant. There is over 95% confidence that area fraction increases with distance from the gate. The reason

may be related to flow properties and particle properties. The higher density particles tend to move further in the cavity after it is filled. There is over 99% confidence that area fraction varies with level. This could arise due to particle settling and particle migration [Huang 04]. Particle settling is described as filler particles “sinking” under their own weight. Particle migration is a phenomenon in which particles gradually migrate from regions of higher shear rate towards those with lower shear rate until they reach a steady configuration due to interparticle interactions, such as hydrodynamic, electrostatic, and surface interactions. Particle migration is likely to be seen in high aspect ratio channels. Both mechanisms will result in more particles at the lower level. The thinner the package, the greater the occurrence of the two mechanisms.

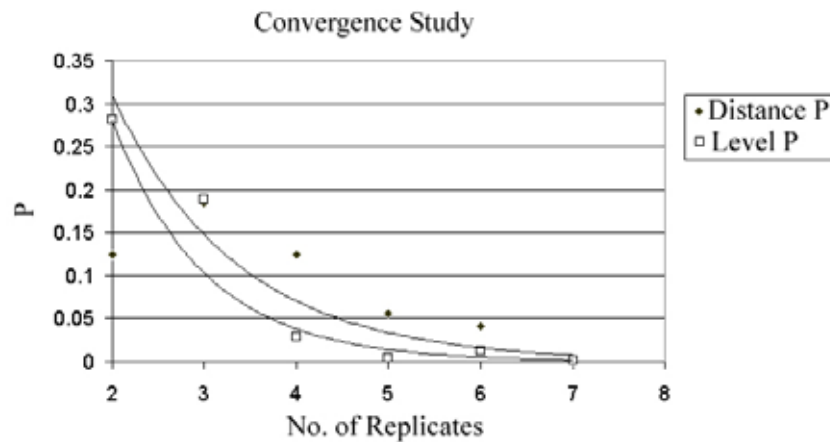


Figure 3.25 Convergence study for area fraction

	Area Fraction of 6 × 6 samples – Levels 1 & 2						Average Area Fraction
L1 (-1)	0.541	0.327	0.529	0.159	0.544	0.615	
L2 (-1)	0.493	0.516	0.818	0.358	0.405	0.534	
L1 (0)	0.404	0.465	0.487	0.276	0.834	0.184	L2
L2 (0)	0.378	0.711	0.924	0.544	1.079	0.444	
L1 (1)	0.866	0.121	0.282	0.275	1.097	0.362	L2
L2 (1)	1.655	1.146	0.971	0.581	1.068	0.88	

Table 3.6 Area fraction (%) results with 6 replicates, L1 & L2 indicate level

	Area Fraction of 6 × 3 samples – Level 3						Average Area Fraction
L3 (-1)	0.214	0.175	0.327	0.683	0.379	0.284	
L3 (0)	0.403	1.138	0.412	1.183	0.898	0.46	
L3 (1)	0.42	0.639	0.926	0.731	0.773	0.647	

Table 3.7 Area fraction (%) results with 6 replicates, L3 indicates level

ANOVA: Area Fraction, versus Distance, Level			
Factor	Type	Levels of a factor	Values
Distance	fixed	3	-1 0 1
Level	fixed	2	-1 1
Analysis of Variance for Area Fraction			
Source	Degree of freedom	F	P
Distance	2	3.56	0.041
Level	1	9.78	0.004
Distance*Level	2	2.32	0.116

Table 3.8 ANOVA test results

The particle size distribution results are shown in Tables 3.9 – 3.11. The mean diameter measurement is defined as the average length of diameters measured at two degree intervals and passing through the object’s centroid. Thus the various shapes of the particles can be compared using mean diameter. The average observable diameter $d_n = \sum d_i / N$ and the volume average diameter $d_v = \sum d_i^4 / d_i^3$, where i indicates each particle, are

defined the same as in [Huang 03]. However, the image obtained for a particle will most often not coincide with the maximum diameter. Corrections can be made to estimate diameters from cross-sections, and it will have the similar size distribution as the measured mean diameters.

	Level & Factor			
	L1 (-1) by the gate	L1 (0)	L1 (1)	Average
No. of Particles	122	172	182	159
d_n (μm)	7.95	6.97	7.28	7.4
d_v (μm)	26.28	19.87	24.91	23.69

Table 3.9 Results of particle number and size for six cells of level 1

	Level & Factor			
	L2 (-1) by the gate	L2 (0)	L2 (1)	Average
No. of Particles	226	251	281	253
d_n (μm)	6.91	7.32	8.14	7.46
d_v (μm)	13.22	19.06	30.74	21.01

Table 3.10 Results of particle number and size for six cells of level 2

	Level & Factor			
	L3 (-1) by the gate	L3 (0)	L3 (1)	Average
No. of Particles	175	250	311	245
d_n (μm)	6.54	7.39	6.63	6.85
d_v (μm)	14.26	31.01	18.44	21.24

Table 3.11 Results of particle number and size for six cells of level 3

Based on measurements or measured (or observable) particle diameter at level 2, d_v is increasing with the distance from the gate. One explanation is that the larger particles have more time to settle down as they are flowing away from the gate. This also affects the size distribution with respect to distance from the gate.

The average number of particles in level 3, d_n and d_v are similar to level 2. Both have more particles than level 1. Table 3.7 shows that the area fraction of level 3 is larger than level 1, however it is not larger than level 2, possibly because the leads and die can influence the particle distribution. However, the results indicate that particle settling and particle migration occur.

The particle distribution between the leads was studied in more depth. Since the space between the leads is small, a much smaller frame (cell) is used for the analysis. The size of the frame is $300\mu\text{m} \times 200\mu\text{m}$. The average observable particle sizes are: $d_n = 5.55 \mu\text{m}$ and $d_v = 19.82 \mu\text{m}$. These are the smallest among all the levels. On the other hand, the average area fraction is 0.75%, which is the same as that of level 2, and larger than level 1. If the numbers of particles are compared, the average number density is $58/\text{mm}^2$ for the images between the leads, and the number density for levels 1 to 3 are $19.5/\text{mm}^2$, $31/\text{mm}^2$, and $30.2/\text{mm}^2$ respectively. Thus, although particles appear to be smaller between leads, the number density is the largest, which is why it has the largest area fraction.

3.3.3.2 Area fraction and size distribution results for the package with 7351UL

In the assessment of the part using Sumitomo 7351UL, Table 3.12 and 3.13 show the selected area fraction data for each factor from each level. The ANOVA test results in Table 3.14 show that the effects of distance and level are significant. There is over 75% confidence that area fraction varies with distance and over 97% confidence that area fraction varies with level.

The data mean plot for area fraction is shown in Figure 3.26. It shows that the area

fraction increases as the distance from the gate increases. The reason may be related to flow properties and particle properties. Level 2 has a larger area fraction than level 1. This could arise from particle settling and particle migration [Huang 04]. Both mechanisms will result in more particles at the lower level. A larger area fraction means either more or larger particles.

	Area Fraction of 6× 9 samples – Levels 1 & 2						Average Area Fraction
L1 (-1)	0.4302	0.4117	0.2858	0.7033	0.5734	0.6539	L1
L2 (-1)	0.7256	0.5771	0.6318	0.6849	0.9651	0.8487	
L1 (0)	0.5686	0.4526	0.7481	0.6054	0.6333	0.7117	0.596
L2 (0)	0.5702	0.5216	0.4806	1.019	0.9947	0.6644	
L1 (1)	0.506	0.5508	0.634	0.8449	0.7422	0.6722	L2
L2 (1)	0.9691	0.6835	0.8467	0.7512	0.9382	0.7248	0.755

Table 3.12 Area fraction (%) results with 6 replicates, L1 & L2 indicate level

	Area Fraction of 6× 9 samples – Level 3						Average Area Fraction
L3 (-1)	0.4665	0.4839	0.4518	0.4578	0.9527	0.3318	0.581
L3 (0)	0.7092	0.3258	1.0915	0.3741	0.6699	0.4231	
L3 (1)	0.5903	0.4181	0.8646	0.6277	0.7852	0.4363	

Table 3.13 Area fraction (%) results with 6 replicates, L3 indicates level

ANOVA: Area Fraction, versus Distance, Level			
Factor	Type	Levels of a factor	Values
Distance	fixed	3	-1 0 1
Level	fixed	2	-1 1
Analysis of Variance for AF			
Source	Degree of freedom	F	P
Distance	2	1.486	0.242
Level	1	5.209	0.03
Distance*Level	2	0.989	0.384

Table 3.14 ANOVA test results

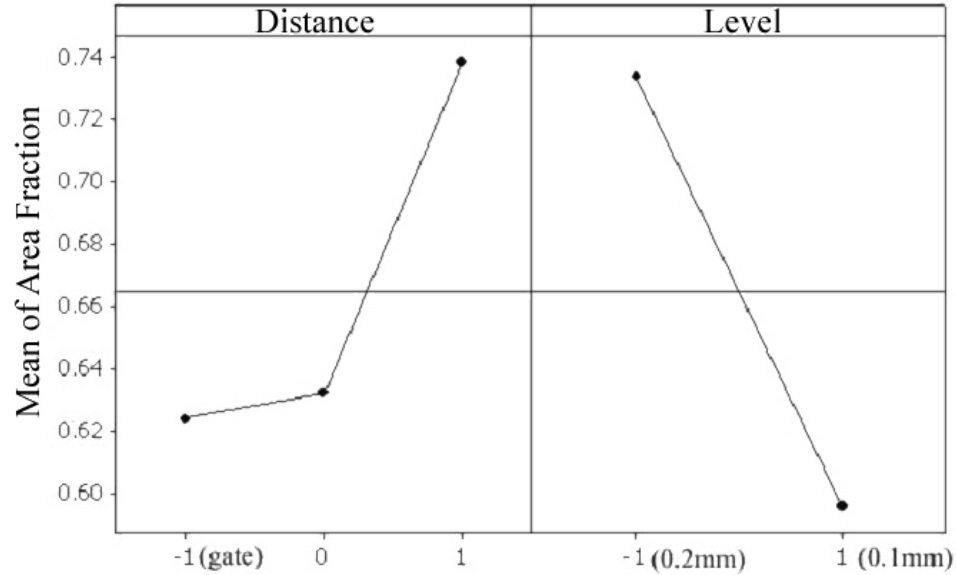


Figure 3.26 Plot of mean area fraction as a function of distance from the gate and level

The particle size distribution results are shown in Tables 3.15 – 3.17. For all levels there is only a slight difference in d_n , but the number of particles increases significantly with distance factor away from the gate. The smallest d_v is located far from the gate. Levels 2 and 3 have a larger d_v . These results only slightly different from the package with 7351UT. It appears that area fraction differences result from the difference of the number of particles. For d_{vmax} (= the largest value of d_v for a level), level 3 > level 2 > level 1 for both compounds, so the largest particles seem to settle to somewhere along the leadframe.

The particle distribution between the leads was studied and the observable average particle sizes are: $d_n = 4.88 \mu\text{m}$ and $d_v = 11.76 \mu\text{m}$. All other trends are similar to the case with the 7351UT mold compound.

	Level & Factor			
	L1 (-1) by the gate	L1 (0)	L1 (1)	Average
No. of Particles	376	351	546	424
d_n (μm)	5.35	5.93	5.25	5.51
d_v (μm)	16.79	18.55	14.46	16.6

Table 3.15 Results of particle number and size for six cells of level 1

	Level & Factor			
	L2 (-1) by the gate	L2 (0)	L2 (1)	Average
No. of Particles	436	444	510	463
d_n (μm)	6.53	5.61	4.9	5.68
d_v (μm)	22.07	18.4	18.73	19.73

Table 3.16 Results of particle number and size for six cells of level 2

	Level & Factor			
	L3 (-1) by the gate	L3 (0)	L3 (1)	Average
No. of Particles	372	452	517	447
d_n (μm)	5.4	5.2	5.15	5.25
d_v (μm)	20.37	28.74	12.98	20.7

Table 3.17 Results of particle number and size for six cells of level 3

3.3.4 Conclusions

The distance from the gate and the depth (level) within the package are factors that will affect the distribution of a minor constituent in a molded microcircuit package. In fact, there is significant confidence that area fraction varies with distance from the gate and that area fraction varies with level. In addition, the number of particles increases as the distance from the gate increases. This trend is the same for the area fraction indicating that the area fraction trends result from the difference of the number of

particles. Particle migration and particle settling can explain these results.

The average area fraction found between the leads is the same as that of level 2, and is bigger than level 1. Also the number of particles is the largest between the leads, even though the average particle size found between the leads is the smallest among all 3 levels.

Chapter 4: Modeling and Numerical Simulation

This study will be the first time of a simulation demonstrating the effect of chaotic advection during the filling of an empty cavity and the combining of the molding and mixing processes. To demonstrate the mixing efficiency of the novel feed protocol, we chose to apply it to a square rectangular cavity. A common molding process fills into a given volume. The ability to repeat the process for the number of cycles, which make demonstration of the chaos, is not easy to do. The numerical simulation of mixing for fully filled cavity flow that have been reported in the literature have multiple, non-constant, time-varying boundaries. There is no report found that has studied the mixing during a cavity filling process due to its difficulty, which lies in the much less time for mixing.

Several software have been developed to simulate the flow of the molding process using various molding machines, such as injection molding, extrusion, and transfer molding, etc. They are focusing on the gate location, cured properties, etc; the mixing within the flow has never been touched. One contribution of this study is the development of the numerical method to simulate the mixing of solid particles for a molding process. The program developed in this study to quantify the mixing could be incorporated in the commercial molding software, thus expanding the functions of these software to a brand new level.

This chapter will first present the governing equations for creeping flow. Then the procedure of the cavity modeling and the flow and mixing simulation process is

described. Also the development of the numerical method and the design of experiment for the numerical simulation are discussed.

4.1 Governing Equations

4.1.1 Equations of motion

The equations governing the theoretical flow are the mass and momentum balances which in dimensionless form for incompressible and isothermal fluids are:

$$\text{Mass: } \nabla \cdot \mathbf{v} = 0 \quad (4.1)$$

$$\text{Momentum: } \frac{\partial \mathbf{v}}{\partial t} + \mathbf{v} \cdot \nabla \mathbf{v} = -\nabla p + \left(\frac{1}{\text{Re}}\right) \nabla^2 \mathbf{v} = 0 \quad (4.2)$$

where v , p and t are dimensionless velocity, pressure and time respectively. $Re = \rho UL/\eta$ is the *Reynolds* number, ρ is the density of the fluid, and U is the mean flow velocity. Since the *Reynolds* number is very small (i.e. $Re \ll 1$), the flow is a creeping flow.

The periodic or aperiodic flows studied here will have alternating flows inside the cavity. The alternate feeding will be transmitted throughout the flow nearly instantaneously. Therefore the velocity field throughout the cavity domain can be assumed to switch instantaneously from the steady flow produced by one feed gate to the steady flow produced by another one. This assumption is supported by Leong's experimental work [Leong 90], which showed that the slow unsteady flow was reversible.

So once the steady flow field is obtained, we can simulate the periodic or aperiodic flow by switching on and off two steady cavity flows according to the sequence rule, and particle trajectories can be integrated.

The definition of T , the nondimensional period of the flow, is different from the cavity flow with moving walls. Here we define the period T as the ratio of combined fluid volume coming through the gates during one period to the total volume of the cavity. Thus for periodic flow the fluid will be pushed through each gate for a time $T/2$. $T/2$ will also be the motions a and b for aperiodic flow.

4.1.2 Boundary and initial conditions

The initial conditions imposed by this study are the particles that will be placed at certain positions in the cavity or within the gates. The fluid will be pushed through the gates with constant velocity V_g for a half period, so the volume of fluid pushed into the cavity will be proportional to $h \cos \theta \times V_g \times T/2$. And the pressure in the cavity before filling will be atmospheric pressure. The cavity boundary will also supply the fluid boundary conditions; the flow will have zero velocity at the cavity walls.

The velocity field of the flow at the gates will be assumed to be like an ideal step response, which means there is no transient before the flow reaching the desired velocity profile. This assumption is validated when considering Stokes first problem of an instantaneously moving plate and seeing that the polymer viscosity is so that the characteristic time to steady state is much smaller than the step time. The resulting position of the fluid from the previous step will serve as the initial conditions of the following step.

4.1.3 Integration of the dynamical system

Since we can compute the steady-state velocity fields, the particle position x can be determined by the integration of the equation:

$$dx/dt = v(x, t); \quad x_{t=0} = X_0 \quad (4.3)$$

where X_0 is the initial position of the particle.

4.2 Modeling procedure

This section will detail a procedure to model the flow system. One of the goals of this study has been to develop a model for the highly filled flow system using a novel feed protocol. Such a model should be able to provide us information on flow front, streamlines, mixing efficiency, and how to optimize the dimensions of the part and gates.

In order to achieve chaos for creeping flow we need periodic or aperiodic flow with cross streamlines. Since we are unable to move any part of the mold in the transfer molding process, it is necessary to design a new feed protocol so that we can realize cross streamlines by using periodic or aperiodic flow. The idea of this novel feed protocol is to introduce two or more gates. Through control of the transfer process, the molding compound will be pushed through each of the gates using predefined periodic or aperiodic flow patterns.

The flow geometry's dimensions, gates locations and numbers, the pressure of the press, and the material properties are important parameters in determining the flow and

mixing efficiency. To simplify the problem, the processing parameters will be fixed; only the gate location and bump patterns will be changed.

4.2.1 Flow geometry

The flow geometry is chosen to be a square cavity so as to reflect the real electronic packages. A mid-plane cavity flow is captured. Though we only analyze the flow and particle distribution in this plane, it is come from 2.5-D flow simulation results. Since this 2-D model is adequate to provide information of the flow and mixing, we will leave the 3-D model as a future topic and it will not used in this study.

The flow geometry is shown in Figure 4.1. It depicts a two gates square rectangular cavity. The distance between the gates and the left upper vertices are d_1 and d_2 , and the cavity length is L . Other parameters are also important and need to be optimized to achieve maximum mixing efficiency.

4.2.2 MoldFlow®

MoldFlow® is one of the most popular software package used in molding industry. This program includes pre-processor and post processor and was developed by MoldFlow Corporation. It can perform the simulation of injection molding, extrusion and resin transfer molding, etc. The finite element method is used to calculate the values of interest, such as velocity, fill time, etc., at the centroid of the triangular elements. MoldFlow® itself is a 2.5D simulation software, to demonstrate our idea, a 2D simulation is chosen. The main reason is that first, there is no big difference in terms of the trend of particle distribution between different layers in a thin package; second, we only want to show our point, which is the novel feed protocol can improve mixing, it

doesn't matter we do a 3D or 2D simulation. Also it is more consistent with the way of our experiments which analyze the particle distribution in a plane.

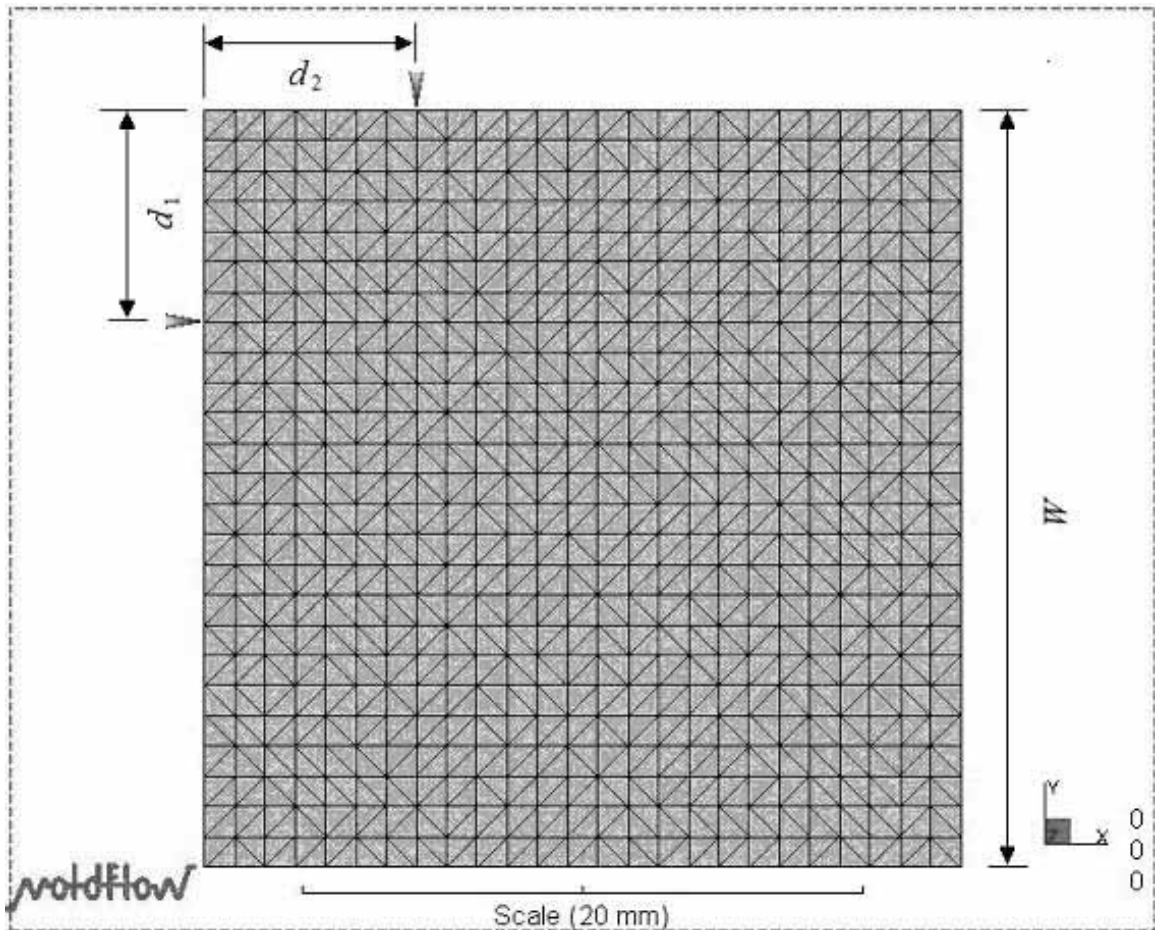


Figure 4.1 Flow geometry

4.2.3 Cavity construction

The first task in the simulation is to construct a 3D model. Though MoldFlow® has the function to construct 3D model, it can also import any standard CAD models. This is a very good feature so we used Pro/E to construct the CAD model. To reflect the actual

package, we generated a square cavity with a dimension of $27\text{mm} \times 27\text{mm}$, which has the same size of the Sumitomo overmold package we have studied. The thickness or height of the cavity is chosen to be small, here it is 3mm. This makes the 2D simulation more reasonable.

Cavities with different geometries were modeled. These geometries include stager array bumps and regular array bumps, which can be compared with the solder balls or leadframe. Figure 4.2 and 4.3 show the stager and regular array bumps models.

4.3 MoldFlow® simulation procedure

4.3.1 Mesh and gates locations

The 2nd step is to import the CAD file to MoldFlow® and select Midplane. Then we can generate mesh as shown in Figure 4.2 and 4.3. The global edge length is chosen to be 1.08 mm, while the mesh size around the solder balls is getting smaller gradually, i.e. from 0.5 mm to 0.25. We have found that 1.08 mm mesh will have enough accuracy in our study. Two gates are located at 5.4mm and 7.56mm to the left upper vertices. The mesh and injection locations are also shown in the Figure 4.2. There are total 1250 triangle elements and 676 nodes.

4.3.2 Material and molding conditions

The material used for simulation is Polydac PA-737 from Chi Mei Corporation. Since we only want to demonstrate our point, it is doesn't matter what material we use, as long as it is polymer which has a very low *Reynolds* number. The process settings of

temperature are shown in Table 4.1.

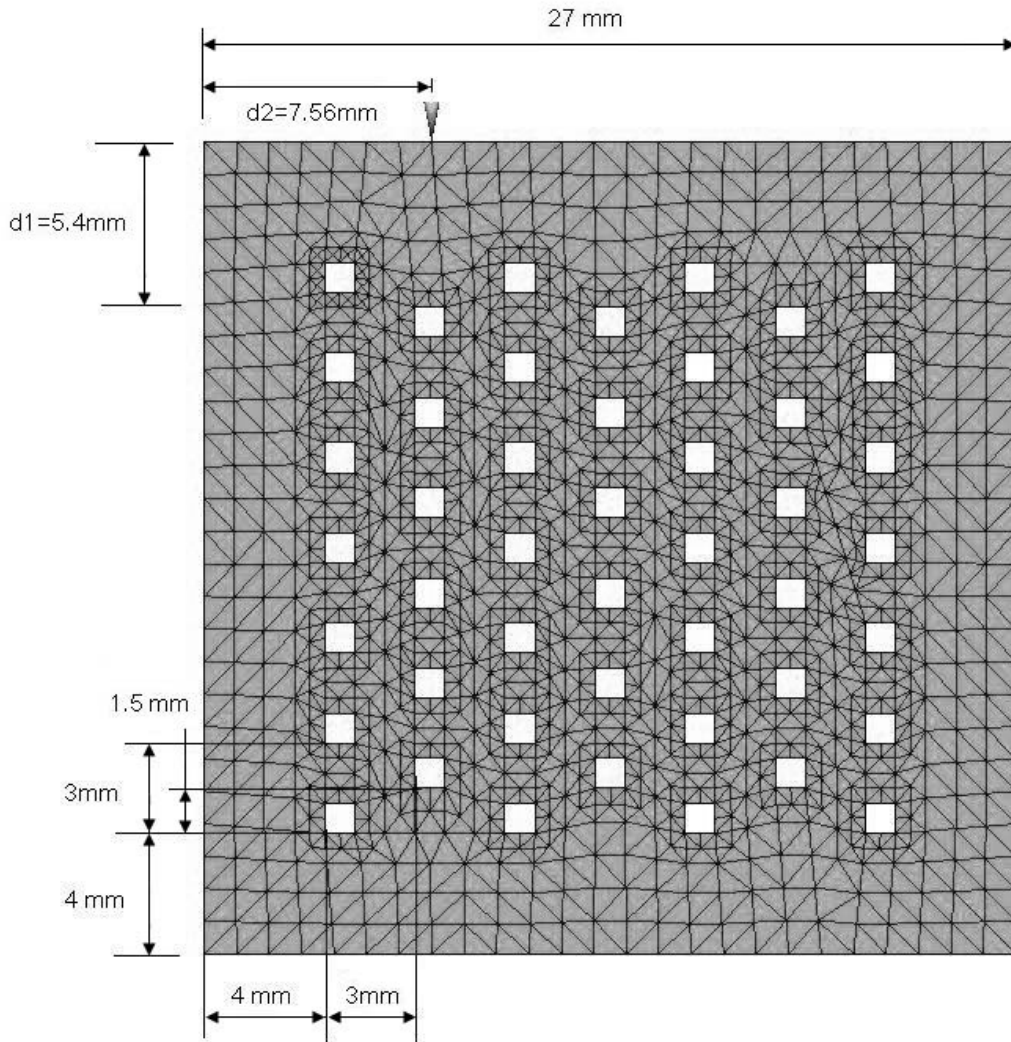


Figure 4.2 Stagger array bumps model and mesh

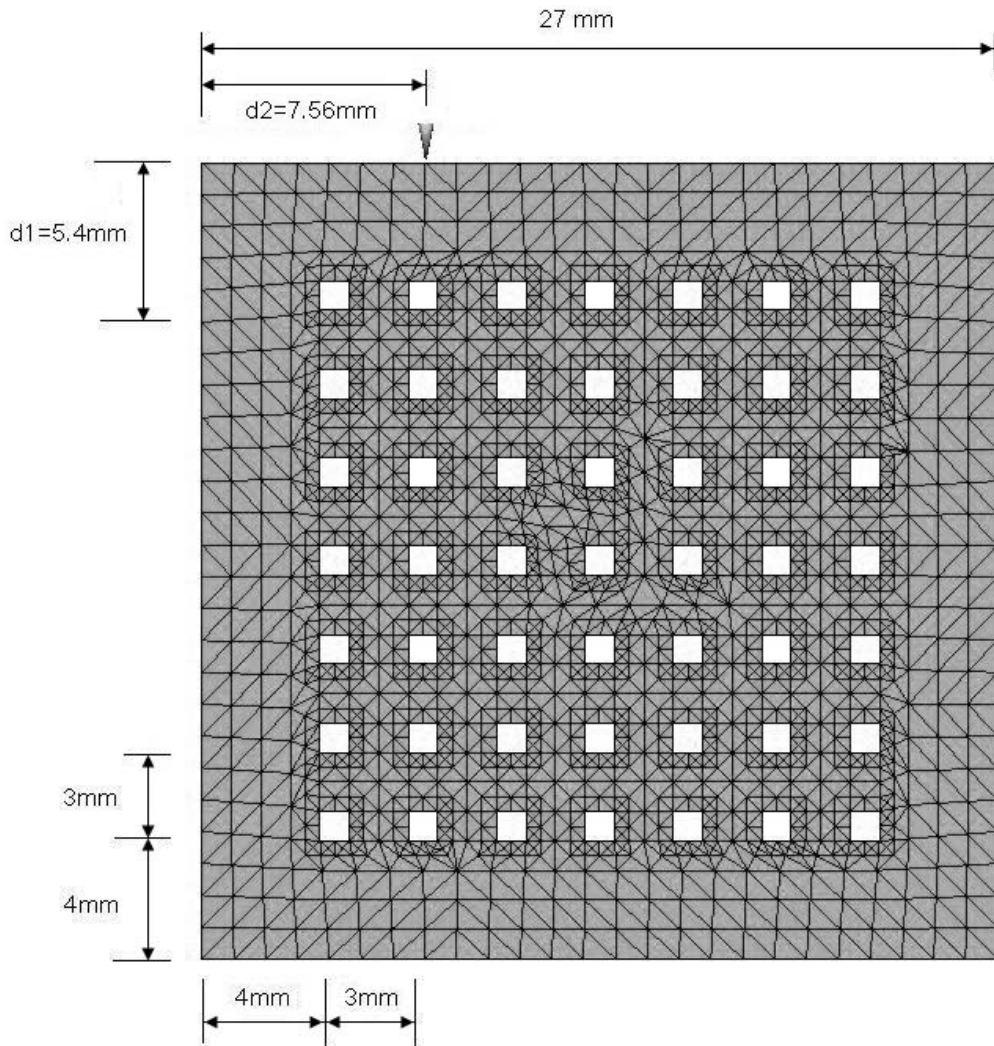


Figure 4.3 Regular array bumps model and mesh

Mold Surface temperature (°C)	40
Melt temperature (°C)	230

Table 4.1 Process settings

4.3.3 Velocity field and streamline construction

From the Moldflow® simulation we obtained the velocity data and from here we can construct streamlines of mold compound flow and perform particle tracking by interpolating the velocity of any arbitrary point inside the velocity field.

4.3.4 Velocity field reconstruction

The Moldflow® analysis can give us the average velocity results only at the centroid of each triangle element. We can save the data in a file 'avnew.ele'. The information on node position and the numbers of the three nodes which have built a triangle can be exported in ASCII format with a file type of *.udm and name of 'Meshexport.udm'.

One disadvantage of the Moldflow® is that the data obtained are not consecutive and we must modify the data to be used for particle tracking. The procedures are:

1. Open 'Meshexport.udm' with MSWord, then find the portion for triangular elements data and save it with a file name 'elementsnode.txt'. Since the format is still not usable, we need to use Excel to open it, chose 'Delimited' at 1st step, chose 'Space', 'other }' at 2nd step, then finish. Copy last 3 columns into Notepad (close Excel file) and save as 'elementsnode.txt'. This file has the node number of each element.
2. Save 'Beginning of node data set.' part with file name 'nodeXY.txt'. Use Excel to open it, chose 'Delimited' at 1st step, chose 'Space', 'other }' at 2nd step, then finish. Copy last 3 columns into Notepad (close Excel file) and save as 'nodeXY.txt'. Remember to check the starting node #, let 'startnode = starting node # -1'. This file has the x, y coordinates of each node.

All these data then are ready to be loaded to any post processing software. From this point we start our own programming. Matlab® is chosen to be the software used to do the rest of the work. This includes velocity field reconstruction, velocity interpolation, particle tracking and all the chaos and mixing analysis.

4.3.5 Velocity at nodes

Since we want to interpolate the velocity at any arbitrary point, we first need to find the velocity at the nodes. However, the Moldflow® analysis only give us the average velocity at the centroid of each triangle element, and these centroids are randomly distributed. So the usual way for interpolating velocity with four nodes at the apex of a square rectangle is not feasible. Thus we have designed a special interpolation method for the arbitrary triangle elements.

To find the velocity at a node, we calculate the average velocity for all the elements around that node, and assign the resulted velocity to that node. To make the results more accurate, it is necessary to reduce the size of the elements, especially the elements around the geometric objects. The flow direction has a much sharper reorientation at these geometric objects. A method of gradual reducing element size is adopted, as shown in Figure 4.2. The element size for the first layer around the object is 0.25 mm, and the second layer is 0.5 mm, then the rest of the elements have the size of 1 mm. The purpose of using this method is to obtain necessary accuracy while keep the computer calculating time reasonable.

4.3.6 Velocity interpolation

To construct the streamlines or track the particles, we have to know the velocity at

any point inside the flow field. Since we only have the data at the nodes, we must do the velocity interpolation.

It is convenient to use the method for finding velocity gradient in a triangular mesh of constant velocity triangles. This is because all of the elements are triangles. For an arbitrary point p , the first thing to do is to find the triangle element which the point belongs to. An effective way is to see if the area of the triangle element will be equal to the area sum of the three triangles formed by connecting the point to three vertices of the triangle element. Figure 4.4 illustrates how it works.

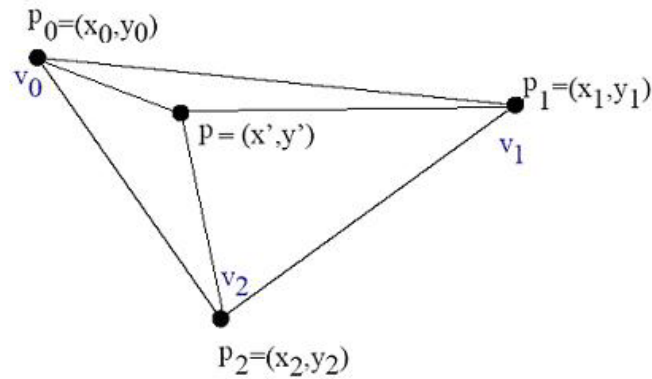


Figure 4.4 Determine a point inside a triangle

First, we calculate the length of the three sides, p_0p_1 , p_0p_2 , and p_1p_2 , as in Equation (4.4). Then we obtain the length of the point $p(x', y')$ to the three nodes of an element, pp_0 , pp_1 , and pp_2 , as in Equation (4.5). So the perimeter s of the triangle $p_0p_1p_2$, can be calculated as in Equation (4.6). Also the perimeters s_1 , s_2 , and s_3 of the triangles pp_0p_1 , pp_0p_2 , and pp_1p_2 can be calculated as in Equation (4.7). Thus the area of each triangle is

determined by using Equations (4.8 – 4.10). If the result from Equation (4.8) is equal to the result from Equation (4.10), then it means that the point p is inside this triangle element. This way the element embracing the point can be found. Then the method of linear interpolation from vertices of a triangle is used to interpolate the velocity at that point.

$$\begin{aligned}
 p_0p_1 &= \sqrt{(x_0-x_1)^2 + (y_0-y_1)^2} \\
 p_0p_2 &= \sqrt{(x_0-x_2)^2 + (y_0-y_2)^2} \\
 p_1p_2 &= \sqrt{(x_1-x_2)^2 + (y_1-y_2)^2}
 \end{aligned} \tag{4.4}$$

$$\begin{aligned}
 pp_0 &= \sqrt{(x-x_0)^2 + (y-y_0)^2} \\
 pp_1 &= \sqrt{(x-x_1)^2 + (y-y_1)^2} \\
 pp_2 &= \sqrt{(x-x_2)^2 + (y-y_2)^2}
 \end{aligned} \tag{4.5}$$

$$s = (p_0p_1 + p_1p_2 + p_0p_2) / 2 \tag{4.6}$$

$$\begin{aligned}
 s_1 &= (pp_0 + pp_1 + p_0p_1) / 2 \\
 s_2 &= (pp_0 + pp_2 + p_0p_2) / 2 \\
 s_3 &= (pp_1 + pp_2 + p_1p_2) / 2
 \end{aligned} \tag{4.7}$$

$$A = \sqrt{s(s-p_0p_1)(s-p_1p_2)(s-p_0p_2)} \tag{4.8}$$

$$\begin{aligned}
A_1 &= \sqrt{s_1(s_1 - p_0 p_1)(s_1 - p p_0)(s_1 - p p_1)} \\
A_2 &= \sqrt{s_2(s_2 - p_1 p_2)(s_2 - p p_1)(s_2 - p p_2)} \\
A_3 &= \sqrt{s_3(s_3 - p_0 p_2)(s_3 - p p_0)(s_3 - p p_2)}
\end{aligned} \tag{4.9}$$

$$A = A_1 + A_2 + A_3 \tag{4.10}$$

‘Real’ functions are rarely given by an explicit formula allowing us to evaluate them anywhere. More frequently, only ‘sample’ values of the function are given at certain points and, in order to estimate the value at some place, which is not a sample, we need to somehow combine the available information. This is the goal of interpolation. By doing interpolation one can, for example, build a complete elevation map of a terrain when only an array of height values is given (this is what happens in practice: height cannot be measured everywhere; no matter how you do it, you end up with only finite number of measurements). We used interpolation to estimate the velocity over a triangle when velocities at vertices are given.

An example of the variant of linear interpolation follows: Let’s say that we have a triangle as shown in Figure 4.5. It has vertices $p_0 = (x_0, y_0)$, $p_1 = (x_1, y_1)$, and $p_2 = (x_2, y_2)$. At each vertex we have a velocity value, let’s say that they are v_0, v_1 and v_2 . There is exactly one linear function which takes the value of v_0 at p_0 , v_1 at p_1 and v_2 at p_2 (We can prove that by ‘embedding’ our triangle and the values at vertices in 3D: say that the triangle lies in the ground plane; lift p_0 to height v_0 , p_1 to height v_1 and p_2 to height v_2 . This yields 3 points in 3D-space. Now, find the plane passing through the three points. This plane is the graph of the linear function we are looking for). The following shows

how to compute algebraically.

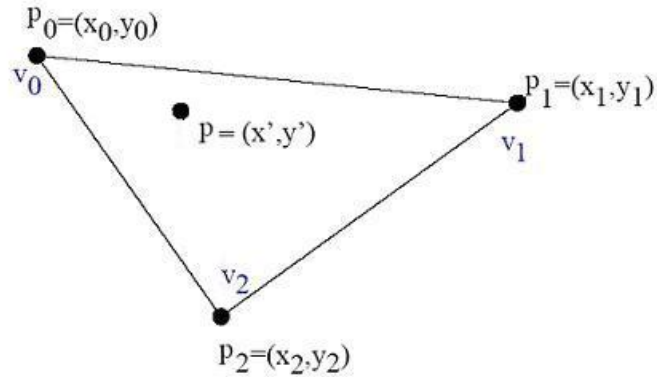


Figure 4.5 Linear interpolation from triangle's vertices

We seek a function of the form $f(x, y) = Ax + By + C$ (A, B, C to be determined). The requirement that the values at the vertices are v_0, v_1 and v_2 leads to three linear equations:

$$Ax_0 + By_0 + C = v_0 \quad (4.11)$$

$$Ax_1 + By_1 + C = v_1 \quad (4.12)$$

$$Ax_2 + By_2 + C = v_2 \quad (4.13)$$

We can solve them, obtaining A, B and C . So, for example, to compute the interpolated value at the point $p = (x', y')$ we need to evaluate

$$f(p) = f(x', y') = A * x' + B * y' + C \quad (4.14)$$

4.3.7 Streamline construction

Determination of the streamlines is the next step that is critical to being able to calculate laminar mixing. To construct the streamlines, a few particles are placed at the desired initial positions and are tracked to the end of filling positions. Here only streamlines in the cavity with stager bump pattern are constructed. Figure 4.6 shows the streamlines for feeding from both left gate and top gate with $d_1 = 5.4\text{mm}$ and $d_2 = 7.56\text{mm}$. Streamlines of top gate are in blue and streamlines of left gate are in red. The most important characteristic of chaotic flow – crossing streamlines can be seen clearly. This means by alternate feeding from both gates we are able to generate chaotic mixing.

Another advantage of two gates filling is that it can diminish the effect of stagnant point. As can be seen from the figure, some of the streamlines are stopped in the middle of the cavity, this is because that they encountered the bumps and the velocity is reduced to 0. But the velocities at these points are generally not equal to 0 for the other gate filling. Thus the particles can be spread into everywhere within the cavity.

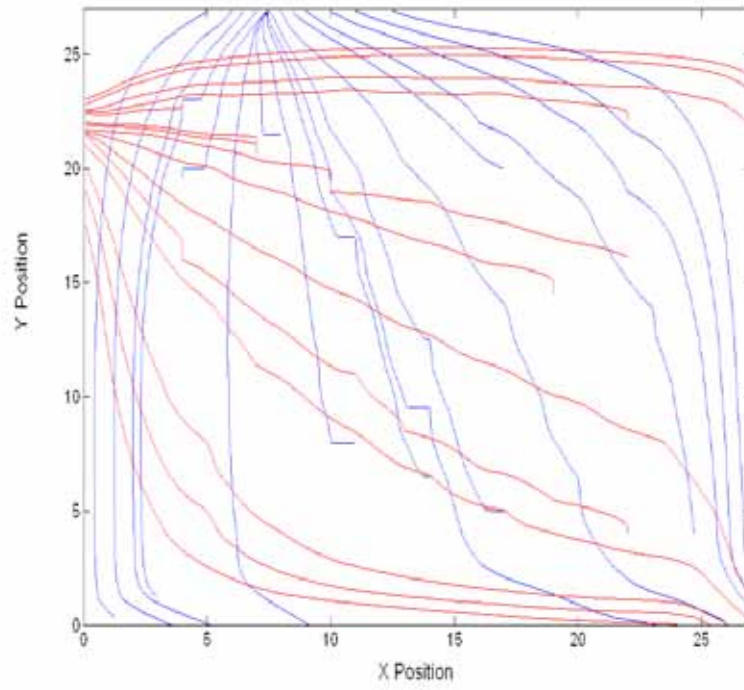


Figure 4.6 Streamlines obtained from $d_1 = 5.4\text{mm}$ and $d_2 = 7.56\text{mm}$

Chapter 5: Model of mixing and measures of mixing

5.1 Model of mixing

5.1.1 Mixing Simulation - Particle tracking

We assume the particles are passively conveyed by the flow, so that we can track the particle through the streamlines they are traveling. We assigned 0 velocity at normal directions at the ball and used 30% slip velocity along the ball. The time step is 0.01s, and the total tracking time is 1.6 s. This is also the time to fill the cavity.

5.1.2 Two important parameters

There are many factors affecting the flow and mixing. One of them is the gate location. The distance of the gates to the left upper corner is indicated by d_1 and d_2 , as show in Figure 4.1. Since the length of the square cavity is L , the normalized distance can be described as

$$d_n^* = d_n / L, n = 1, 2 \quad (5.1)$$

The value of this parameter cannot be too small or too big. Small distances will not generate enough reorientation because in order to achieve chaos, particles need to flow past hypergeometric points. When these hypergeometric points are crossed, adjacent particles will separate exponentially when the flow direction is changed. In the other

aspect, if it is too big, the two flow fronts will not reach for a long time, and the weld line will become bigger. This is not good for the final product property and should be avoided. Two distance values have been chosen in this study.

$$d_n^* = 0.2 \text{ and } 0.28 \quad (5.2)$$

The other important parameter is the filling period denoted by T . This parameter is used to define the periodic motion. Other than the definition given by previous researchers, here it is defined as the time of filling from one gate at a time which is the approximate time of fluid flow from one ball to another ball when $T = 0.2\text{s}$. Since the more important thing is to see the time flow from one ball to another ball, so it is better to make this filling period dimensionless according to the ball distance as expressed in Equation (5.2). This dimensionless period is denoted by f .

$$f = \frac{\frac{T}{P}}{\frac{t_{total}}{L}} \quad (5.3)$$

For this study, $t_{total} = 1.6 \text{ s}$, $P = 3 \text{ mm}$, $L = 27 \text{ mm}$. So f is 1.125 at $T = 0.2\text{s}$.

Thus if we alternatively fill through gates 1 and 2, the whole period is $2T$. Aperiodic filling can be obtained by assigning a random number to multiply T as the filling time at each gate. Here this number is between 0.5 and 2. The periodic and aperiodic procedures are given in Table 5.1 and 5.2.

Left	0 – 0.2		0.4 – 0.6		0.8 – 1.0		1.2-1.4	
Top		0.2 – 0.4		0.6 – 0.8		1.0-1.2		1.4-1.6

Table 5.1 Periodic procedure

Left	0 – 0.36		0.44 – 0.68		0.84 – 1.16		1.44-1.6
Top		0.36– 0.44		0.68 – 0.84		1.16-1.44	

Table 5.2 Aperiodic procedure

The initial center positions of two particle balls are located at (6, 22) and (6, 20), the radius is 0.9 as in Figure 5.1. The total particle number is 522.

5.1.3 Design of experiment

5.1.3.1 One gate and two gates filling

The most important thing is to see the effects of one gate and two gates filling. A basic assertion the cavity filling model is that two gates are required for chaos to be created. The entropic study and stretching analysis will be conducted; the difference between one gate, two gates periodic filling and two gates aperiodic filling will be quantified.

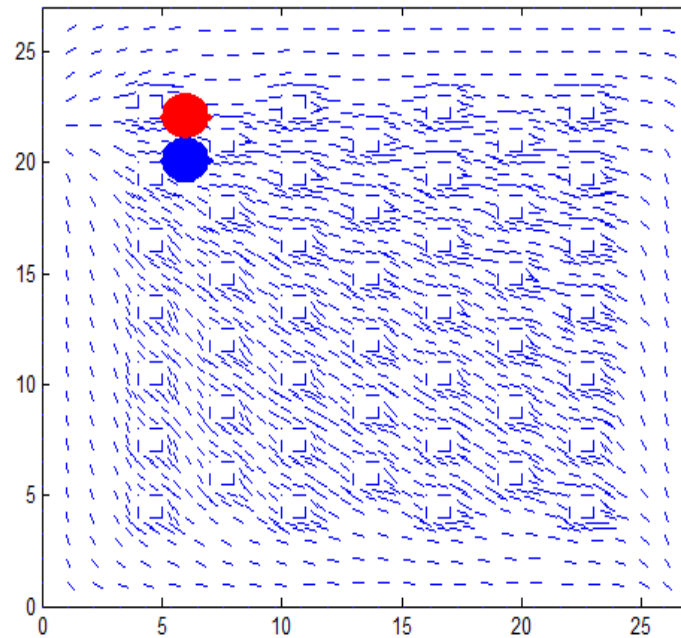


Figure 5.1 Initial positions of two particle balls

5.1.3.2 Effects of f and ball pattern

In order to see the effects of f and ball pattern on the mixing, a full $3 \times 3 \times 2$ factorial design of experiment is constructed as shown in Table 5.3. There are 3 levels for f which are 0.2813, 1.125 and 1.9687. These correspond to T at 0.05s, 0.2s, and 0.35s respectively. The second factor is the gate location. Also 3 levels are given by the first level: left gate d1 at 5.4mm and top gate d2 at 5.4mm, the second level: left gate d1 at 5.4mm and top gate d2 at 7.56mm, the third level left gate d1 at 7.56mm and top gate d2 at 7.56mm. Two levels for ball patterns; these are stagger and regular patterns as shown in Figure 4.2 and 4.3. The relations between f and mixing will be plotted and modeled. The effects of change of gate location and ball pattern on the mixing will also be studied.

	Factor 1	Factor 2		Factor 3
Run	A: f	B:d1	C:d2	D:Ball Pattern
1	0.2813	5.4	5.4	Stagger
2	1.125	5.4	5.4	Stagger
3	1.9687	5.4	5.4	Stagger
4	0.2813	5.4	7.56	Stagger
5	1.125	5.4	7.56	Stagger
6	1.9687	5.4	7.56	Stagger
7	0.2813	7.56	7.56	Stagger
8	1.125	7.56	7.56	Stagger
9	1.9687	7.56	7.56	Stagger
10	0.2813	5.4	5.4	Regular
11	1.125	5.4	5.4	Regular
12	1.9687	5.4	5.4	Regular
13	0.2813	5.4	7.56	Regular
14	1.125	5.4	7.56	Regular
15	1.9687	5.4	7.56	Regular
16	0.2813	7.56	7.56	Regular
17	1.125	7.56	7.56	Regular
18	1.9687	7.56	7.56	Regular

Table 5.3 DOE study of f and ball pattern

5.2 Stretching

Chaotic flow can produce exponential stretching rate and it is convinible to use stretching rate as a measure of chaotic flow. In calculation, the stretching rate λ is defined as the ratio of the length of an infinitesimal segment at the end of filling to its original length. First the ratio of all particle pairs at final position d_f to the initial position d_i is calculated, and the mean is obtained by simply divided the sum of the ratio by the total number of particle pairs N . Then the mean $\log(\lambda)$ can be calculated as in Equation (5.4).

$$\text{mean } \log(\lambda) = \log\left(\sum_{j=1}^N \frac{d_f}{d_i} / N\right) \quad (5.4)$$

The evolution of mean $\log(\lambda)$ vs. time is plotted to view the trend. If a line with positive slope can be fitted to the curve, then it is recognized as exponential stretching and thus chaotic flow.

5.3 Entropic mixing characterization

5.3.1 Background on Shannon Entropy

The Shannon entropy is used to quantitatively characterize color homogeneity as a measure of distributive mixing in numerical simulations and experiments performed in a single screw extruder by Wang and Manas [Wang 01, Manas 04]]. Entropy is the rigorous measure of mixing. It is determined by the probabilities p_i from:

$$S = -\sum_{i=1}^M p_i \ln p_i \quad (5.5)$$

here M is the total number of the outcomes and p_i is the probability of outcome i to occur.

Equation (5.5) is the standard measure [Shannon 1948] of homogeneity as it satisfies the following requirements:

- (i) The lowest entropy ($S = 0$) corresponds to one of the p 's being 1 and the rest being zero (i.e., segregation);

- (ii) The largest value for the entropy is achieved when all p 's are equal (i.e., complete mixing);
- (iii) S is additive over partitions of the outcomes.

In numerical simulations particles are used as a mean to study the dynamics of the mixing process and assess mixing quality. In particular, the total domain of study (such as the midplane of the square cavity) is divided into small regions (bins). It calculates particle concentrations in each bin as estimators of the probabilities. Calculation of Shannon entropy reveals the homogeneity of particle distribution in the system.

5.3.2 Entropic Characterization of Mixing

When assessing distributive mixing in a system, we have to consider the relative concentration of blue and red particles at each location in the system. We then, divide the space of interest in M bins labeled $j = 1, 2, \dots, M$. There are also two species of particles (blue and red) labeled $c = 1$ and 2 . In view of Equation (5.5), the overall quality of mixing is described by:

$$S = - \sum_{c=1}^2 \sum_{j=1}^M p_{c,j} \ln p_{c,j} \quad (5.6)$$

where $p_{c,j}$ is the joint probability for a particle to be of species “ c ” and in bin “ j ”. It is estimated by the fraction of particles of species c located in bin j out of all particles. The joint probability for a particle to be located in bin j and to be of species c is given by Bayes’ theorem:

$$p_{c,j} = p_{c|j} p_j \quad (5.7)$$

where $p_{c|j}$ is the probability of finding a particle of species c conditional on the bin j and p_j is the probability for bin j . By substituting equation (5.7) into equation (5.6) we get:

$$S = -\sum_{c=1}^2 \sum_{j=1}^M [(p_{c|j} p_j) \ln(p_{c|j} p_j)] p_{c,j} \ln p_{c,j} \quad (5.8)$$

and finally because $\sum_{c=1}^2 p_{c|j} = 1$ for all values of j

$$S = \sum_{j=1}^M [p_j S_j(\text{species})] + S(\text{locations}) \quad (5.9)$$

where

$$S = -\sum_{c=1}^2 \sum_{j=1}^M p_{c,j} \ln p_{c,j} \quad (5.10)$$

$$S_j(\text{species}) = -\sum_{c=1}^2 p_{c|j} \ln p_{c|j} \quad (5.11)$$

$$S(\text{locations}) = -\sum_{j=1}^M p_j \ln p_j \quad (5.12)$$

$S_j(\text{species})$ is the entropy of mixing the two species (blue and red) at the location of bin j and $S(\text{locations})$ is the entropy associated with the overall spatial distribution of

particles irrespective of species. It can be written more compactly as

$$S = S(locations) + S_{locations}(species) \quad (5.13)$$

where

$$S_{locations}(species) = \sum_{j=1}^M [p_j S_j(species)] \quad (5.14)$$

$S_{locations}(species)$ is a spatial average of the entropy of mixing of species conditional on location. It is maximized for the particular homogeneous state characterized by: $p_{c/j} = 1/2$, for $c = 1, 2$ and $j = 1, 2, \dots, M$. The maximum value of $S_{locations}(species)$ is $\ln(2)$, so we normalize this entropy by $\ln(2)$ to get the relative entropy, which takes values between 0 and 1. It is a measure of the system being homogeneous as well as having the particular color or shade of gray that corresponds to having equal concentrations of blue and red particles in each bin. In this work we will use this particular entropy to characterize color and homogeneity by employing two species of particles, namely blue and red.

5.4 Analysis of mixing and stretching in empty cavity without bumps

An empty cavity without bumps is not reflecting the actual application in electronic packaging industry, but it worth to learn and it could give us some insight into the theory of filling a cavity. The streamlines for filling from left gate at $d1 = 7.56\text{mm}$ and top gate at $d2 = 7.56\text{mm}$ are shown in Figure 5.2. The crossing streamlines are verified, however, whether it will give us chaotic mixing is to be studied.

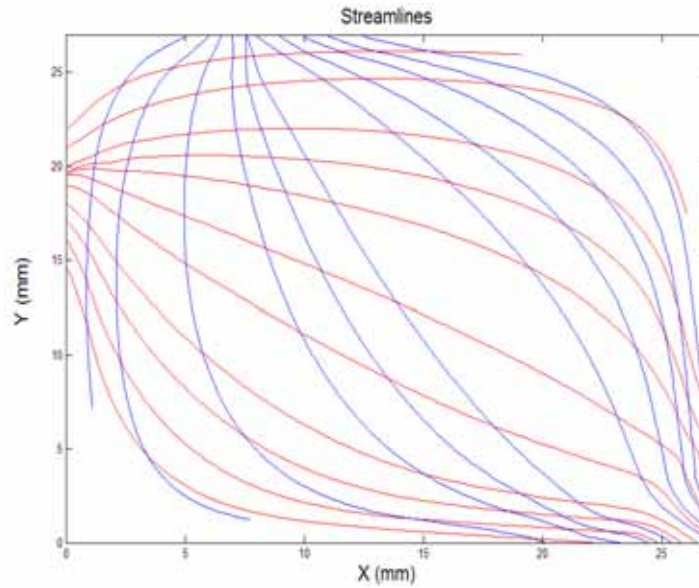


Figure 5.2 Streamlines obtained from $d_1 = 7.56\text{mm}$ and $d_2 = 7.56\text{mm}$

5.4.1 Mixing study

The simulation of mixing is conducted by placing two particle balls inside the cavity, and then filling the empty cavity with single gate and two gates. The initial center positions of two particle balls are located at (6, 22) in red and (6, 20) in blue; the radius is 0.9 as in Figure 5.3. The total particle number is 522. Figure 5.3 also shows the final particles position at $t = 1\text{s}$ for single left gate filling with $d_1 = 7.56\text{ mm}$. The particle balls are just elongated with neither mixing nor dispersion. The final particles position at $t = 1\text{s}$ for two gates filling with $d_1 = 7.56\text{ mm}$, $d_2 = 7.56\text{ mm}$ and $f = 1.125$ so $T = 0.2\text{s}$ is shown in Figure 5.4. We can see that the particles are still bounded together as in the single gate filling. Only the location is different.

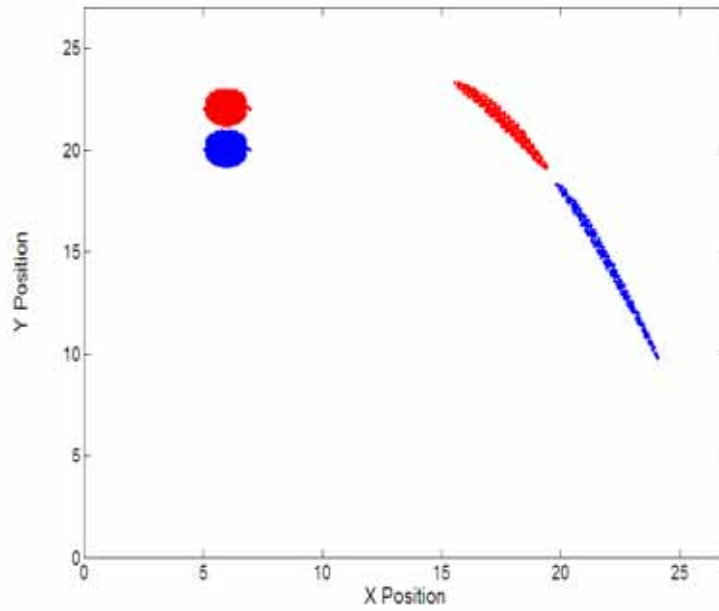


Figure 5.3 Initial and final particles position with single gate filling

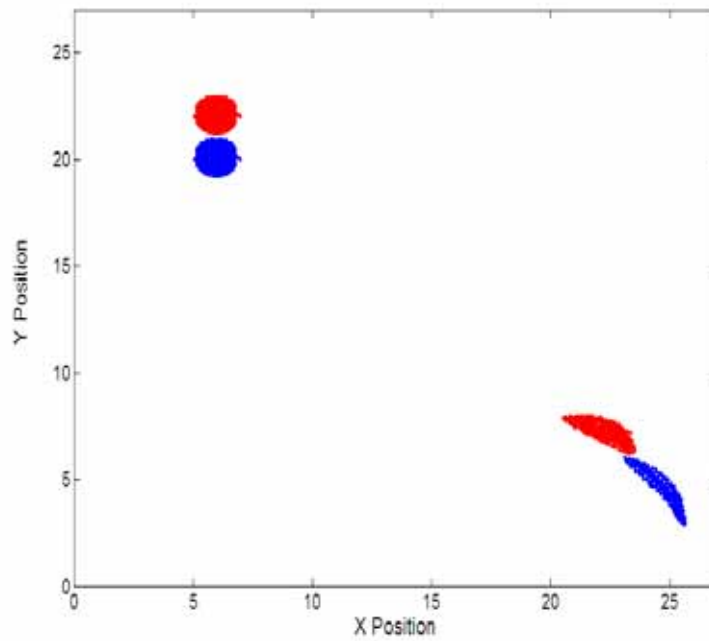


Figure 5.4 Initial and final particle positions with two gates filling

Figure 5.5 – 5.7 show the entropy $S_{\text{locations}}$ (species), $S(\text{locations})$ and S for left gate filling (blue) and two gates periodic filling (cyan). In theory, the best $S_{\text{location}}(\text{species})$ (Normalized), $S(\text{locations})$ and S values are 1, 5.5645, and 6.2577 respectively. Also the minimum value we can get for $S_{\text{location}}(\text{species})$ (Normalized) is 0, while we can get the initial values for $S(\text{locations})$ and S is 2.0721.

It is a little surprise to see that the left gate filling even has higher $S(\text{locations})$ and S values than two gates filling. On the other hand, we should not be surprised because if we examine the chaotic flow in the fully filled cavity, we can find that besides crossing streamline, there is another critical condition must be met, which is velocity gradient. The moving wall can generate velocity gradient between itself and the other walls, thus can produce hyperbolic points at certain regions. While in the empty cavity, the velocity gradient can only exist at near the walls. In the middle of the cavity, the velocity field is flat. By placing bumps into the cavity, we could produce the stagnation points and velocity gradient in the center of the cavity, and resolve the problem caused by the empty cavity.

5.4.2 Stretching analysis

For stretching, the particles are initially placed at (6, 22) and formed two circular balls. There are total 261 pairs of particles. The distance between a pair of particles is 0.005mm. The result of mean $\log(\lambda)$ vs. time is given in Figure 5.8. Filling from left gate only with $d_1 = 7.56$ mm is shown in blue. Periodic filling with $d_1 = 7.56$ mm, $d_2 = 7.56$ mm and $f = 1.125$ or $T = 20$ is shown in cyan. Both cases have a very small amount of stretching. Periodic filling has slightly higher stretching than single gate filling.

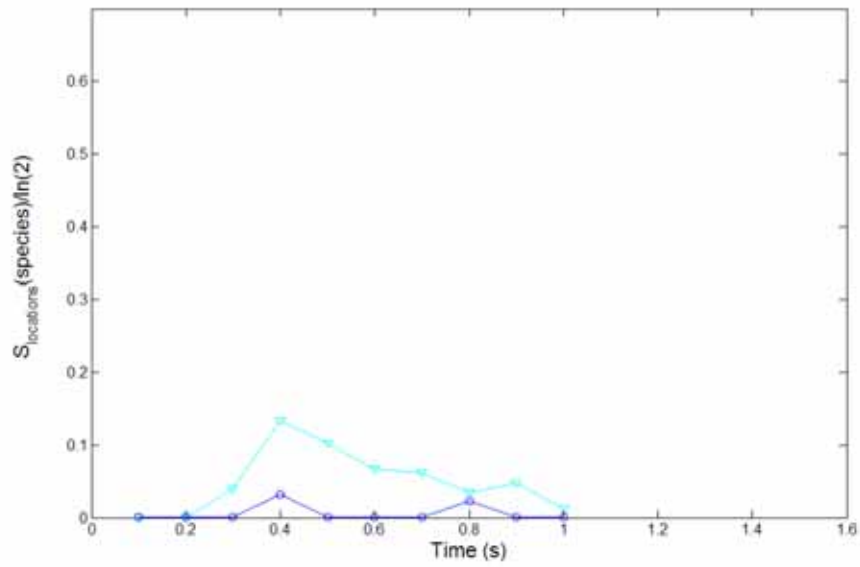


Figure 5.5 $S_{\text{locations}}(\text{species})/\ln(2)$ vs. time for left gate filling (blue) and two gates filling with $f = 1.125$ (cyan)

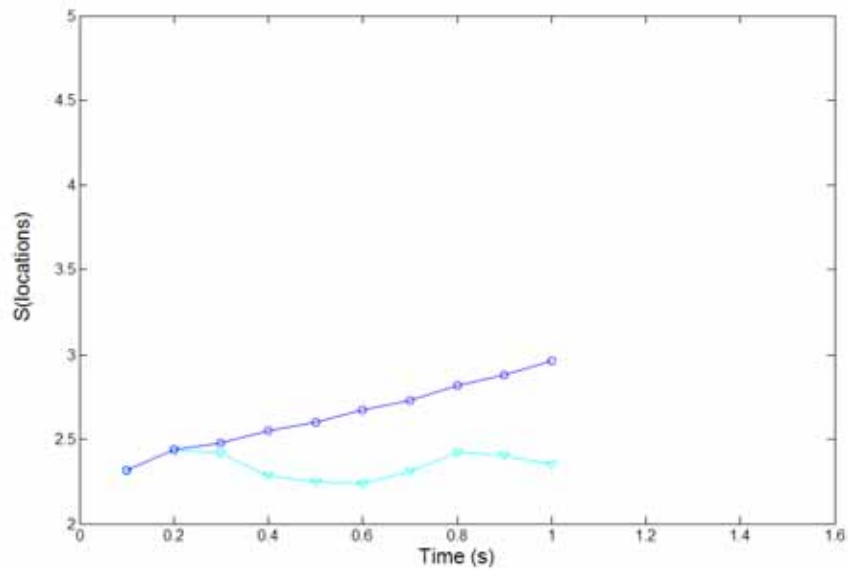


Figure 5.6 Entropy $S(\text{locations})$ for left gate filling (blue) and two gates periodic filling with $f = 1.125$ (cyan)

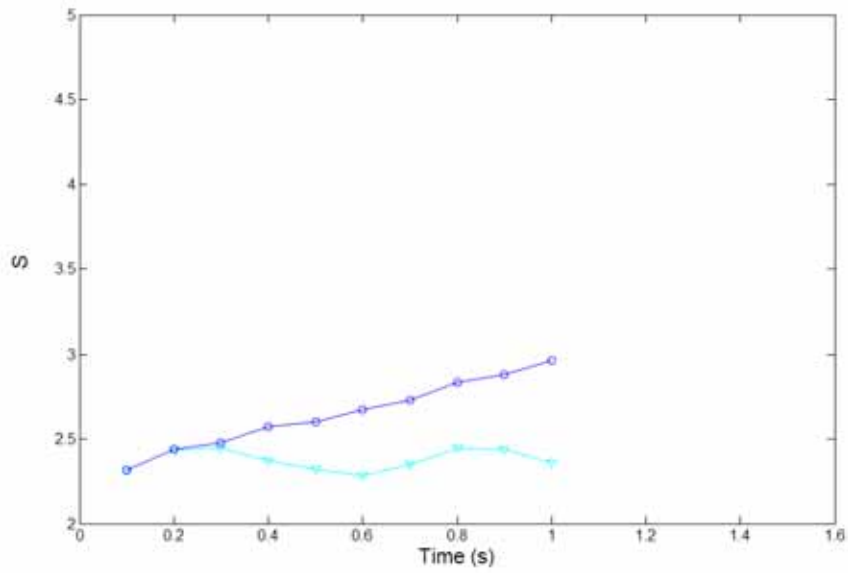


Figure 5.7 Entropy S for left gate filling (blue) and two gates periodic filling with $f=1.125$ (cyan)

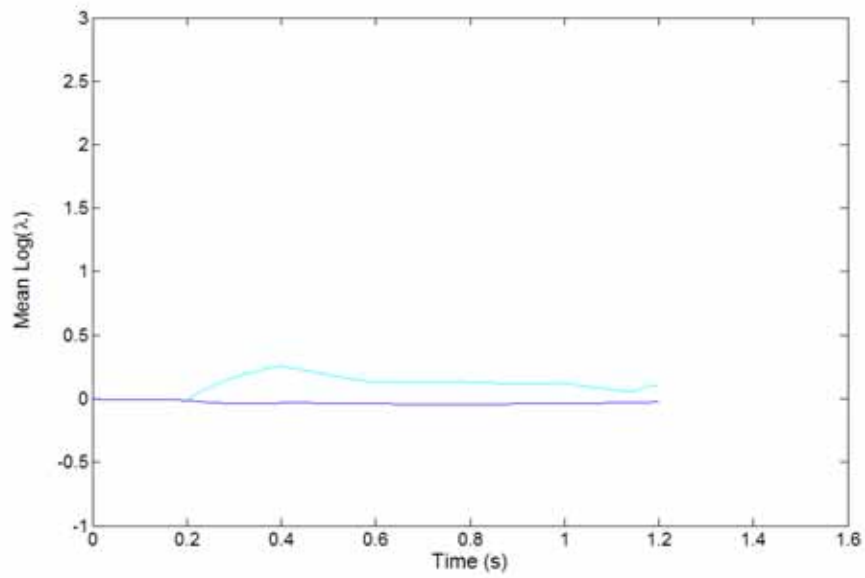


Figure 5.8 Mean $\log(\lambda)$ vs. time for left gate (red) and two gates $f=1.125$ (blue), $d_1=7.56\text{mm}$, $d_2=7.56\text{mm}$

Table 5.4 shows entropy and stretch values at $t = 1s$. All the values are relatively small, means poor mixing. No chaotic flow is presented. Can we expect to see chaotic flow once we have added bumps into the cavity? Next chapter we will find the answer.

f	$S_{\text{location}}(\text{species})$	$S(\text{locations})$	S	Stretch
Left	0	2.9647	2.9647	-0.0225
1.125	0.013	2.3491	2.3581	0.1066

Table 5.4 Simulation results for filling the clear cavity

Chapter 6: Chaotic mixing analysis

The analysis is focus on the stretching and mixing. Exponential stretching is an important measure of chaotic flow. Entropic is a non-chaotic measure, which can reveal the effectiveness of the mixing resulted from the novel feed protocol.

6.1 Analysis of flow and mixing in cavity with stagger bumps

6.1.1 Particle distribution

First to see is the final particle distribution. Total 522 particles were tracked through the flow field for different f values and aperiodic procedure. This section will show visually the distribution of particle balls, which are colored by red and blue, at $t = 1.6s$.

6.1.1.1 $d1 = 5.4mm$ and $d2 = 5.4mm$

The results of filling from left gate $d1 = 5.4mm$ only is given in Figure 6.1. The particles are compressed closer and spread into very limited spaces. Thus we could expect poor mixing. Figure 6.2 – 6.4 show two gates filling for $f = 0.2813$, 1.125 , and 1.9687 respectively with $d1 = 5.4mm$ and $d2 = 5.4mm$. Figure 6.5 shows aperiodic filling. By looking at the final particle distributions, it is clear that all two gates filling are having superior mixing results than one gate filling.

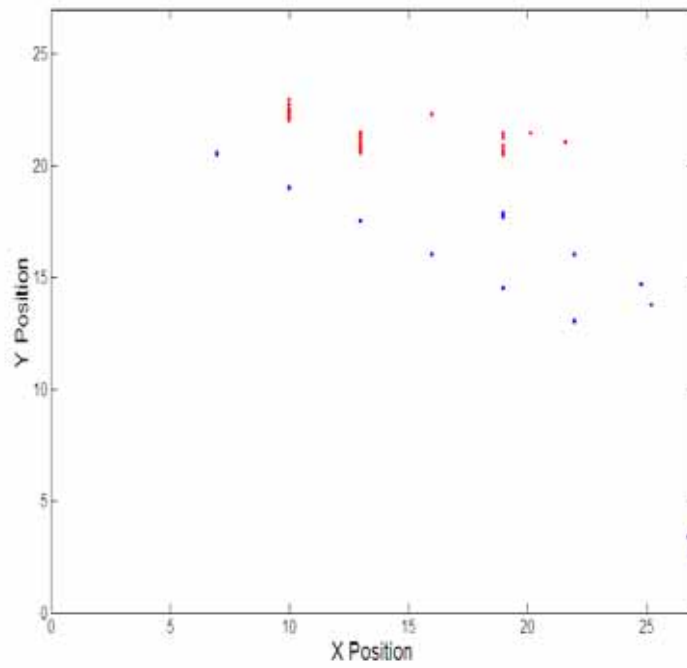


Figure 6.1 Distribution of particles at $t = 1.6\text{s}$ with left gate filling at $d1 = 5.4\text{ mm}$

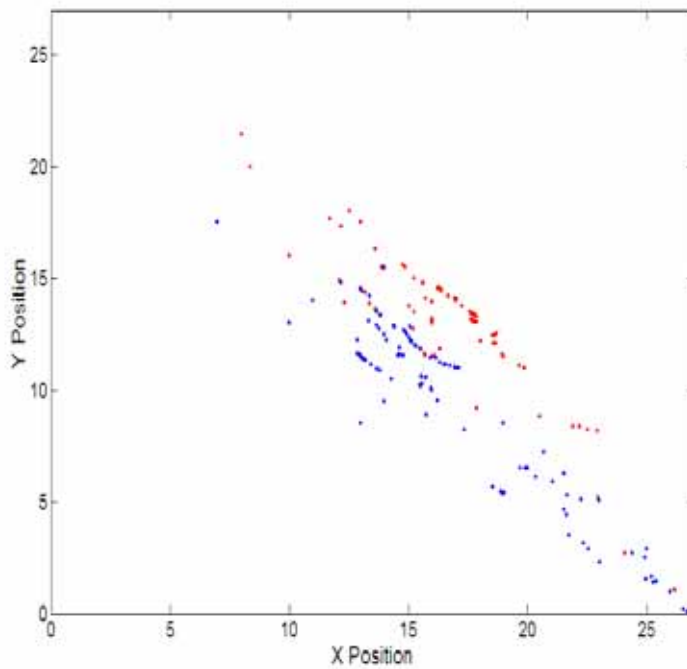


Figure 6.2 Distribution of particles at $t = 1.6\text{s}$ for $f = 0.2813$

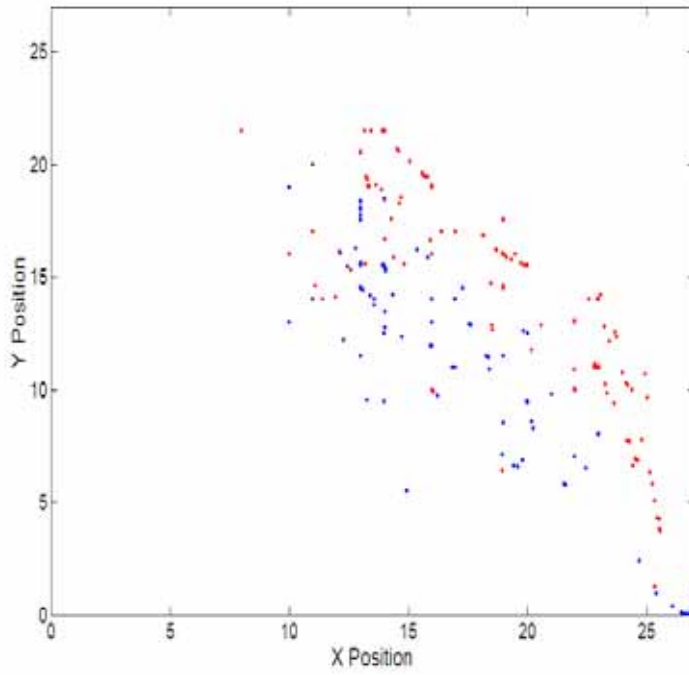


Figure 6.3 Distribution of particles at $t = 1.6s$ for $f = 1.125$

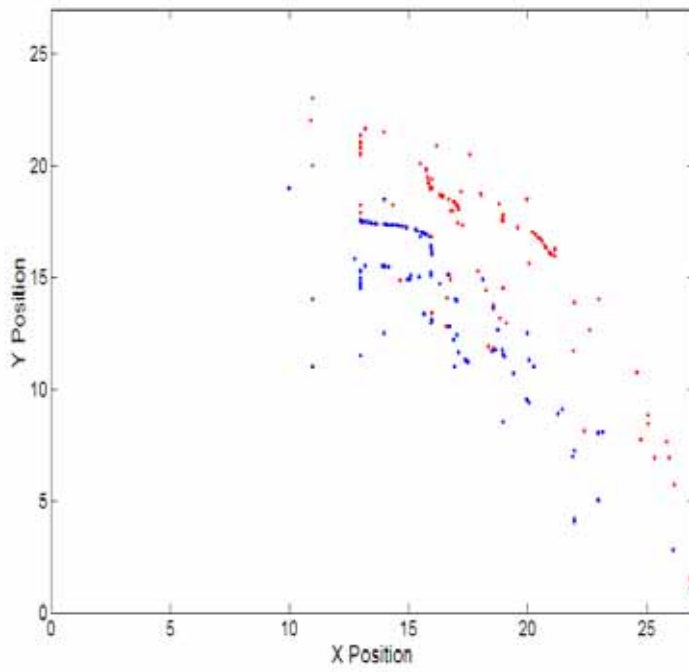


Figure 6.4 Distribution of particles at $t = 1.6s$ for $f = 1.9687$

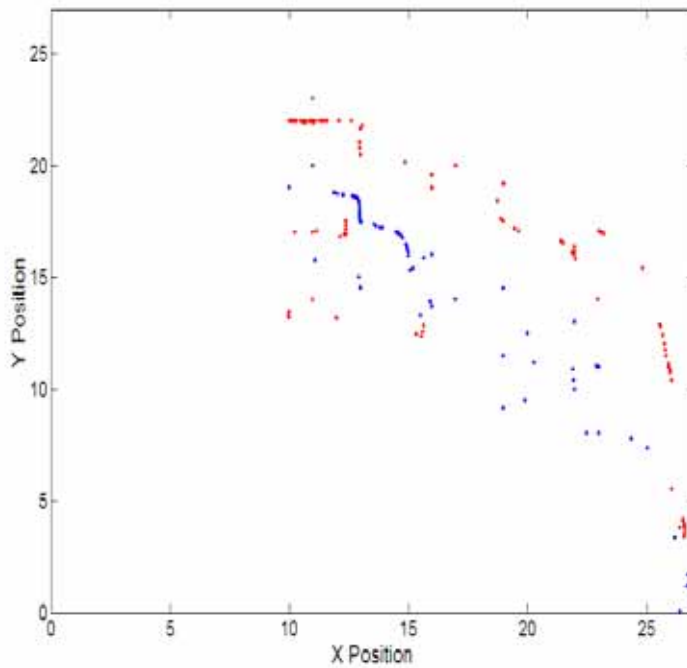


Figure 6.5 Distribution of particles at $t = 1.6s$ for aperiodic filling

6.1.1.2 $d_1 = 5.4mm$ and $d_2 = 7.56mm$

The left gate filling is the same as above. Figure 6.6 – 6.8 show two gates filling for $f = 0.2813$, 1.125 , and 1.9687 respectively with $d_1 = 5.4mm$ and $d_2 = 7.56mm$. Figure 6.9 shows aperiodic filling. By looking at the final particle distributions, it is clear that all two gates filling are having superior mixing results than one gate filling. Larger f may result in better mixing.

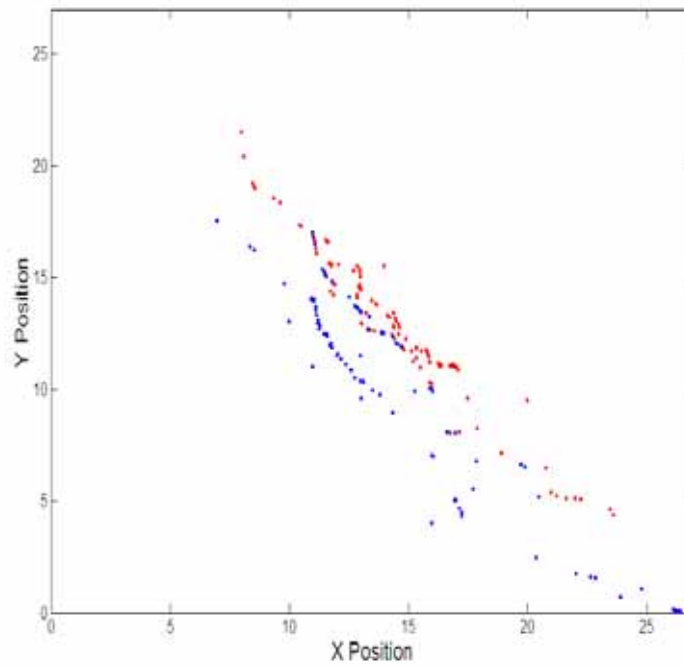


Figure 6.6 Distribution of particles at $t = 1.6s$ for $f = 0.2813$

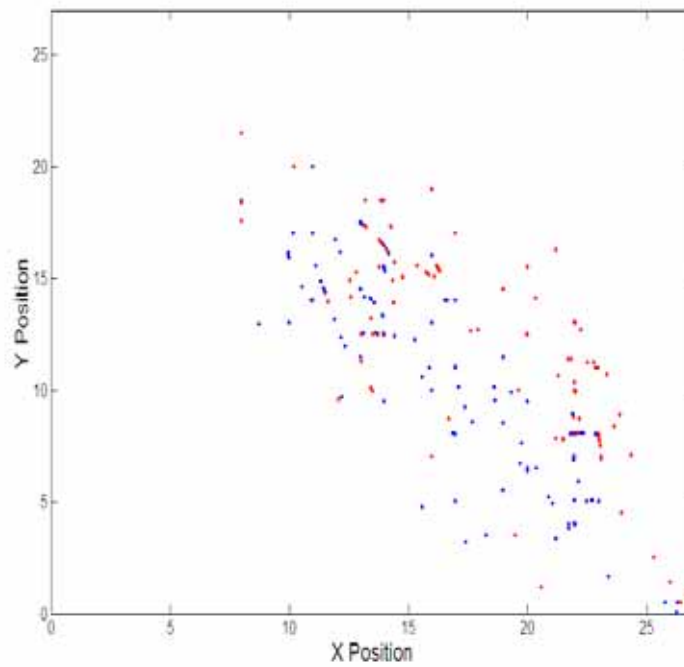


Figure 6.7 Distribution of particles at $t = 1.6s$ for $f = 1.125$

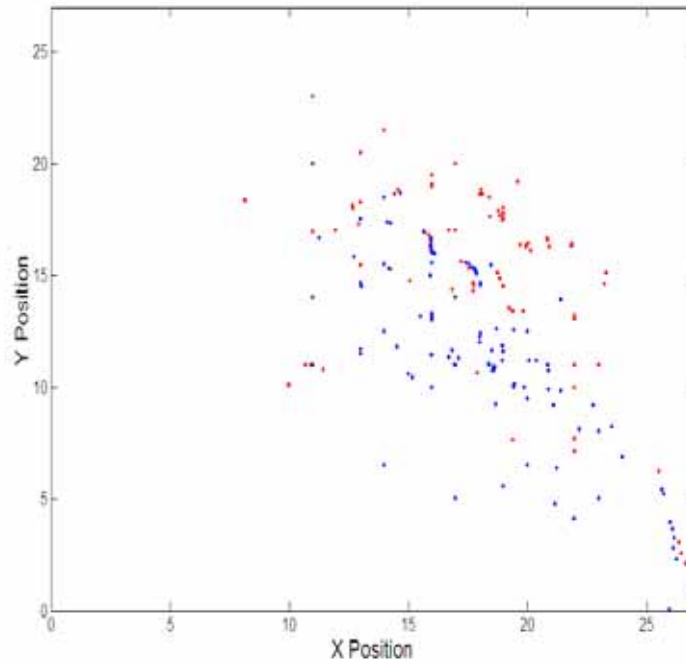


Figure 6.8 Distribution of particles at $t = 1.6s$ for $f = 1.9687$

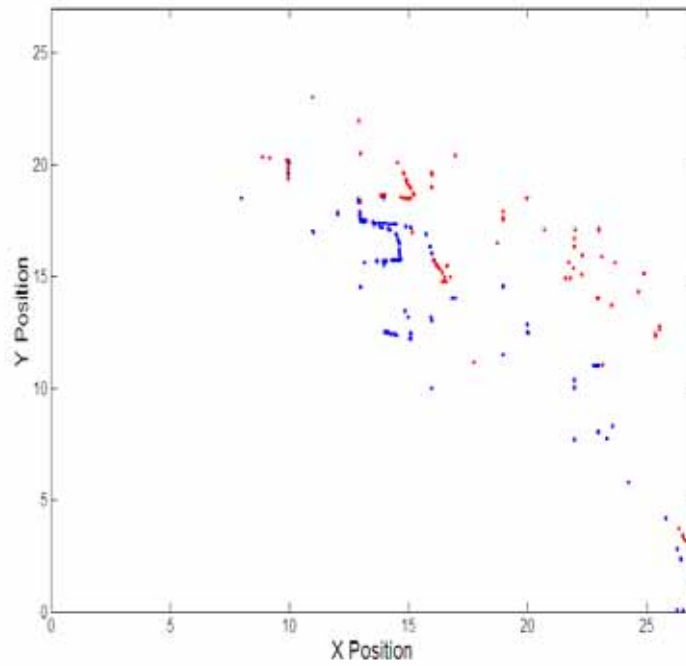


Figure 6.9 Distribution of particles at $t = 1.6s$ for aperiodic filling

6.1.1.3 $d_1 = 7.56\text{mm}$ and $d_2 = 7.56\text{mm}$

The results of filling from single left gate at $d_1 = 7.56\text{mm}$ is given in Figure 6.10. Again the particles are compressed closer and spread into very limited spaces. This further confirms that one gate filling is not a good practice for mixing. Figure 6.11 – 6.13 show two gates filling for $f = 0.2813$, 1.125 , and 1.9687 respectively with $d_1 = 7.5\text{mm}$ and $d_2 = 7.5\text{mm}$. Figure 6.14 shows aperiodic filling. By looking at the final particle distributions, it is clear that all two gates filling are having superior mixing results than one gate filling.

For all the cases of two gates filling, we observed better spreading and mixing compared to single gate filling. To quantify the mixing, and numerically compare them, the next step is to calculate entropic value for all these filling conditions.

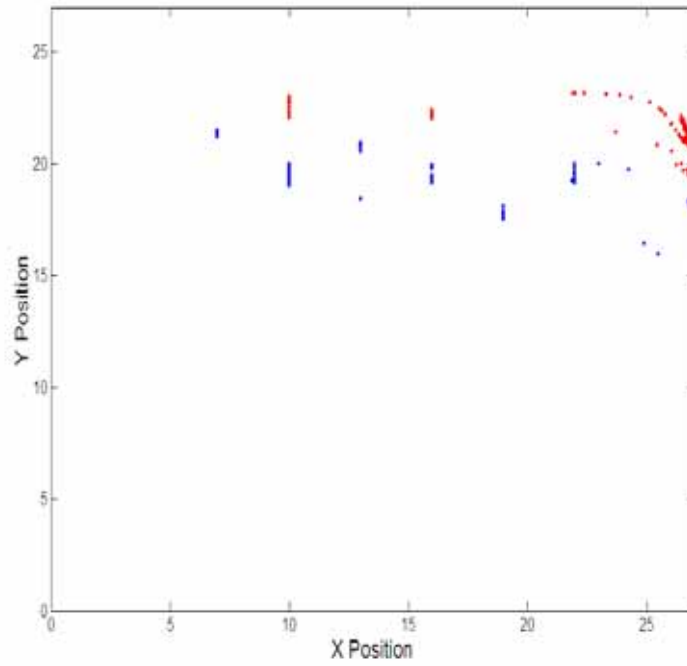


Figure 6.10 Distribution of particles at $t = 1.6s$ with left gate filling at $d1 = 7.5$ mm

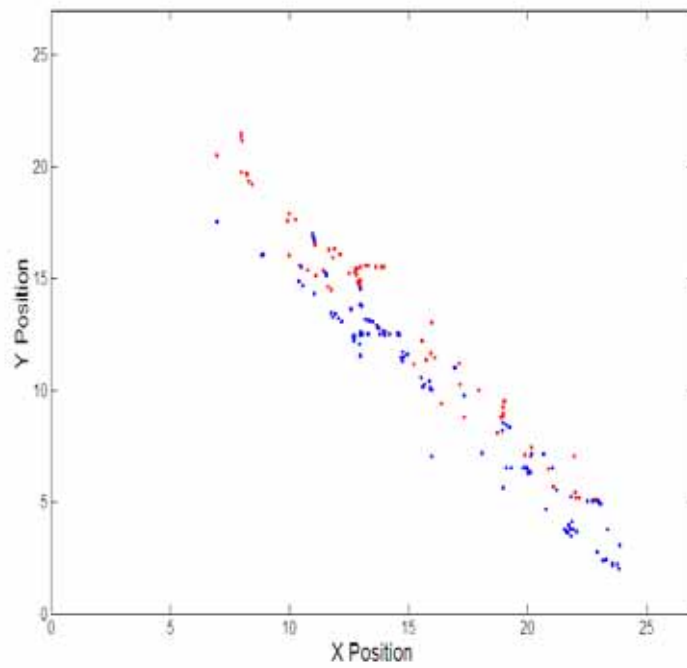


Figure 6.11 Distribution of particles at $t = 1.6s$ for $f = 0.2813$

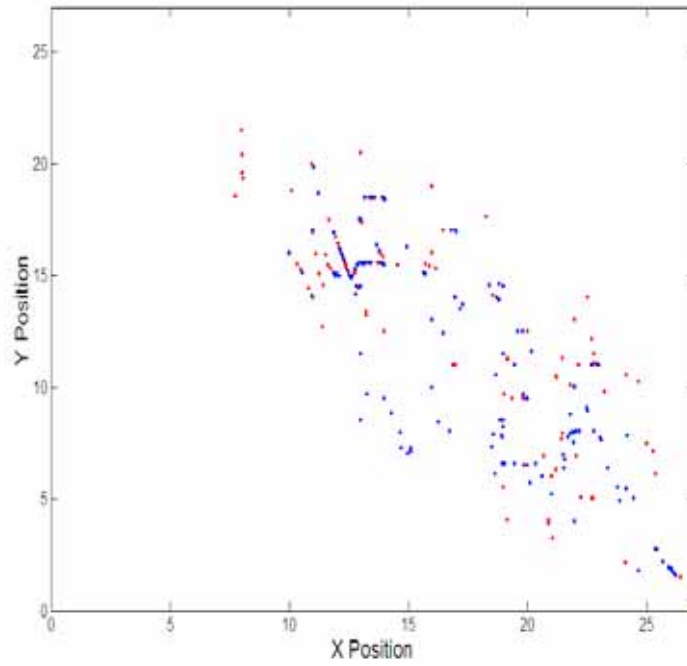


Figure 6.12 Distribution of particles at $t = 1.6s$ for $f = 1.125$

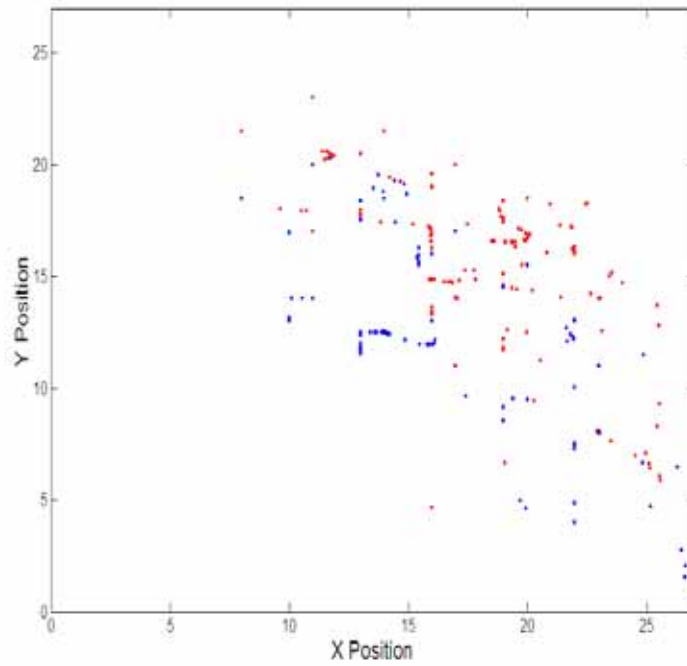


Figure 6.13 Distribution of particles at $t = 1.6s$ for $f = 1.9687$

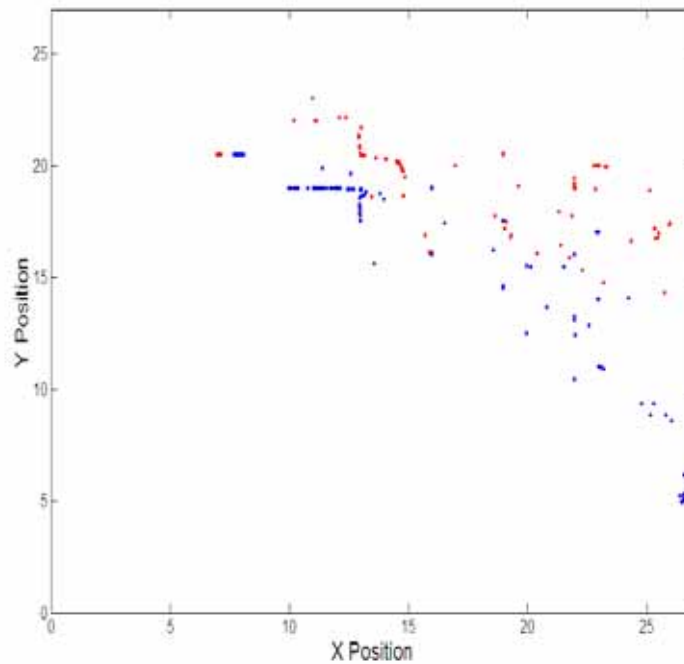


Figure 6.14 Distribution of particles at $t = 1.6s$ for aperiodic filling

6.1.2 Entropy study

To quantitatively study the mixing, the entropic plot for $S_{\text{location}}(\text{species})$, $S(\text{locations})$ and S are given in Figure 6.15 - 6.23. It would be very helpful to understand the best Entropy values we can get for mixing 261 red and 261 blue particles. By evenly distributing one red particle and one blue particle into one bin; with a total of 261 bins, we have the best condition. The best $S_{\text{location}}(\text{species})$ (Normalized), $S(\text{locations})$ and S values are 1, 5.5645, and 6.2577 respectively. Also the minimum value we can get for $S_{\text{location}}(\text{species})$ (Normalized) is 0, while we get the initial values for $S(\text{locations})$ and S is 2.0721.

6.1.2.1 $d_1 = 5.4\text{mm}$ and $d_2 = 5.4\text{mm}$

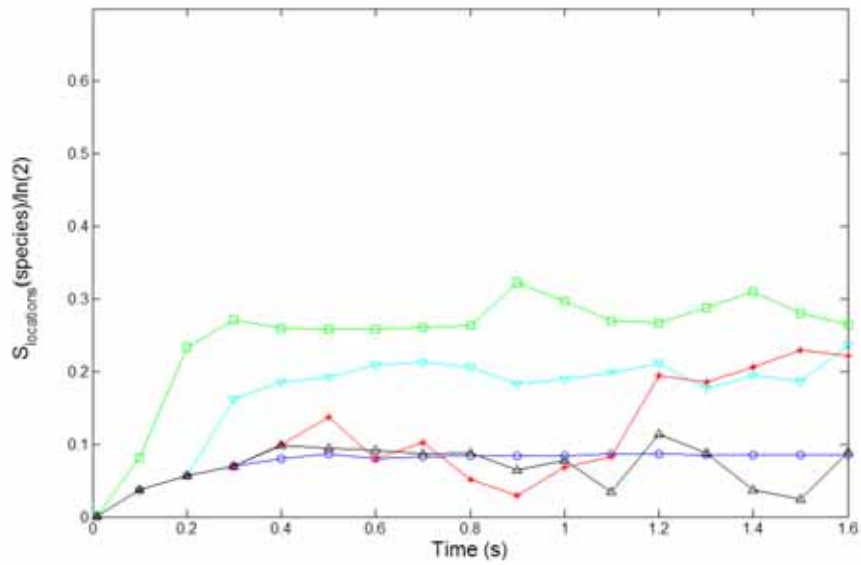


Figure 6.15 $S_{\text{locations}}(\text{species})/\ln(2)$ vs. time for left gate filling (blue) and two gates filling with $f=0.02813$ (green), $f=1.125$ (cyan), $f=1.9687$, (red), aperiodic (black)

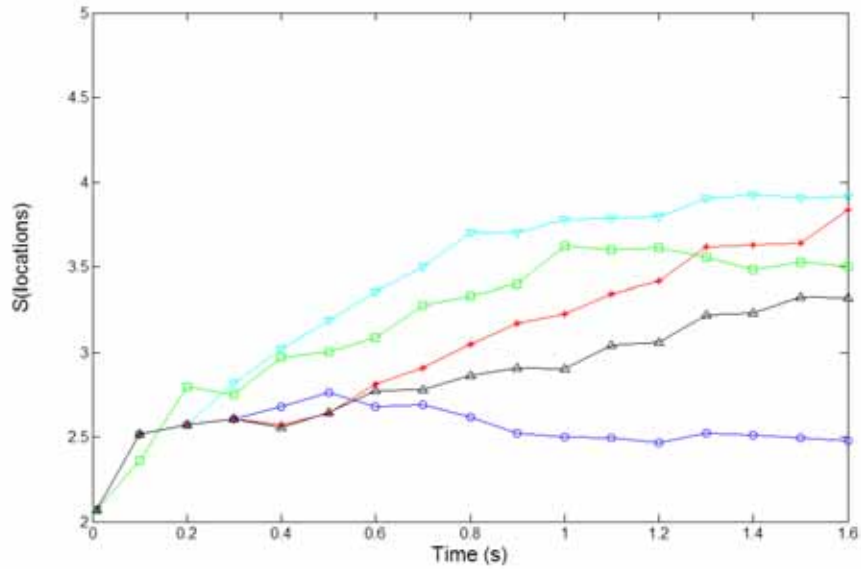


Figure 6.16 $S(\text{locations})$ vs. time for left gate filling (blue) and two gates filling with $f=0.02813$ (green), $f=1.125$ (cyan), $f=1.9687$, (red), aperiodic (black)

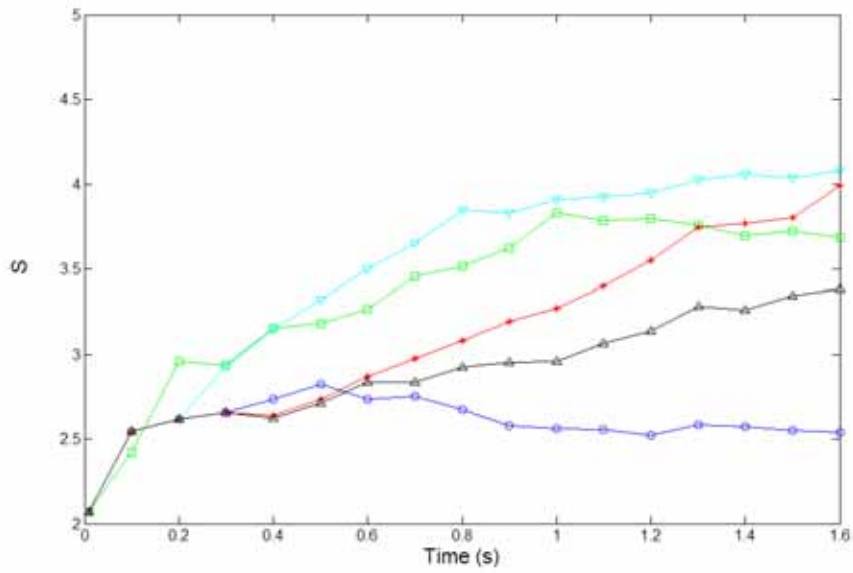


Figure 6.17 S vs. time for left gate filling (blue) and two gates filling with $f=0.02813$ (green), $f=1.125$ (cyan), $f=1.9687$ (red), and aperiodic (black)

6.1.2.2 $d1 = 5.4\text{mm}$ and $d2 = 7.56\text{mm}$

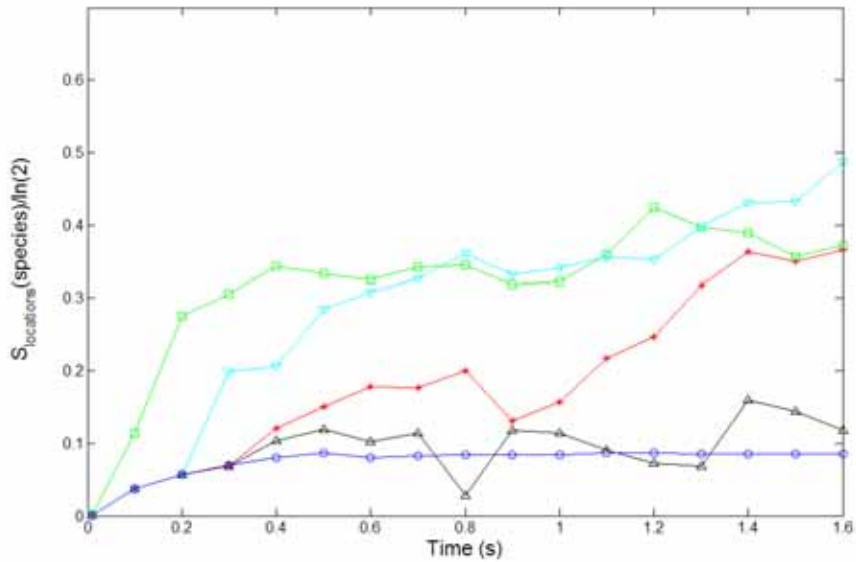


Figure 6.18 $S_{\text{locations}}(\text{species})/\ln(2)$ vs. time for left gate filling (blue) and two gates filling with $f=0.02813$ (green), $f=1.125$ (cyan), $f=1.9687$ (red), aperiodic (black)

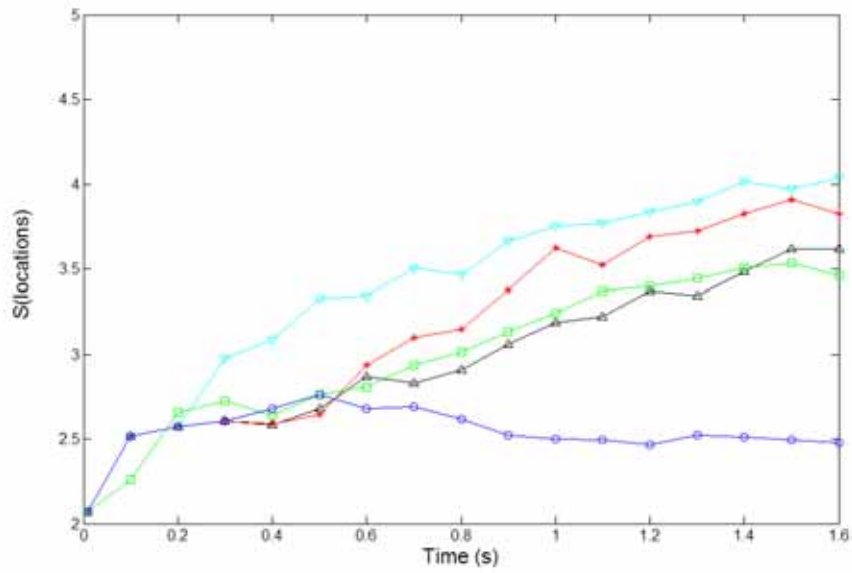


Figure 6.19 $S(\text{locations})$ vs. time for left gate filling (blue) and two gates filling with $f=0.02813$ (green), $f=1.125$ (cyan), $f=1.9687$, (red), aperiodic (black)

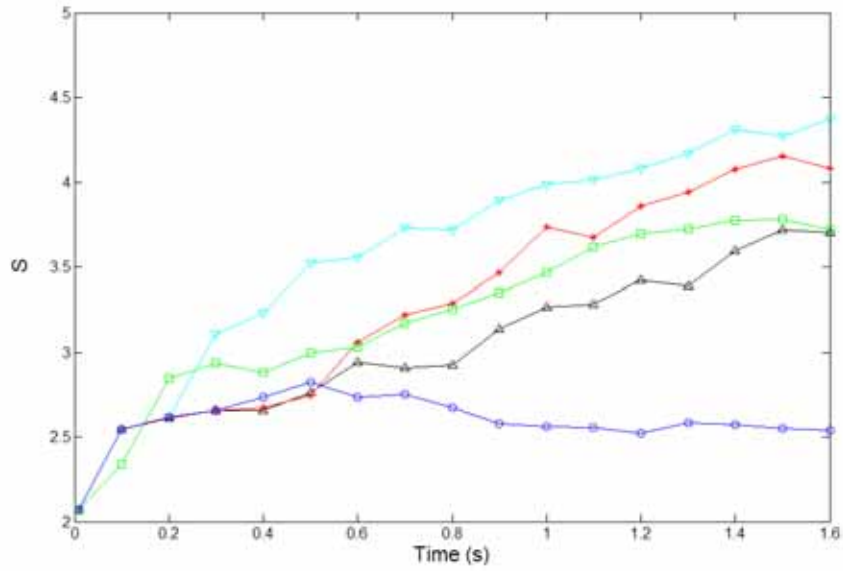


Figure 6.20 S vs. time for left gate filling (blue) and two gates filling with $f=0.02813$ (green), $f=1.125$ (cyan), $f=1.9687$ (red), and aperiodic (black)

6.1.2.3 $d1 = 7.56\text{mm}$ and $d2 = 7.56\text{mm}$

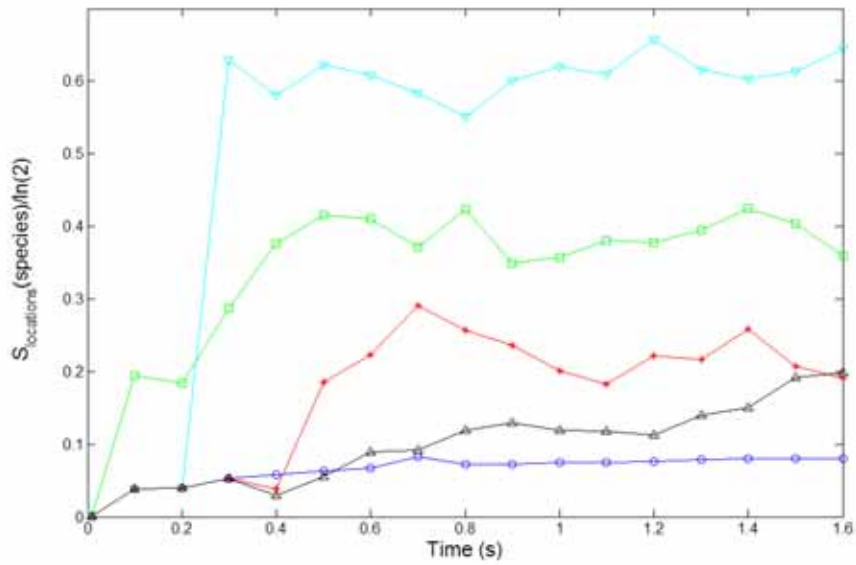


Figure 6.21. $S_{\text{locations}}(\text{species})/\ln(2)$ vs. time for left gate filling (blue) and two gates filling with $f=0.02813$ (green), $f=1.125$ (cyan), $f=1.9687$, (red), aperiodic (black)

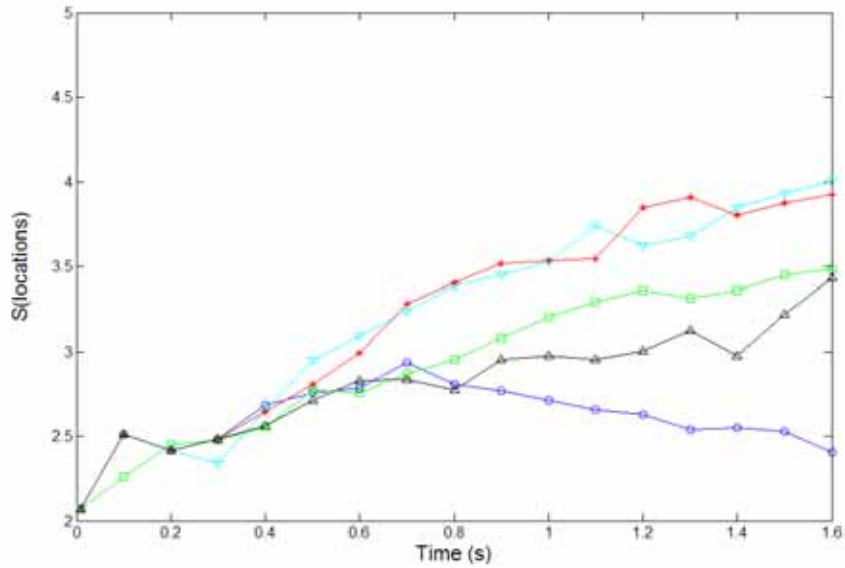


Figure 6.22 $S(\text{locations})$ vs. time for left gate filling (blue) and two gates filling with $f=0.02813$ (green), $f=1.125$ (cyan), $f=1.9687$, (red), aperiodic (black)

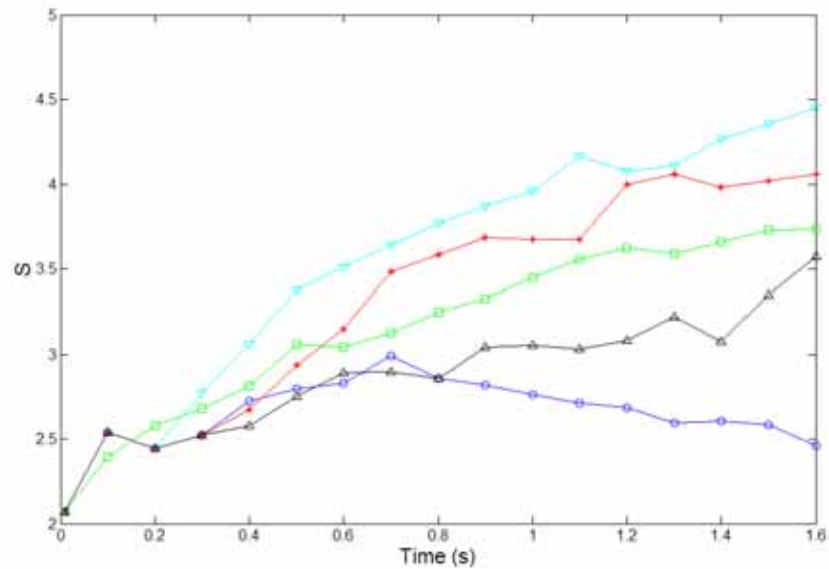


Figure 6.23 S vs. time for left gate filling (blue) and two gates filling with $f=0.02813$ (green), $f=1.125$ (cyan), $f=1.9687$ (red), and aperiodic (black)

6.1.2.4 Analysis of entropy

In general, the entropy for one gate filling is the smallest, which confirms our observation that it has the worst mixing. The f value is a key factor to entropy. Low value of f has the worst mixing. Aperiodic filling is not the best case in the study. It is in contrast with previous studies on aperiodic flow. This means here aperiodic flow no longer provides more uniform mixing than periodic filling. Though carefully selected aperiodic flows could get good results. This is not a surprise at all due to that the totally different flow characteristics. Filling the empty cavity will not generate any periodic points due to no returning flow, and since the primary function of the aperiodic flow is to break the periodic points, so that the aperiodic flow will not necessarily better than periodic flow.

6.1.2.5 Entropy as a function of f

Design-Expert, commercial software used for DOE study, is used to analyze the final value of Entropy. A quadratic model is chosen to fit the data since it is nonlinear in nature. The DOE result is shown in Table 6.1. All the values are obtained at $t = 1.6s$. N is the number of periods.

Factor 1		Factor 2	Response 1	Response 2	Response 3	Response 4
f	n	d1, d2	$S_{\text{location}}(\text{species})$	$S(\text{locations})$	S	Stretch
Left		5.4	0.0849	2.4788	2.5377	-0.2705
0.2813	16	5.4, 5.4	0.2651	3.501	3.6848	2.3174
1.125	4	5.4, 5.4	0.2363	3.9146	4.0784	2.0678
1.9687	2.3	5.4, 5.4	0.2223	3.8363	3.9904	1.6413
Aperiodic		5.4, 5.4	0.0887	3.3189	3.3804	1.3465
Left		5.4	0.0849	2.4788	2.5377	-0.2705
0.2813	16	5.4, 7.56	0.3719	3.4597	3.7175	2.4422
0.5625	8	5.4, 7.56	0.2998	3.6852	3.8930	2.2922
0.8438	5.3	5.4, 7.56	0.5563	3.8790	4.2647	2.4722
1.125	4	5.4, 7.56	0.4874	4.0363	4.3742	2.3462
1.4063	3.2	5.4, 7.56	0.3791	3.9536	4.2164	-
1.9687	2.3	5.4, 7.56	0.3661	3.8248	4.0786	1.9637
Aperiodic		5.4, 7.56	0.118	3.6185	3.7003	1.6465
Left		7.56	0.0797	2.4051	2.4604	0.4688
0.2813	16	7.56, 7.56	0.3591	3.4852	3.7341	2.4649
0.5625	8	7.56, 7.56	0.3231	3.7642	3.9882	-
0.8438	5.3	7.56, 7.56	0.6835	3.8628	4.3366	-
1.125	4	7.56, 7.56	0.6441	4.0042	4.4507	2.4227
1.9687	2.3	7.56, 7.56	0.1913	3.9264	4.0591	2.1177
Aperiodic		7.56, 7.56	0.1984	3.4344	3.5719	1.8192

Table 6.1 DOE result for irregular bump pattern

One gate filling has the lowest entropic values. Two gates filling has much higher entropic values. The one factor plots for $S_{\text{location}}(\text{species})$, $S(\text{locations})$, and S with respect to f between 0.02813 and 1.9687 are shown in Figure 6.24 – 6.26 respectively. The red curve is for $d1 = 5.4\text{mm}$ and $d2 = 5.4\text{mm}$; the blue curve is for $d1 = 5.4\text{mm}$ and $d2 = 7.56\text{mm}$; the green curve is for $d1 = 7.56\text{mm}$ and $d2 = 7.56\text{mm}$. It is clear that f is critical to the mixing. Neither high nor low f will result in good mixing. This is because at low f , there is not enough movement to stretch the particles, so that the particles are trapped in a narrow strip and therefore poor mixing. On the other hand, at high f , there is not enough alternating numbers of two gates filling, for example at $f = 1.9687$ only two complete cycles is observed, so that the mixing is not good. The $S(\text{locations})$ and S values are generally higher for larger f than for smaller f . This could be understood by the longer distance traveled by the particles for each gate filling at larger f . There exists an f value that can achieve highest entropic value and thus the best mixing. The best mixing is obtained at f around 0.8 and 1.2.

To exam in more details for f around 1, we simulated and calculated entropy at $f = 0.5625, 0.8437, \text{ and } 1.4063$ for $d1 = 5.4\text{mm}, d2 = 7.56\text{mm}$. The results are recorded in Table 6.1 and $S_{\text{location}}(\text{species})$ as a function of f is plotted in Figure 6.27, $S(\text{locations})$ and S as a function of f is plotted in Figure 6.28. From Figure 6.27 we can see that there is a critical value of f between around 0.84, above this value, the mixing is substantially improved. This is very similar to Zerafati's f_c , which is between 0.58 and 1.16 [Zerafati 94]. Here different geometries and different flow result in a similar f_c value further proved that this critical f value is a characteristic of chaotic flow. The entropic values

drops at high f could mostly result from the low number of periods.

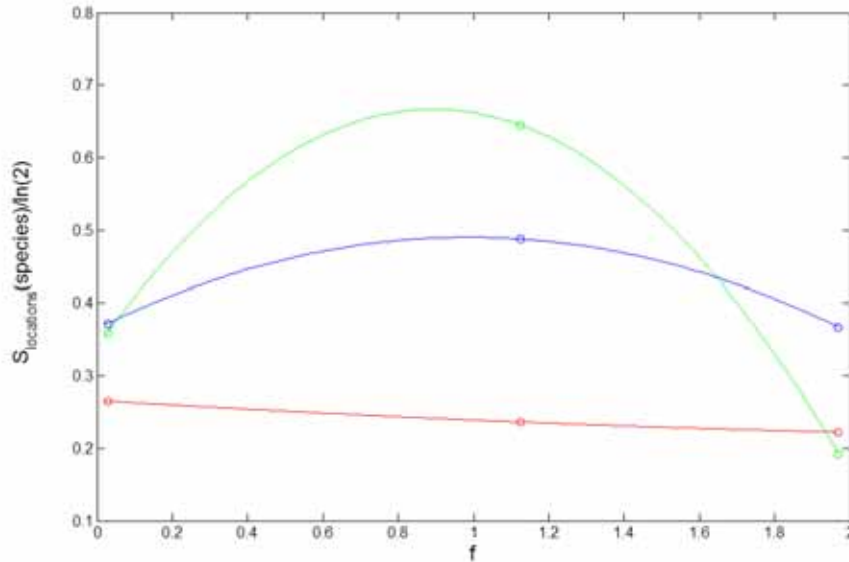


Figure 6.24 $S_{\text{location}}(\text{species})$ vs. f , red: $d1 = 5.4\text{mm}$, $d2 = 5.4\text{mm}$; blue: $d1 = 5.4\text{mm}$, $d2 = 7.56\text{mm}$; green: $d1 = 7.56\text{mm}$, $d2 = 7.56\text{mm}$

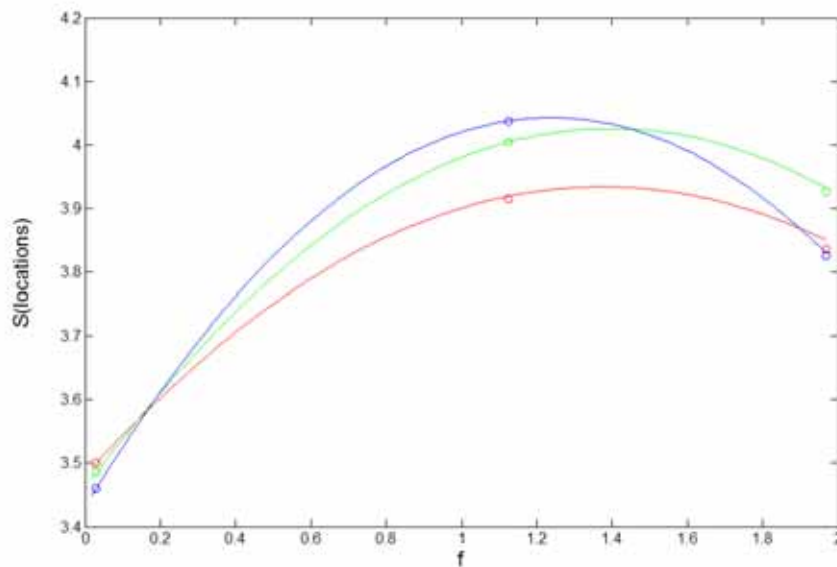


Figure 6.25 $S(\text{locations})$ vs. f , red: $d1 = 5.4\text{mm}$, $d2 = 5.4\text{mm}$; blue: $d1 = 5.4\text{mm}$, $d2 = 7.56\text{mm}$; green: $d1 = 7.56\text{mm}$, $d2 = 7.56\text{mm}$

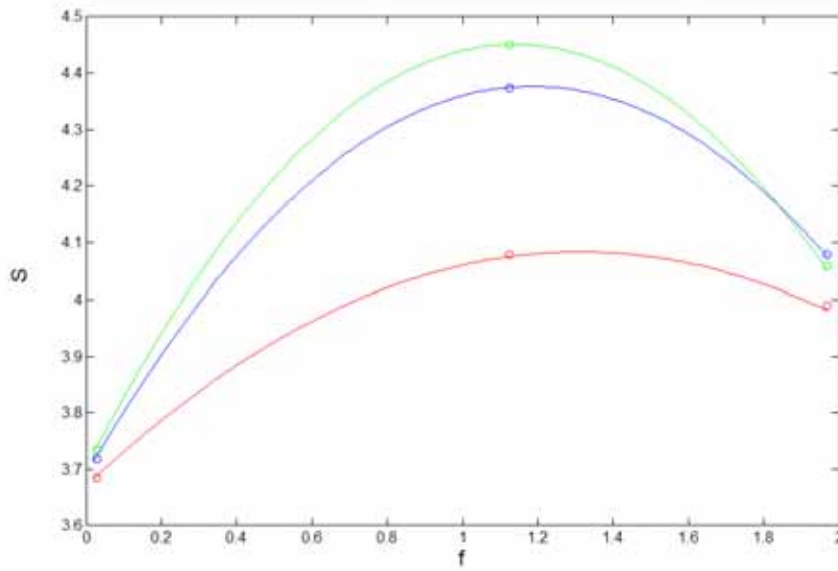


Figure 6.26 S vs. f , red: $d1 = 5.4\text{mm}$, $d2 = 5.4\text{mm}$; blue: $d1 = 5.4\text{mm}$, $d2 = 7.56\text{mm}$;
green: $d1 = 7.56\text{mm}$, $d2 = 7.56\text{mm}$

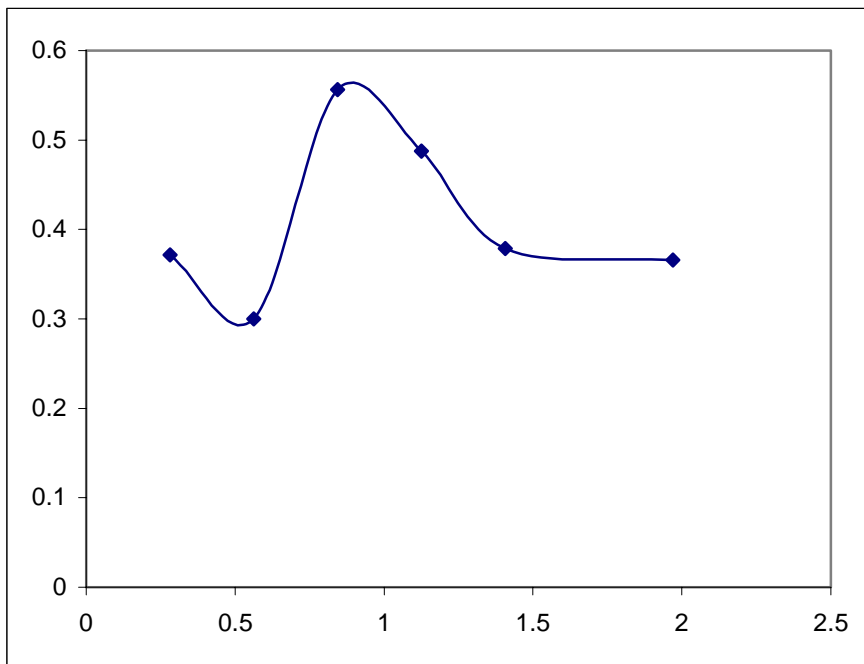


Figure 6.27 $S_{\text{location}}(\text{species})$ vs. f , $d1 = 5.4\text{mm}$, $d2 = 7.56\text{mm}$

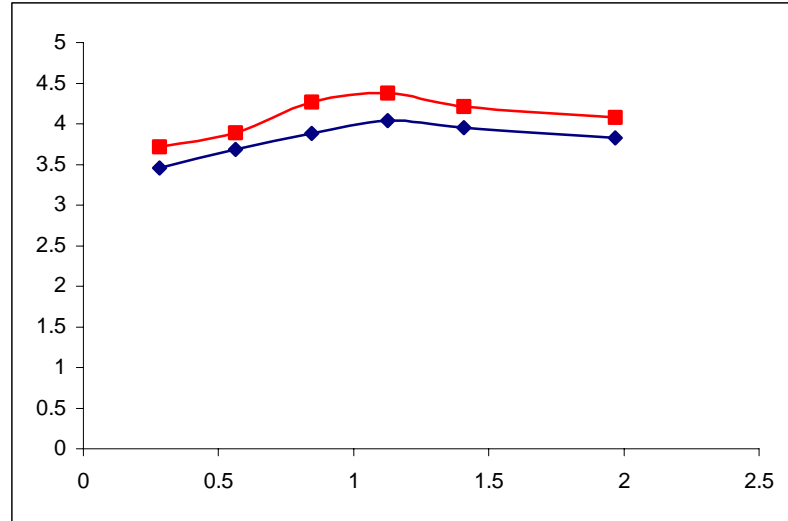


Figure 6.28 S(locations) (blue) and S (red) vs. f , $d1 = 5.4\text{mm}$, $d2 = 7.56\text{mm}$

S(locations) and S on the other hand show still higher values at higher f . This indicates that these two parameters do not depend on the number of periods.

6.1.2.6 Effects of $d1$ and $d2$

From the figures we can see that $d1$ and $d2$ play a very important role too. All entropic values are the smallest for $d1 = 5.4\text{mm}$ and $d2 = 5.4\text{mm}$. The best $S_{\text{location}}(\text{species})$ and S values occur at $d1 = 7.56\text{mm}$ and $d2 = 7.56\text{mm}$. While the best S(locations) value occurs at $d1 = 5.4\text{mm}$ and $d2 = 7.56\text{mm}$.

To see the effects of $d1$ and $d2$ on the critical value of f we simulated and calculated Entropy at $f = 0.5625$ and 0.8437 for $d1 = 7.56\text{mm}$, $d2 = 7.56\text{mm}$. The results are recorded in Table 6.1 and $S_{\text{location}}(\text{species})$ as a function of f is plotted in Figure 6.29. S(locations) and S as a function of f are plotted in Figure 6.30. Figure 6.29 shows a critical value of f around 0.84 which is the same as in the case of $d1 = 5.4\text{mm}$ and $d2 = 7.56\text{mm}$.

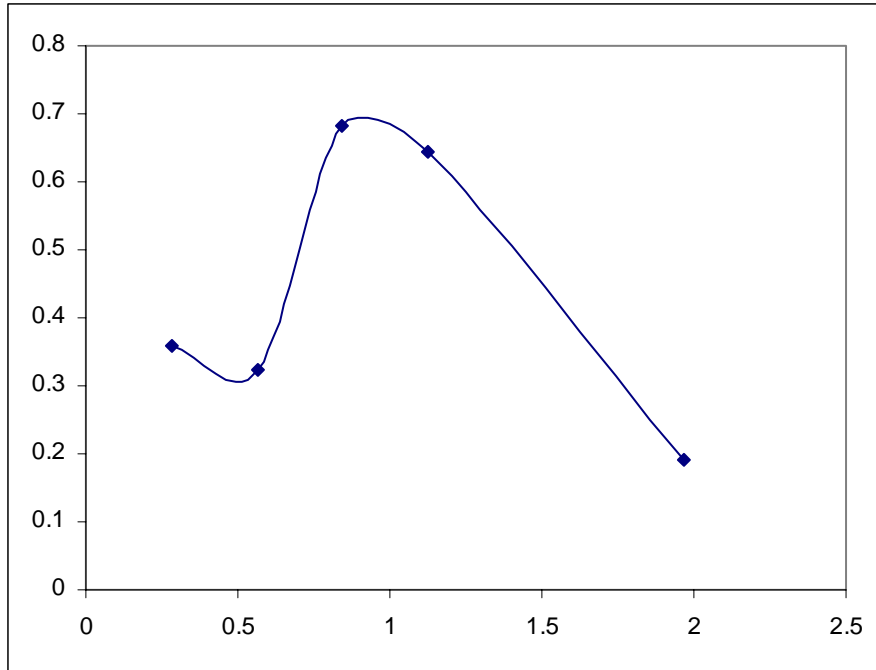


Figure 6.29 $S_{\text{location}}(\text{species})$ vs. f , $d1 = 7.56\text{mm}$, $d2 = 7.56\text{mm}$

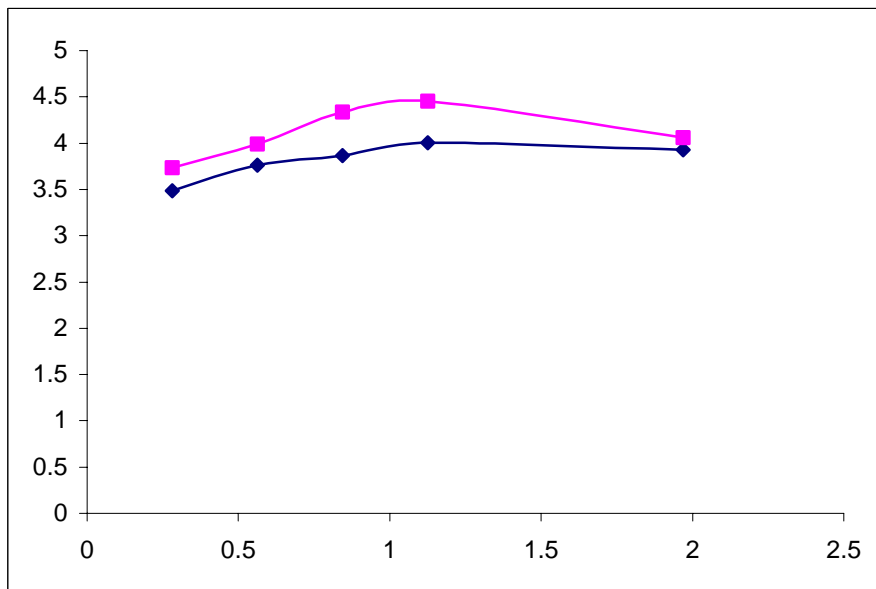


Figure 6.30 $S(\text{locations})$ (blue) and $S(\text{red})$ vs. f , $d1 = 7.56\text{mm}$, $d2 = 7.56\text{mm}$

6.1.2.7 Compare with one gate filling

As an example, we look at entropy with $d1 = 7.56\text{mm}$ and $d2 = 7.56\text{mm}$. The maximum value occurs at approximately $f = 0.84$, and at this f the $S_{\text{location}}(\text{species})$ has increased 8.58 times compared to one gate filling, as shown in Equation (6.1). For $S(\text{locations})$ and S , we will consider the relative increase since the initial $S(\text{locations})$ and S is 2.072. With $d1 = 5.4\text{mm}$ and $d2 = 7.56\text{mm}$, the relative increase is 5.8 times compared to one gate filling, as shown in Equation (6.2).

$$\frac{0.6835}{0.0797} = 8.58 \quad (6.1)$$

$$\frac{4.0363 - 2.072}{2.4788 - 2.072} = 5.8 \quad (6.2)$$

6.1.3 Stretching analysis showing chaotic flow in two gates filling

Figure 6.31 – 6.33 show stretching, mean $\log(\lambda)$, evolution with time in the cavity of filling with gates $d1 = 5.4\text{mm}$ $d2 = 5.4\text{mm}$, $d1 = 5.4\text{mm}$ $d2 = 7.5\text{mm}$, and $d1 = 7.5\text{mm}$ $d2 = 7.5\text{mm}$ respectively. In all the three cases, the stretching of one gate filling is flat or decreasing which means the stretching is linear or even no stretching. All two gates filling have nearly linear increasing of mean $\log(\lambda)$, which indicates the exponential stretching. This is the evidence of chaotic flow inside the cavity. Chaotic flow can dramatically increase the mixing.

Figure 6.34 shows stretch as a function of f . As f increases the stretch is decreasing.

This is because the smaller f has more frequent reorientation thus the higher stretching. Since the flow tends to minimize the stretching, whenever a new flow direction occurs, the stretching will be maximized and then gradually decreasing. So the smaller f changes flow direction more often and maximize the stretching.

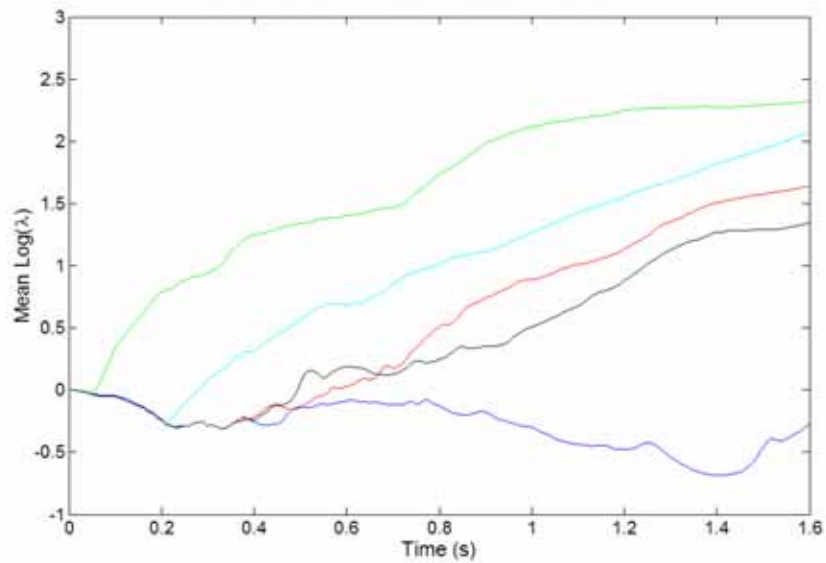


Figure 6.31 Mean λ for Left gate (blue) and two gates $f=0.02813$ (green), $f=1.125$ (cyan), $f=1.9687$ (red), aperiodic (black); $d_1 = 5.4\text{mm}$, $d_2 = 5.4\text{mm}$

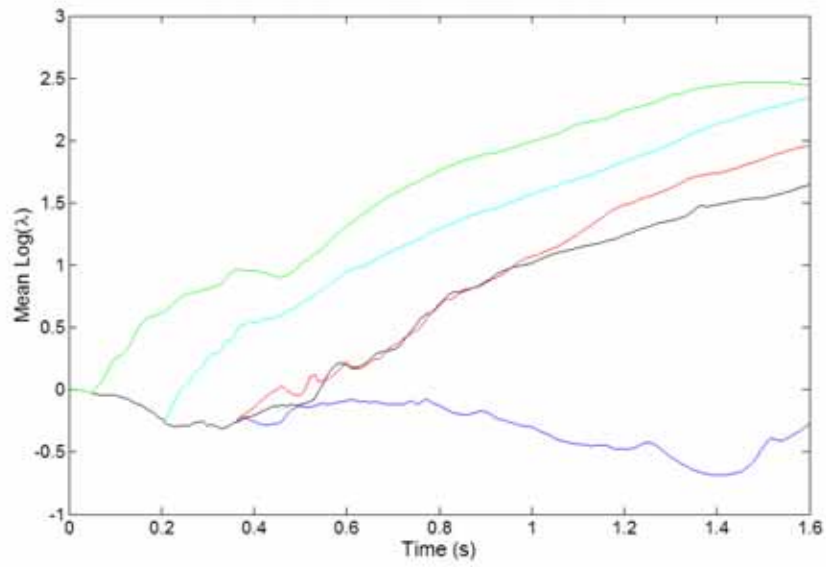


Figure 6.32 Mean λ for Left gate (blue) and two gates $f=0.02813$ (green), $f=1.125$ (cyan), $f=1.9687$, (red), aperiodic (black); $d1 = 5.4\text{mm}$, $d2 = 7.56\text{mm}$

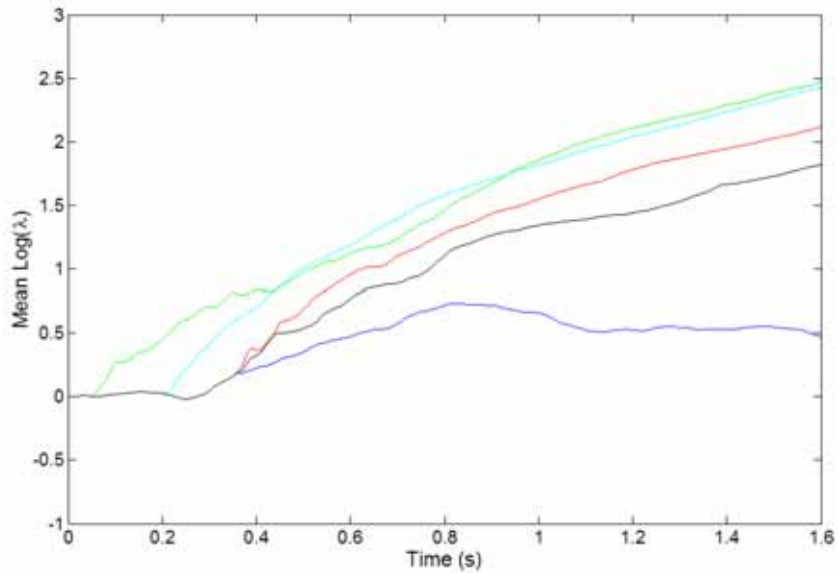


Figure 6.33 Mean λ for Left gate (blue) and two gates $f=0.0281$ (green), $f=1.125$ (cyan), $f=1.9687$, (red), aperiodic (black); $d1 = 7.56\text{mm}$, $d2 = 7.56\text{mm}$

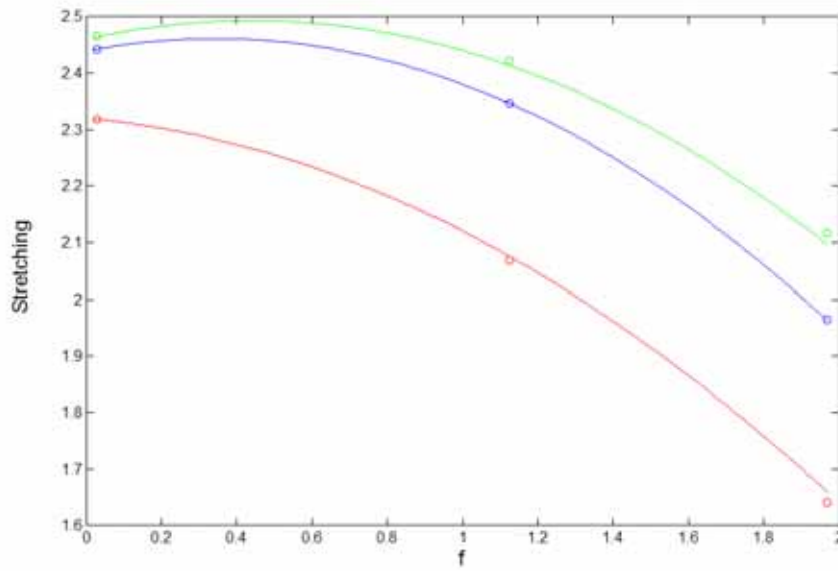


Figure 6.34 Stretching as a function of f , red: $d1 = 5.4\text{mm}$, $d2 = 5.4\text{mm}$; blue: $d1 = 5.4\text{mm}$, $d2 = 7.56\text{mm}$; green: $d1 = 7.56\text{mm}$, $d2 = 7.56\text{mm}$

Stretching is also governed by gate location. The largest stretching is obtained at $d1 = 7.56\text{mm}$ and $d2 = 7.56\text{mm}$, while the smallest stretching is obtained at $d1 = 5.4\text{mm}$ and $d2 = 5.4\text{mm}$. However, the maximum stretching happens at low f , while the best mixing occurs at mid f values. This means stretching is not a rigorous measure for mixing.

6.1.4 Conclusion

Two gates filling can generate chaotic flow, and much better mixing. The f value and $d1$, $d2$ values are important parameters to Entropy and stretching. The gates further away from each other will have the best results. But this distance will be restricted by the final packaging requirements on weld line, since we want to minimize the weld line too. There is a critical value of f around 0.84, above this value, the mixing is substantially

improved. In the case of $d1 = 7.56\text{mm}$ and $d2 = 7.56\text{mm}$, the maximum value of $S_{\text{location}}(\text{species})$ has increased 8.58 times compared to one gate filling. For $S(\text{locations})$ and S , the relative increase is 5.8 times compared to one gate filling when $d1 = 5.4\text{mm}$ and $d2 = 7.56\text{mm}$. All two gates filling have nearly linear increasing of mean $\log(\lambda)$, which indicates the exponential stretching. This is the evidence of chaotic flow inside the cavity.

6.2 Analysis of flow and mixing in cavity with regular bumps

This section discusses the effect of bump patterns. The regular bump pattern has been shown in Figure 4.3 in Chapter 4. Since we are only concerned with the difference between two grid patterns, the rest of the study only contains results of f equal to 0.2813, 1.125 and 1.9687. The same initial particle balls locations and the total number of particles were used as for stagger pattern.

6.2.1 Particle distribution

6.2.1.1 $d1 = 5.4\text{mm}$ and $d2 = 5.4\text{mm}$

The results of filling from left gate at $d1 = 5.4\text{mm}$ only is given in Figure 6.35. It is very similar to the stagger bump pattern that the particles are compressed closer and spread into very limited spaces. This demonstrates that single gate filling will have poor mixing regardless of the bump patterns. Figure 6.36 – 6.38 show two gates filling for $f = 0.2813$, 1.125, and 1.9687 respectively with $d1 = 5.4\text{mm}$ and $d2 = 5.4\text{mm}$. By looking at the final particle distributions, two gates filling have substantially improved the mixing.

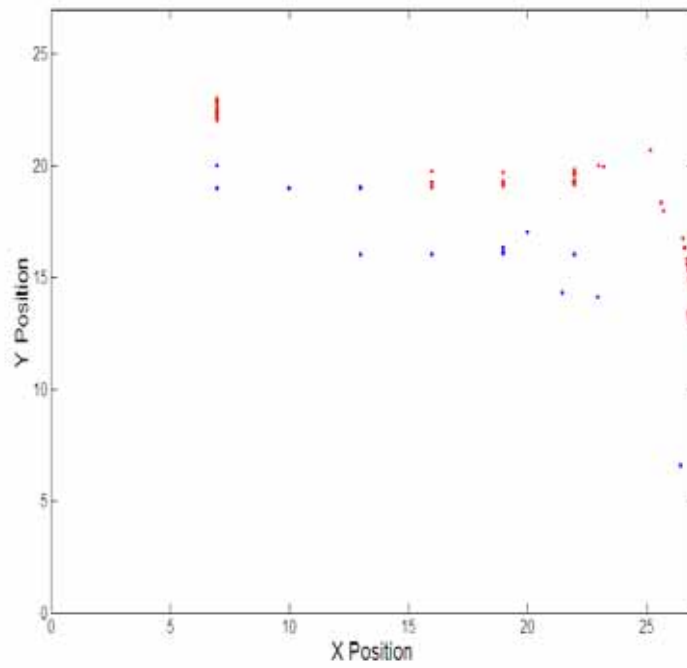


Figure 6.35 Distribution of particles at $t = 1.6$ s with left gate filling at $d_1 = 5.4$ mm

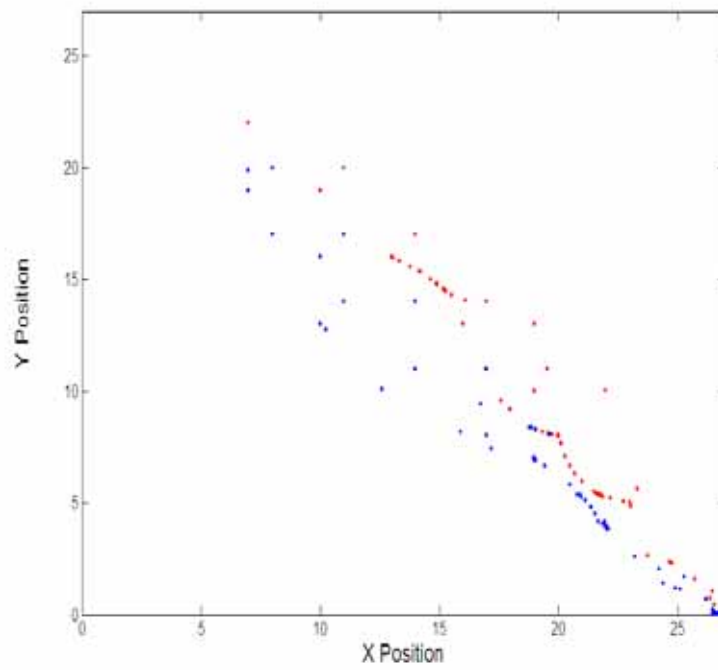


Figure 6.36 Distribution of particles at $t = 1.6$ s for $f = 0.2813$

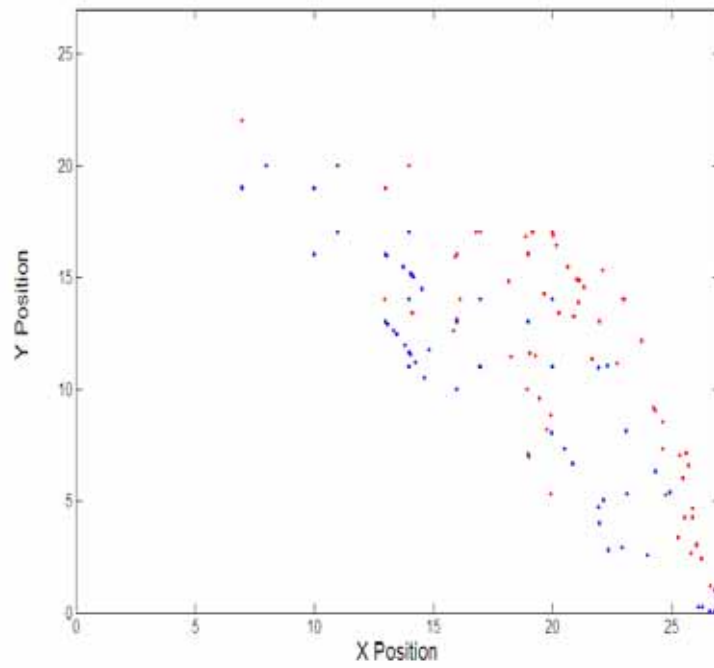


Figure 6.37 Distribution of particles at $t = 1.6s$ for $f = 1.125$

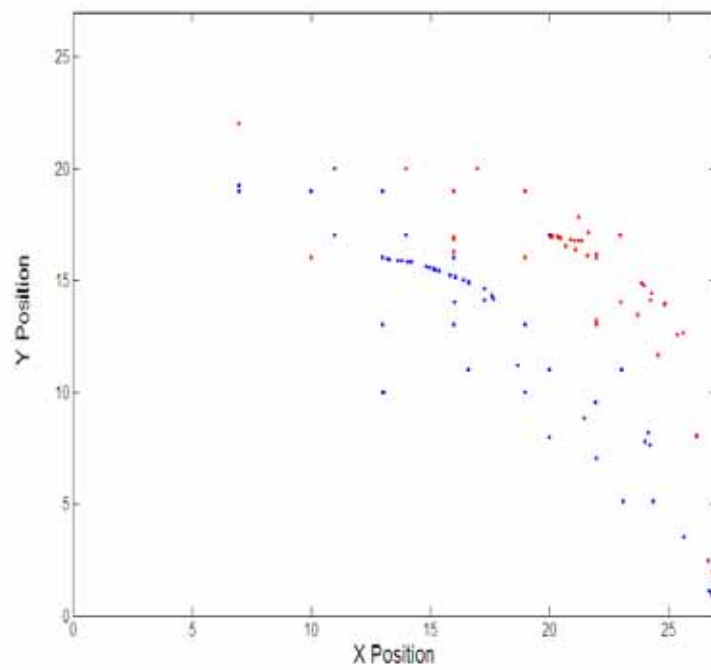


Figure 6.38 Distribution of particles at $t = 1.6s$ for $f = 1.9687$

6.2.1.2 $d1 = 5.4\text{mm}$ and $d2 = 7.56\text{mm}$

Figures 6.39 – 6.41 show two gates filling for $f = 0.2813$, 1.125, and 1.9687 respectively with $d1 = 5.4\text{mm}$ and $d2 = 7.56\text{mm}$.

6.2.1.3 $d1 = 7.56\text{mm}$ and $d2 = 7.56\text{mm}$

Figures 6.42 – 6.44 show two gates filling for $f = 0.2813$, 1.125, and 1.9687 respectively with $d1 = 7.56\text{mm}$ and $d2 = 7.56\text{mm}$.

By looking at the final particle distributions, it is clear that two gates filling have substantially improved the mixing for all the $d1$ and $d2$ combinations.

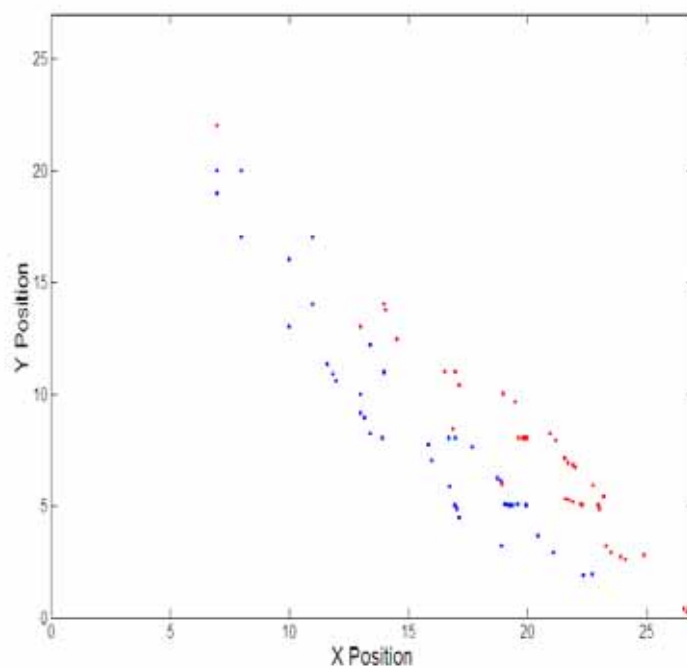


Figure 6.39 Distribution of particles at $t = 1.6\text{s}$ for $f = 0.2813$

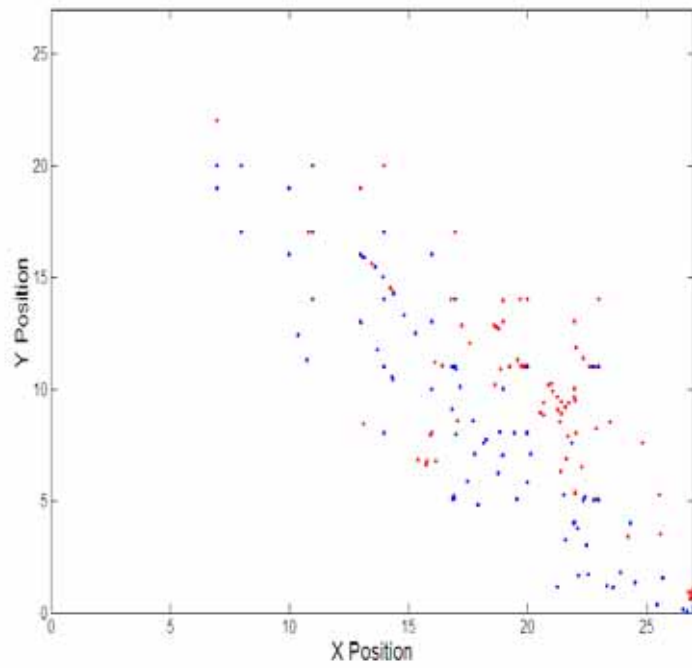


Figure 6.40 Distribution of particles at $t = 1.6s$ for $f = 1.125$

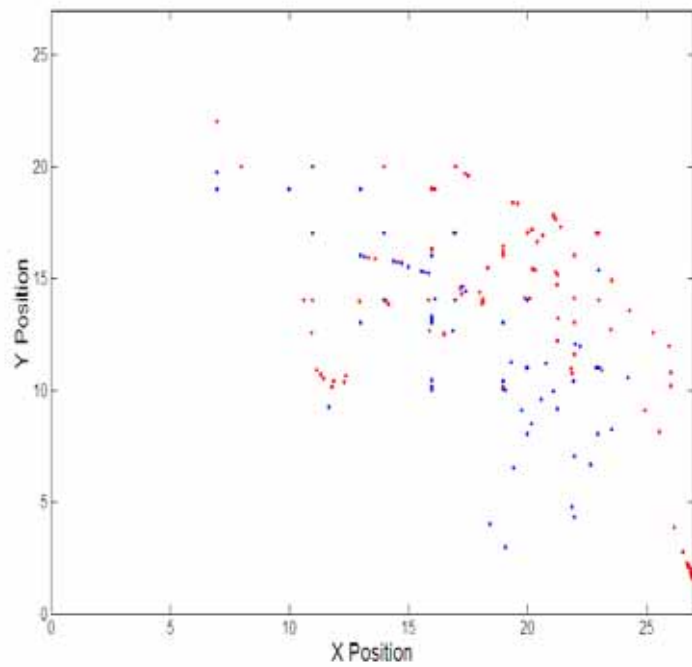


Figure 6.41 Distribution of particles at $t = 1.6s$ for $f = 1.9687$

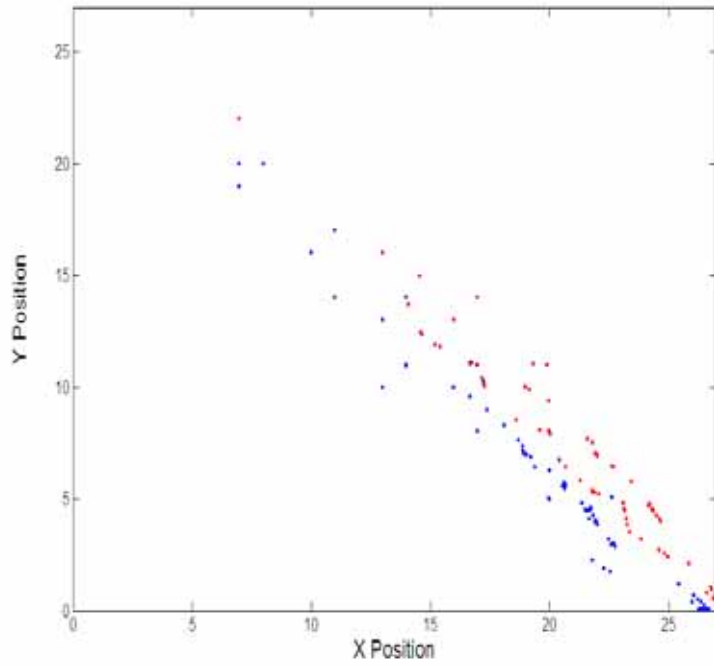


Figure 6.42 Distribution of particles at $t = 1.6s$ for $f = 0.2813$

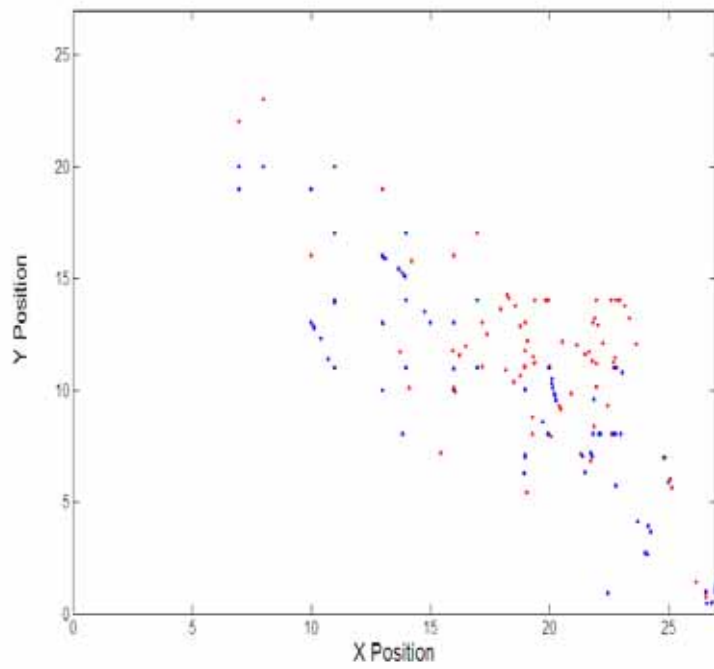


Figure 6.43 Distribution of particles at $t = 1.6s$ for $f = 1.125$

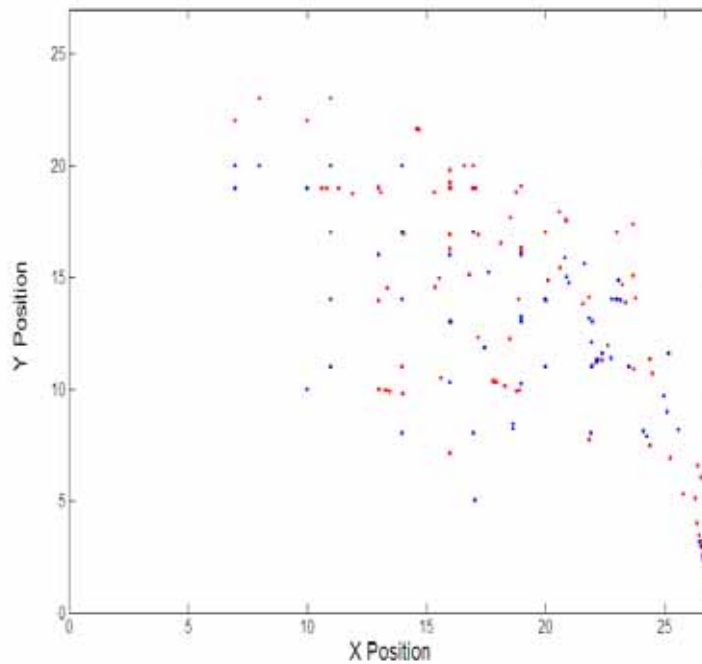


Figure 6.44 Distribution of particles at $t = 1.6s$ for $f = 1.9687$

6.2.2 Entropy

The Entropy function as a function of time is plotted in Figure 6.45 - 6.53 for $S_{\text{location}(\text{species})}$, $S(\text{locations})$, S and different gate locations. From the plots, we can see that the f value is a key factor to entropy. The same is true to the $d1$ and $d2$. Table 6.2 summarizes the simulation results for regular bump pattern. Figure 6.54 shows $S_{\text{location}(\text{species})}$ as a function of f for $d1 = 5.4\text{mm}$ and $d2 = 7.56\text{mm}$ obtained at $t = 1.6s$. Figure 6.55 shows the same plot as Figure 6.54 with all $S_{\text{location}(\text{species})}$ values obtained at the end of two periods. Figure 6.56 shows $S(\text{locations})$ and S as a function of f for $d1 = 5.4\text{mm}$ and $d2 = 7.56\text{mm}$. Here again we see that there is a critical value of f between 0.56 and 0.84, above this value, the mixing is substantially improved.

6.2.2.1 $d_1 = 5.4\text{mm}$ and $d_2 = 5.4\text{mm}$

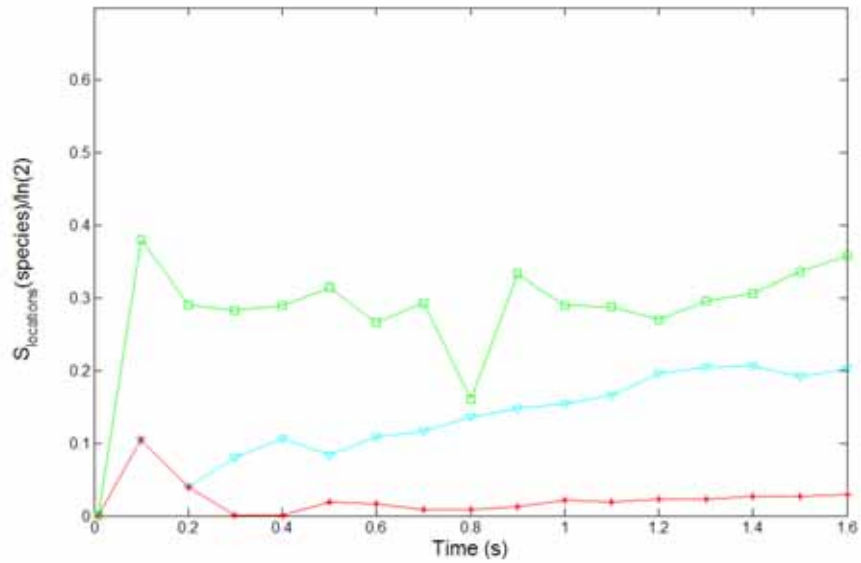


Figure 6.45 $S_{\text{locations}}(\text{species})/\ln(2)$ vs. time for two gates filling with $f = 0.02813$ (green), $f = 1.125$ (cyan), $f = 1.9687$ (red)

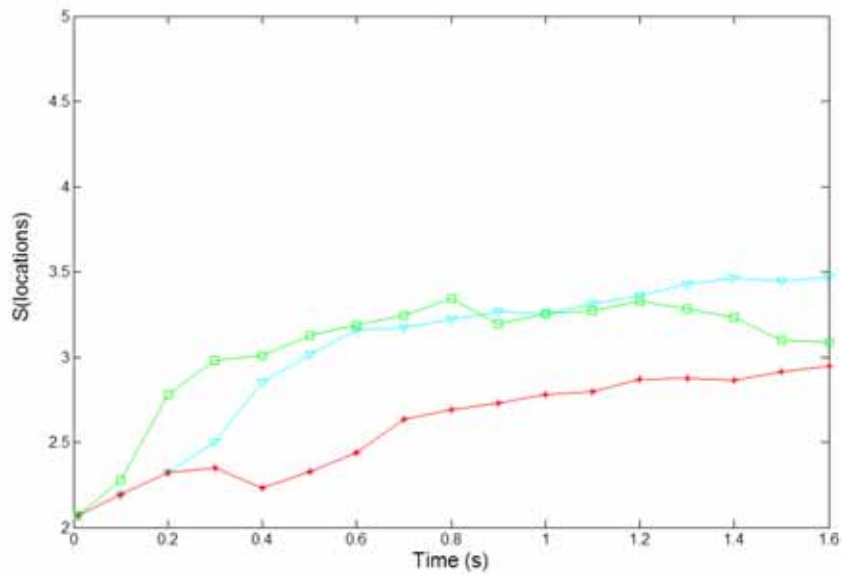


Figure 6.46 $S(\text{locations})$ vs. time for and two gates filling with $f = 0.02813$ (green), $f = 1.125$ (cyan), $f = 1.9687$ (red)

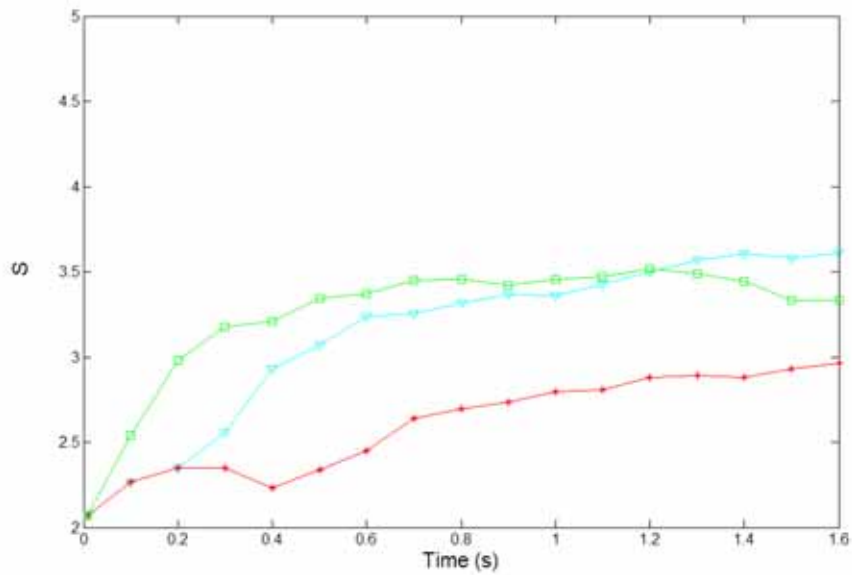


Figure 6.47 S vs. time for two gates filling with $f=0.02813$ (green), $f=1.125$ (cyan), $f=1.9687$ (red)

6.2.2.2 $d1 = 5.4\text{mm}$ and $d2 = 7.56\text{mm}$

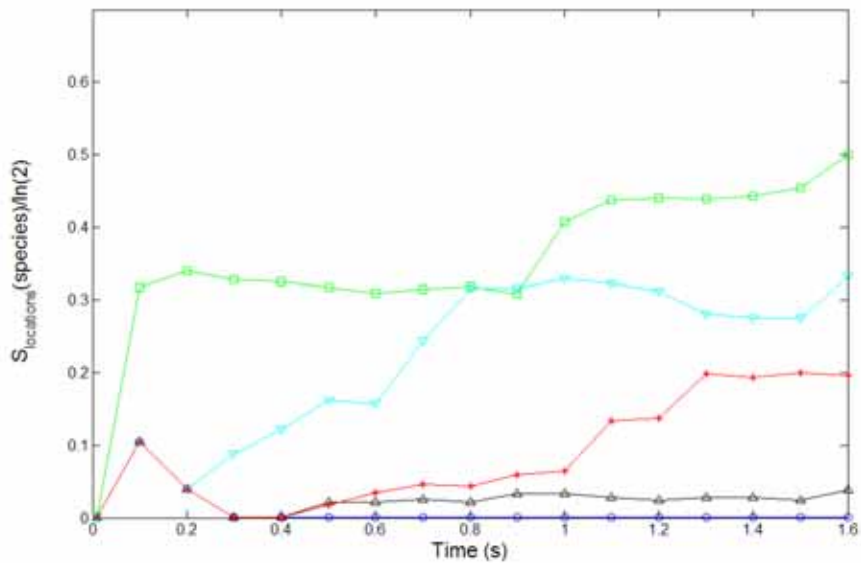


Figure 6.48 $S_{\text{locations}}(\text{species})/\ln(2)$ vs. time for left gate filling (blue) and two gates filling with $f=0.02813$ (green), $f=1.125$ (cyan), $f=1.9687$, (red), aperiodic (black)

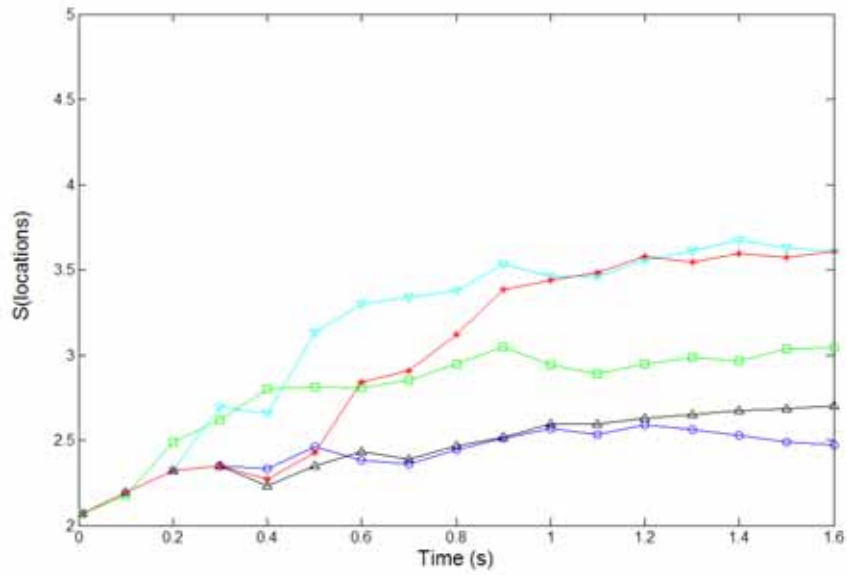


Figure 6.49 S(locations) vs. time for left gate filling (blue) and two gates filling with $f=0.02813$ (green), $f=1.125$ (cyan), $f=1.9687$, (red), aperiodic (black)

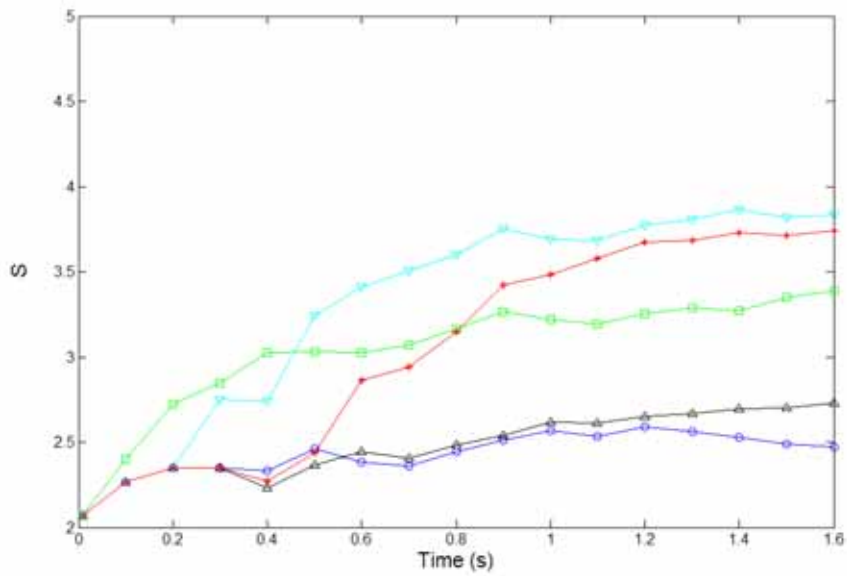


Figure 6.50 S vs. time for left gate filling (blue) and two gates filling with $f=0.02813$ (green), $f=1.125$ (cyan), $f=1.9687$ (red), and aperiodic (black)

6.2.2.3 $d1 = 7.56\text{mm}$ and $d2 = 7.56\text{mm}$

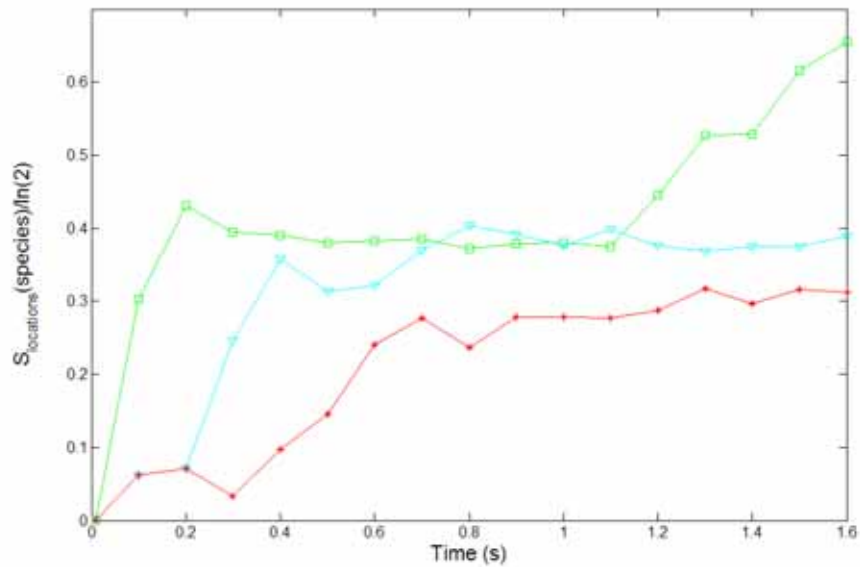


Figure 6.51 $S_{\text{locations}}(\text{species})/\ln(2)$ vs. time for two gates filling with $f = 0.02813$ (green), $f = 1.125$ (cyan), $f = 1.9687$ (red)

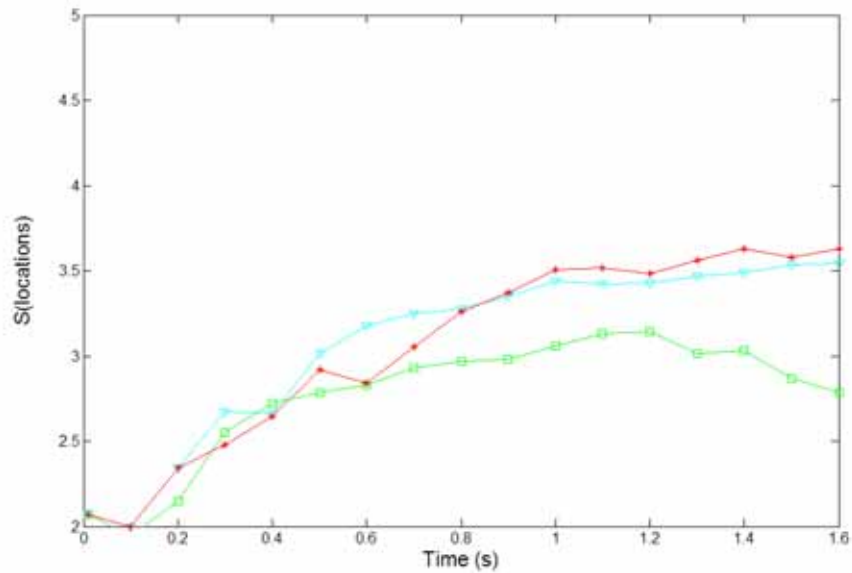


Figure 6.52 $S(\text{locations})$ vs. time for and two gates filling with $f = 0.02813$ (green), $f = 1.125$ (cyan), $f = 1.9687$ (red)

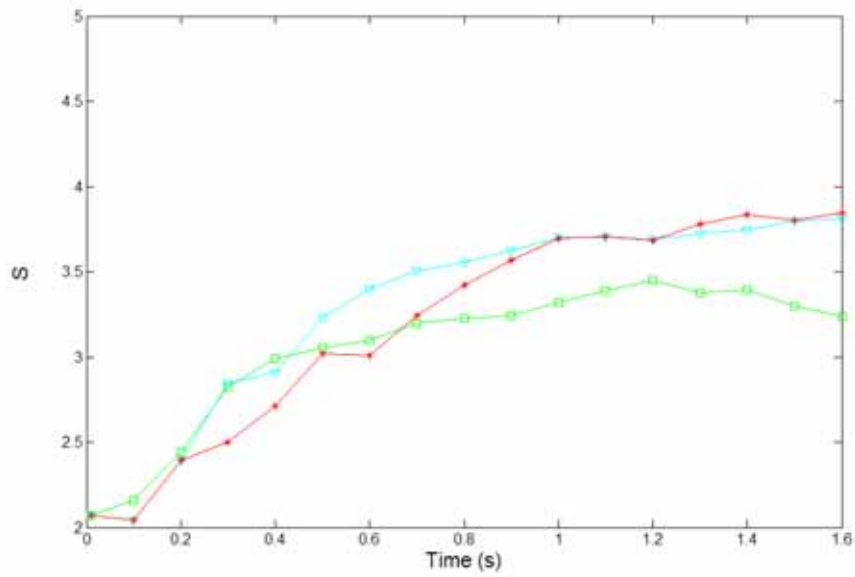


Figure 6.53 S vs. time for and two gates filling with $f = 0.02813$ (green), $f = 1.125$ (cyan), $f = 1.9687$ (red)

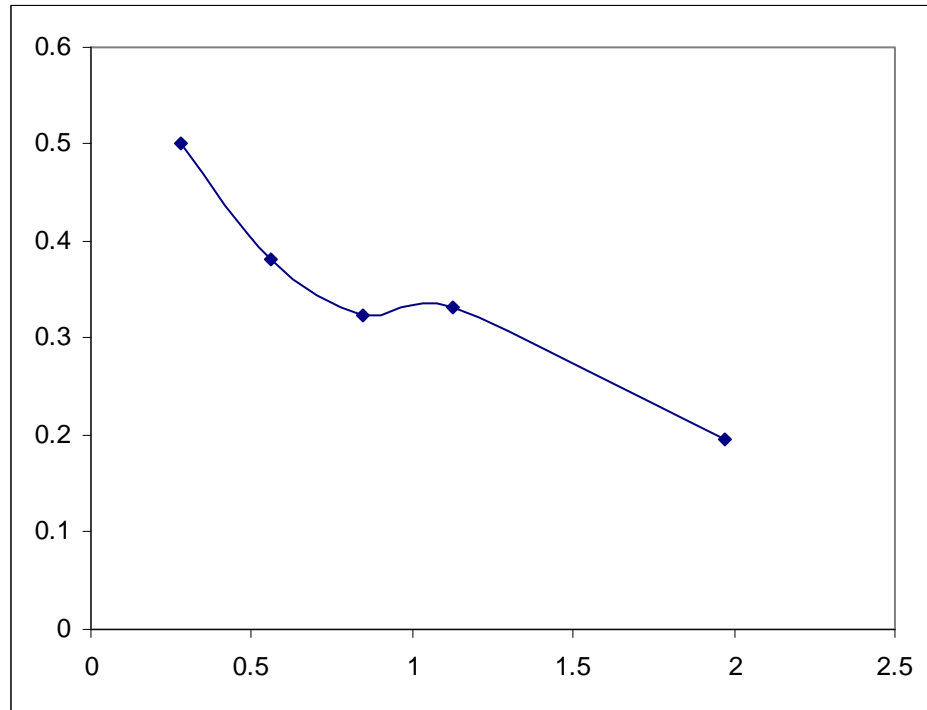


Figure 6.54 $S_{\text{location}}(\text{species})$ vs. f , $d1 = 5.4\text{mm}$, $d2 = 7.56\text{mm}$, $t = 1.6\text{s}$

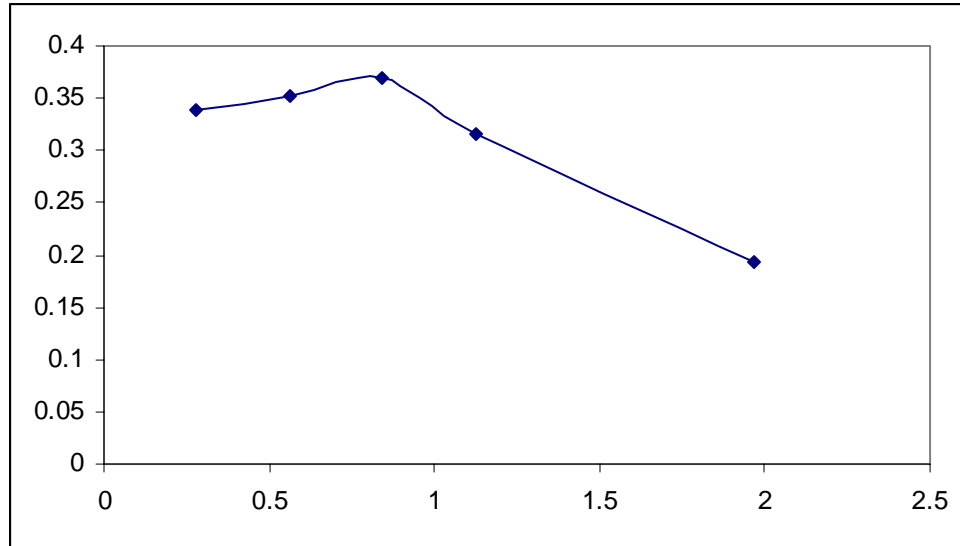


Figure 6.55 $S_{\text{location(species)}}$ vs. f , $d1 = 5.4\text{mm}$, $d2 = 7.56\text{mm}$, $n = 2$

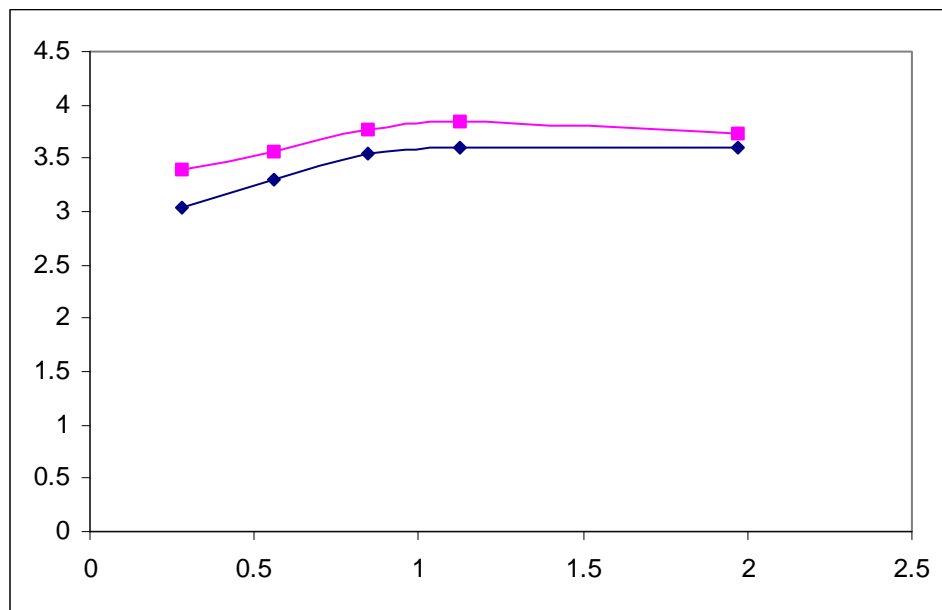


Figure 6.56 $S(\text{locations})$ (blue) and S (red) vs. f , $d1 = 5.4\text{mm}$, $d2 = 7.56\text{mm}$

6.2.2.4 Compare with stagger bump pattern

The average $S_{\text{location(species)}}$, $S(\text{locations})$, and S values are 0.33, 3.3, and 3.53 respectively. To compare with irregular bump pattern results, we calculate the average

$S_{\text{location}}(\text{species})$, $S(\text{locations})$, and S values to be 0.35, 3.78, and 4.02 respectively. There is no significant difference for $S_{\text{location}}(\text{species})$, but the $S(\text{locations})$ and S values are slightly lower than stagger bump pattern. But all these values are much larger than single gate filling, which are 0, 2.47, and 2.47 respectively for regular bump pattern.

Figure 6.57 shows $S_{\text{location}}(\text{species})$ as a function of f . Filling with $d1 = 5.4\text{mm}$ and $d2 = 5.4\text{mm}$, $d1 = 5.4\text{mm}$ and $d2 = 7.56\text{mm}$, $d1 = 7.56\text{mm}$ and $d2 = 7.56\text{mm}$ are shown in red, blue and green respectively, while stagger and regular pattern are indicated by circle and star respectively. The regular pattern results in an almost linear relation slightly higher values for the low f value. The stagger pattern gives the best results with medium f value. And the larger $d1$ and $d2$ results in a sharper curvature and higher values of $S_{\text{location}}(\text{species})$. This shows the strong effects of $d1$ and $d2$ on the mixing.

Factor 1	Factor 2	Response 1	Response 2	Response 3	Response 4
f	d1, d2	$S_{\text{location}}(\text{species})$	$S(\text{locations})$	S	Stretch
0.2813	5.4, 5.4	0.3585	3.0858	3.3343	1.9953
1.125	5.4, 5.4	0.2033	3.4685	3.6094	2.1734
1.9687	5.4, 5.4	0.0295	2.945	2.9655	1.4573
0.2813	5.4, 7.56	0.5004	3.0429	3.3898	1.9224
0.5625	5.4, 7.56	0.3805	3.2998	3.5635	2.2427
0.8438	5.4, 7.56	0.3241	3.5443	3.7689	2.3054
1.125	5.4, 7.56	0.3319	3.6055	3.8355	2.3403
1.9687	5.4, 7.56	0.1956	3.6037	3.7393	1.9967
0.2813	7.56, 7.56	0.6545	2.7852	3.2389	1.9242
1.125	7.56, 7.56	0.389	3.5436	3.8132	2.2776
1.9687	7.56, 7.56	0.3115	3.6302	3.8462	2.1871

Table 6.2 DOE results for regular bump pattern

Figure 6.58 and 6.59 show $S(\text{locations})$ and S as a function of f respectively. Filling with $d1 = 5.4\text{mm}$ and $d2 = 5.4\text{mm}$, $d1 = 5.4\text{mm}$ and $d2 = 7.56\text{mm}$, $d1 = 7.56\text{mm}$ and $d2 = 7.56\text{mm}$ are shown in red, blue and green respectively, while stagger and regular pattern are indicated by circle and star respectively. Both patterns have similar trend except for $d1 = 5.4\text{mm}$ and $d2 = 5.4\text{mm}$. The stagger pattern gives better results in general.

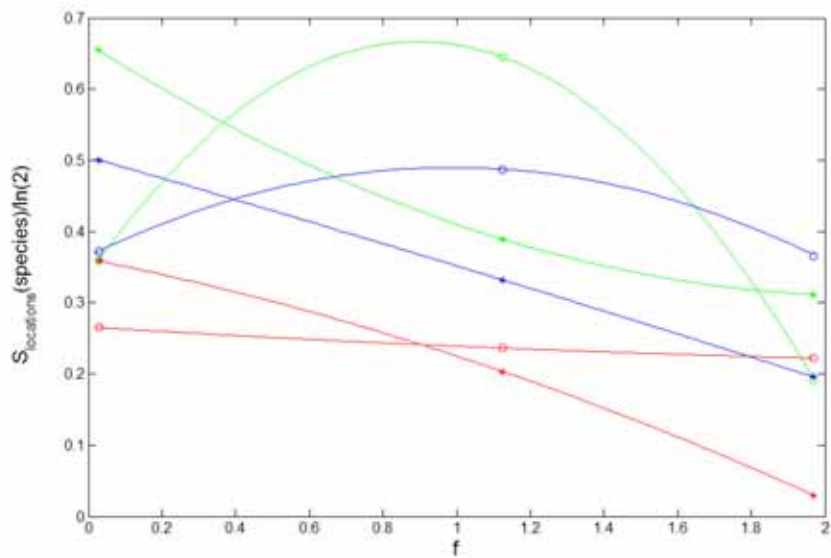


Figure 6.57 $S_{\text{location}}(\text{species})$ vs. f , red for $d1 = 5.4\text{mm}$ and $d2 = 5.4\text{mm}$, blue for $d1 = 5.4\text{mm}$ and $d2 = 7.56\text{mm}$, green for $d1 = 7.56\text{mm}$ and $d2 = 7.56\text{mm}$, stagger pattern – circle, regular pattern – star

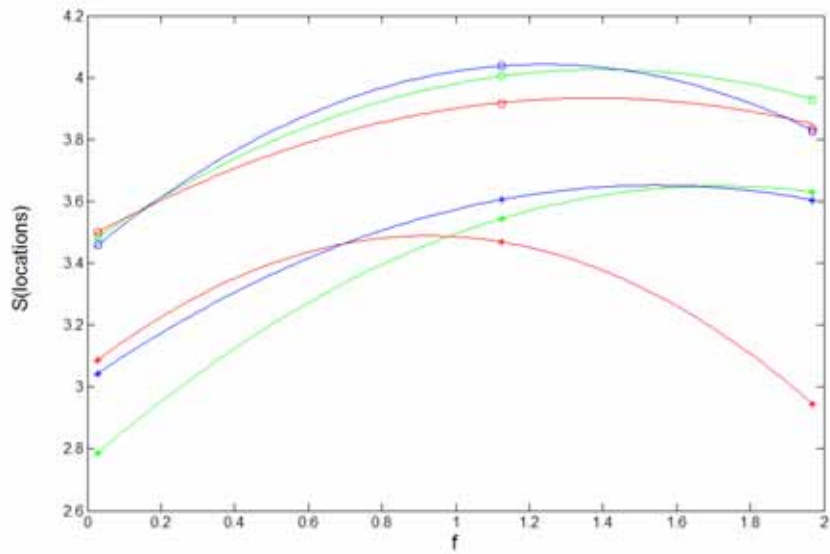


Figure 6.58 $S(\text{locations})$ vs. f , red for $d1 = 5.4\text{mm}$ and $d2 = 5.4\text{mm}$, blue for $d1 = 5.4\text{mm}$ and $d2 = 7.56\text{mm}$, green for $d1 = 7.56\text{mm}$ and $d2 = 7.56\text{mm}$, stagger pattern – circle, regular pattern – star

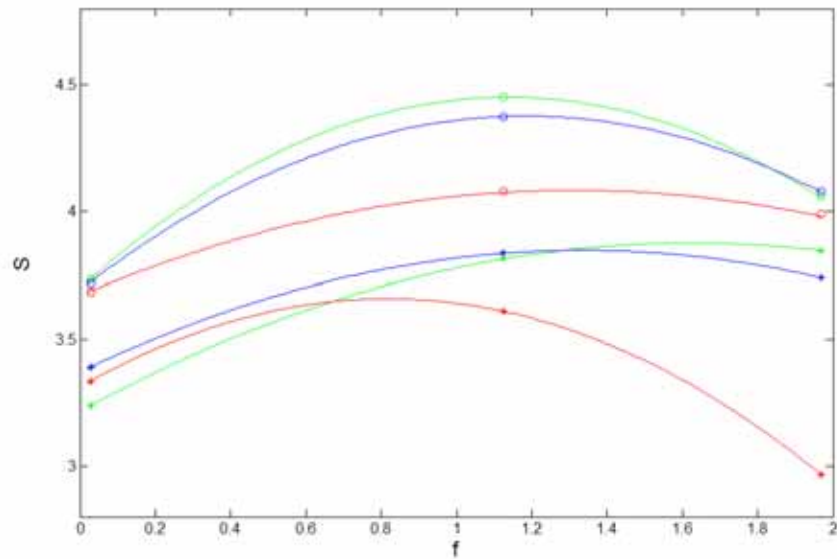


Figure 6.59 S vs. f , red for $d1 = 5.4\text{mm}$ and $d2 = 5.4\text{mm}$, blue for $d1 = 5.4\text{mm}$ and $d2 = 7.56\text{mm}$, green for $d1 = 7.56\text{mm}$ and $d2 = 7.56\text{mm}$, stagger pattern – circle, regular pattern – star

In conclusion, good local mixing will be achieved regardless of bump patterns, however, carefully designed bump patterns could optimize the results. $S(\text{locations})$ and S values are generally larger for stagger pattern. The f value plays an important role and has different trends for different patterns. So the pattern must be considered together with the f value to achieve the best mixing. There is a critical value of f around 0.84, above this value, the mixing is substantially improved. Also the Entropy is affected by gate distance. The gate distance of $d1 = 5.4\text{mm}$ and $d2 = 5.4\text{mm}$ results in the worst mixing for both patterns.

6.2.3 Stretching analysis

Figure 6.60 – 6.62 show stretching, mean $\log(\lambda)$, evolution with time in the cavity of filling with gates $d1 = 5.4\text{mm}$ $d2 = 5.4\text{mm}$, $d1 = 5.4\text{mm}$ $d2 = 7.5\text{mm}$, and $d1 = 7.5\text{mm}$ $d2 = 7.5\text{mm}$ respectively. All two gates filling have nearly linear increasing of mean $\log(\lambda)$, which indicates the exponential stretching. This is the evidence of chaotic flow inside the cavity.

Figure 6.63 shows stretch as a function of f for both patterns. At low f values, the regular pattern has smaller stretching. At higher f values, both patterns have similar stretching. This proves that the bump patterns could affect the stretching.

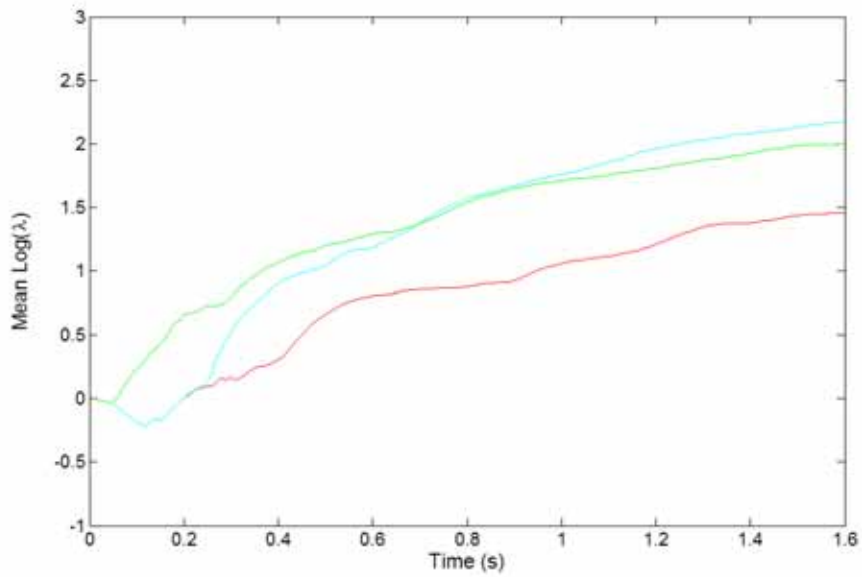


Figure 6.60 Mean λ for two gates $f = 0.02813$ (green), $f = 1.125$ cyan), $f = 1.9687$ (red);
 $d_1 = 5.4\text{mm}$, $d_2 = 5.4\text{mm}$

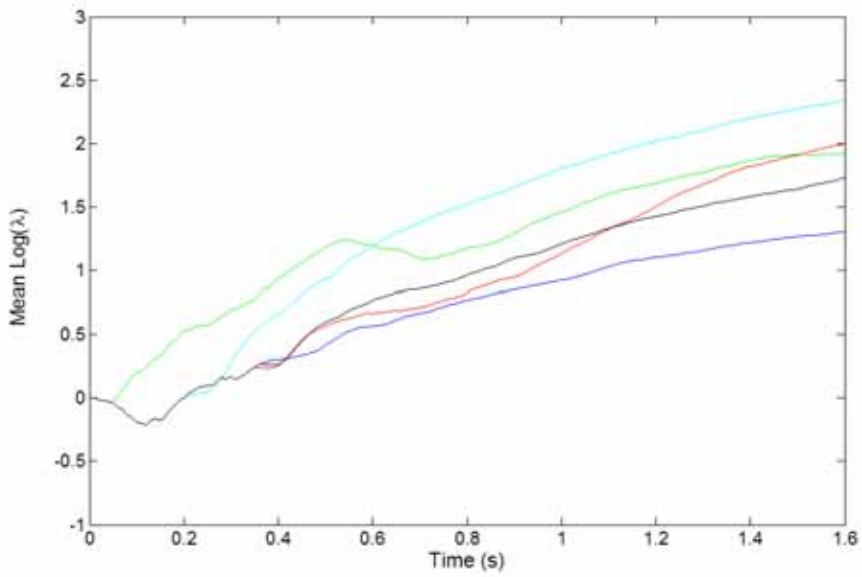


Figure 6.61 Mean λ for two gates $f = 0.02813$ (green), $f = 1.125$ cyan), $f = 1.9687$ (red);
 $d_1 = 5.4\text{mm}$, $d_2 = 7.56\text{mm}$

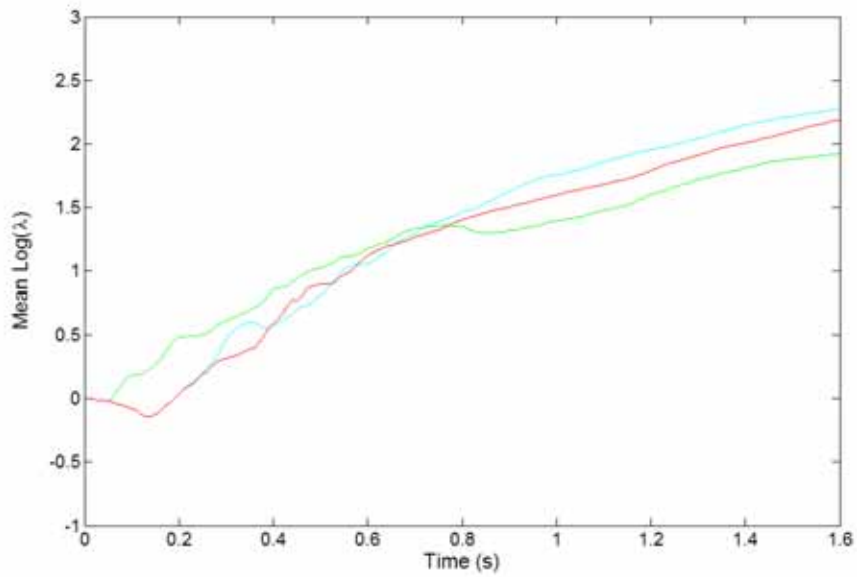


Figure 6.62 Mean λ for two gates $f = 0.02813$ (green), $f = 1.125$ (cyan), $f = 1.9687$ (red);
 $d1 = 7.56\text{mm}$, $d2 = 7.56\text{mm}$

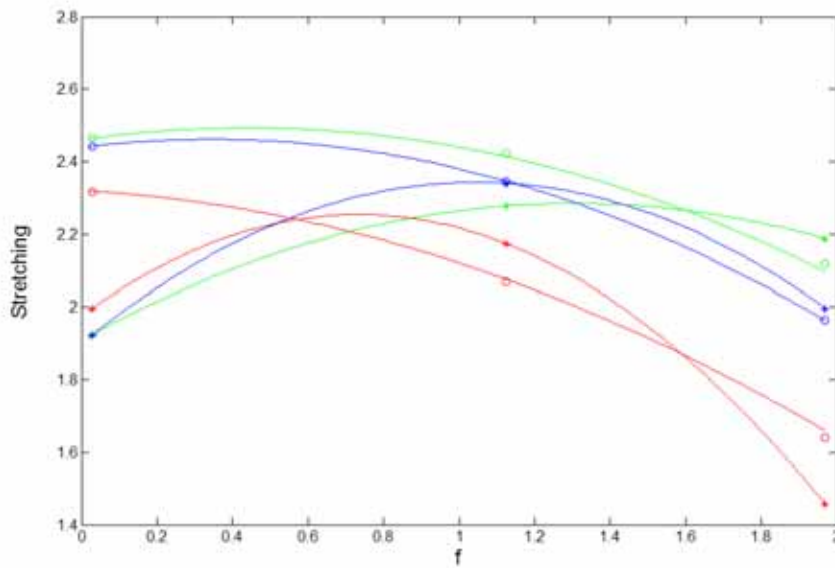


Figure 6.63 Stretching as a function of f , red for $d1 = 5.4\text{mm}$ and $d2 = 5.4\text{mm}$, blue for $d1 = 5.4\text{mm}$ and $d2 = 7.56\text{mm}$, green for $d1 = 7.56\text{mm}$ and $d2 = 7.56\text{mm}$, stagger pattern – circle, regular pattern – star

6.2.4 Improve CTE

To see the improvement of CTE value of mold compound with two gates chaotic filling, we can estimate by using $S_{\text{location}}(\text{species})$ value that has been increased 8.08 times compared to one gate filling when use L75T75 two gates filling. As mentioned before in chapter 3, we know that the AF difference can be as big as 11.4% and a CTE difference of 5.3 ppm/°C. Using novel fed protocol filling the package can reduce the AF difference to approximately 1.97% as shown in Equation (6.3). This in return may reduce the CTE difference to 0.92 ppm/°C, which is shown in Equation (6.4).

$$(43.1\% - 31.7\%) / 5.8 = 1.97\% \quad (6.3)$$

$$\begin{aligned} \Delta\text{CTE} &= 1.41\% / (43.1\% - 31.7\%) \times 5.3 \\ &= 0.92 \text{ ppm/}^\circ\text{C} \end{aligned} \quad (6.4)$$

As a result of reduced CTE difference we will expect the electronic packages to be more reliable and increased lifetime and performance.

Chapter 7: Conclusion

The goal of this research was to determine the nature of the feed protocol necessary to create chaotic laminar mixing during the filling process of an empty cavity. Periodic and aperiodic feed protocols from two feed ports are tested and a domain for chaotic mixing is identified.

The first part of this thesis is the experimental investigation on electronic packages. Both major and minor fillers are analyzed. Two kinds packages with different geometry are studied, one is square, and the other is rectangular. Images obtained from cross sections at various places are analyzed for the particle distribution. A set of measures include d_v , d_n , AF and d_b have been created to assess the particle distribution. These measures are supposed to tie to different properties, and more general work need to be done to determine which measures are the key factors for which property.

The statistical results show that the filler particles are not uniformly distributed within the package. It can be found that different measures vary in different directions. For MQFPs, over 83% confidence that d_v varies with position, over 95% confidence that d_n varies with distance, and over 97% confidence that d_b varies with distance. For Visteon chip, d_v is affected by plane, position and interactions of die position and plane, plane and position; d_n affected by die position, position and interactions of die position and plane, die position and position.

The uneven distribution has a big influence on local CTE property, and could affect the reliability. In this study the CTE is tied to AF. The maximum AF variation is found

about 10% and makes a local CTE difference more than 5 ppm/°C. This value is about 44% of the effective CTE for MQFPs and 27% of the effective CTE for PQFPs. These differences could be harmful to the reliability of the packages.

For minor filler, the distance from the gate and the depth (level) within the package are factors that will affect the distribution of a minor constituent in a molded microcircuit package. In fact, there is significant confidence that area fraction varies with distance from the gate and that area fraction varies with level. In addition, the number of particles increases as the distance from the gate increases. This trend is the same for the area fraction indicating that the area fraction trends result from the difference of the number of particles.

The average area fraction found between the leads is the same as that of level 2, and is bigger than level 1. Also the number of particles is the largest between the leads, even though the average particle size found between the leads is the smallest among all 3 levels.

The second part is the simulation of filling cavity using novel feed protocol. The simulation in an empty cavity without bumps shows no improvements on mixing. This is because that another critical condition must be met, which is velocity gradient. In this kind of cavity, the velocity gradient can only exist at near the walls. In the middle of the cavity, the velocity field is essentially flat.

The most important achievements of this thesis are to prove that two gates filling can generate chaotic flow, and much better mixing. The f value and $d1$, $d2$ values are important parameters to Entropy and stretching. The gates further away from each other will have the best results for stagger bump pattern. But this distance will be restricted by

the final packaging requirements on weld line, since we want to minimize the weld line too. The f value plays an important role and has different trends for different patterns. There is a critical value of f around 0.84, above this value, the mixing is substantially improved. And this critical value of f is affected by the bump patterns. So the pattern must be considered together with the f value to achieve the best mixing. Good local mixing will be achieved regardless of bump patterns, however, carefully designed bump patterns could optimize the results. $S(\text{locations})$ and S values are generally larger for stagger pattern. Also the Entropy is affected by gate distance. The gate distance of $d1 = 5.4\text{mm}$ and $d2 = 5.4\text{mm}$ results in the worst mixing for both patterns.

Filling the empty cavity will not generate any periodic points due to no returning flow, and since the primary function of the aperiodic flow is to break the periodic points, so that the aperiodic flow will not necessarily better than periodic flow

Appendix

1. Program for reconstructing the velocity field in the cavity and defining the initial position of particle balls.

```
close all
clear all
clc

%Load elements' 3 nodes
load 'C:\elementnumber.txt'
nodes = elementnumber;
nodes = elementnumber; %the starting node number -1 ;

%Load coordinates of nodes
load 'C:\nodenumber.txt'
X = nodenumber(:,1)*1000;
Y = nodenumber(:,2)*1000;

%Load top gate flow
load 'C:\T75.txt'
v = T75*1000;
ux = v(:,2); %Velocity in x direction
uy = v(:,3); %Velocity in y direction

% load left gate flow
load 'C:\L54.txt'
vb = L54*1000;
uxb = vb(:,2);
uyb = vb(:,3);

totalnode = max(max(nodes));
totalelement = length(nodes);

%Calculate velocity at nodes
for nn = 1:totalnode
    uxx(nn) = 0; uyy(nn) = 0; kk = 0; uxxb(nn) = 0; uyyb(nn) = 0;
    for k = 1:totalelement
        if (nodes(k, 1) == nn)
            kk = kk + 1;
            uxx(nn) = uxx(nn) + ux(k);
            uyy(nn) = uyy(nn) + uy(k);
            uxxb(nn) = uxxb(nn) + uxb(k);
            uyyb(nn) = uyyb(nn) + uyb(k);
        end
        if (nodes(k, 2) == nn)
            uxx(nn) = uxx(nn) + ux(k);
            uyy(nn) = uyy(nn) + uy(k);
            uxxb(nn) = uxxb(nn) + uxb(k);
            uyyb(nn) = uyyb(nn) + uyb(k);
            kk = kk + 1;
        end
    end
end
```

```

if (nodes(k, 3) == nn);
    uxx(nn) = uxx(nn) + ux(k);
    uyy(nn) = uyy(nn) + uy(k);
    uxxb(nn) = uxxb(nn) + uxb(k);
    uyyb(nn) = uyyb(nn) + uyb(k);
    kk = kk + 1;
end
end
if (kk > 0)
    uxx(nn) = uxx(nn)/kk;
    uyy(nn) = uyy(nn)/kk;
    uxxb(nn) = uxxb(nn)/kk;
    uyyb(nn) = uyyb(nn)/kk;
end
end

percent = 0.3 %Set slip velocity as 30% of the original velocity

%Set velocity to be 0 at boundaries
lxo1 = 7; lyo1 = 5.5; lxo = 4; dball = 1; lyo = 4; e = 1e-6; delty = 3;
for k = 1:totalnode
    if (X(k) <= e)
        uxx(k)=0; uyy(k) = 0; uxxb(k) = 0; uyyb(k) = 0;
    end
    if (X(k) == 27)
        uxx(k) = 0; uyy(k) = 0; uxxb(k) = 0; uyyb(k) = 0;
    end
    if (Y(k) <= e)
        uxx(k) = 0; uyy(k) = 0; uxxb(k) = 0; uyyb(k) = 0;
    end
    if (Y(k) == 27)
        uxx(k) = 0; uyy(k) = 0; uxxb(k) = 0; uyyb(k) = 0;
    end
end

%Set velocity to be 0 at balls
ly = lyo;
for m = 1:7 %y
    lx = lxo;
    for mm = 1:4 %x
        if (X(k) >= lx & X(k) <= lx+dball & Y(k) == ly)
            uyy(k) = 0; uyyb(k) = 0; uxx(k) = percent*uxx(k); uxxb(k) = percent*uxxb(k);
        end
        if (X(k) >= lx & X(k) <= lx+dball & Y(k) == ly + dball)
            uyy(k) = 0; uyyb(k) = 0; uxx(k) = percent*uxx(k); uxxb(k) = percent*uxxb(k);
        end
        if (X(k) == lx & Y(k) >= ly & Y(k) <=ly + dball)
            uxx(k) = 0; uxxb(k) = 0; uyy(k) = percent*uyy(k); uyyb(k) = percent*uyyb(k);
        end
        if (X(k) == lx + dball & Y(k) >= ly & Y(k) <= ly + dball)
            uxx(k) = 0; uxxb(k) = 0; uyy(k) = percent*uyy(k); uyyb(k) = percent*uyyb(k);
        end
        lx = lx + 6;
    end
    ly = ly + delty;
end
ly = lyo1;

```

```

for m = 1:6
    lx = lx01;
    for mm = 1:3
        if (X(k) >= lx & X(k) <= lx + dball & Y(k) == ly)
            uyy(k) = 0; uyyb(k) = 0; uxx(k) = percent*uxx(k); uxxb(k) = percent*uxxb(k);
        end
        if (X(k) >= lx & X(k) <= lx+dball & Y(k) == ly+dball)
            uyy(k) = 0; uyyb(k) = 0; uxx(k) = percent*uxx(k); uxxb(k) = percent*uxxb(k);
        end
        if (X(k) == lx & Y(k) >= ly & Y(k) <= ly + dball)
            uxx(k) = 0; uxxb(k) = 0; uyy(k) = percent*uyy(k); uyyb(k) = percent*uyyb(k);
        end
        if (X(k) == lx + dball & Y(k) >= ly & Y(k) <= ly + dball)
            uxx(k) = 0; uxxb(k) = 0; uyy(k) = percent*uyy(k); uyyb(k) = percent*uyyb(k);
        end
        lx = lx + 6;
    end
    ly = ly + delty;
end
end
% Plot velocity field for top gate filling
figure(1)
gama = sqrt(uxx.*uxx+uyy.*uyy) + e; %Normalize the plot
S = 2;
for k = 1:totalnode
    DX(k) = X(k) + uxx(k) / gama(k) / S;
    DY(k) = Y(k) + uyy(k) / gama(k) / S;
end
for n=1:totalnode
    plot([X(n) DX(n)], [Y(n) DY(n)], '-')
    hold on
end
axis([0 27 0 27])
% Plot velocity field for left gate filling
figure(2)
gama = sqrt(uxxb.*uxxb + uyyb.*uyyb) + e;
for k = 1:totalnode
    DX(k) = X(k) + uxxb(k) / gama(k) / S;
    DY(k) = Y(k) + uyyb(k) / gama(k) / S;
end
for n=1:totalnode
    plot([X(n) DX(n)], [Y(n) DY(n)], '-')
    hold on
end

%Initial positions of particle balls, make sure the ball are not overlap
%Initial particle ball center point, radius, increment
xs = 6; ys = 22;
r = 0.9;
dys = 0.1; dxs = 0.1;
i = 1; j = 1;
x(1,1) = xs - r; xx = x(1,1);
y(1,1) = ys - sqrt(r^2 - (x(1) - xs)^2);
yy=y(1,1);
while (x(j,i) <= (xs+r) )
    y(j,i) = ys - sqrt(r^2 - (x(j,i) - xs)^2);

```

```

while (y(j,i) <= ys+sqrt(r^2 - (x(j,i) - xs)^2) );
x(j, i+1) = x(j,i);
y(j, i+1) = y(j,i)+dys;
xx = [xx x(j, i + 1)];
yy = [yy y(j, i + 1)];
i = i + 1;
end
j = j + 1;
i = 1;
x(j,i) = x(j-1, i) + dxs;
end
y(j,i) = ys - sqrt(r^2 - (x(j,i) - xs)^2);
xx = [xx x(j,i)];
yy = [yy real(y(j,i))];
%End of 1st ball1
xs = 6; ys = 20;
r = 0.9; i = 1; j = 1;
dys = 0.1; dxs = 0.1;
x1(1,1) = xs - r; xx1 = x1(1,1);
y1(1,1) = ys - sqrt(r^2 - (x1(1) - xs)^2);
yy1 = y1(1,1);
while (x1(j,i) < (xs+r))
y1(j,i) = ys - sqrt(r^2 - (x1(j,i) - xs)^2);
while (y1(j,i) < ys + sqrt(r^2 - ( x1(j,i) - xs)^2) );
x1(j, i+1) = x1(j,i);
y1(j, i+1) = y1(j,i) + dys;
xx1 = [xx1 x1(j, i+1)];
yy1 = [yy1 y1(j, i+1)];
i = i+1;
end
j=j+1;
i=1;
x1(j,i)=x1(j-1,i)+dxs;
end
y1(j,i) = ys - sqrt(r^2 - (x1(j,i) - xs)^2);
xx1 = [xx1 x1(j,i)];
yy1 = [yy1 real(y1(j,i))];
%End of 2nd ball1

xx = real([xx xx1]);
yy = real([yy yy1]);
p = length(xx);
ux = zeros(1,p);
uy = zeros(1,p);
plot(xx(:,1:261), yy(:,1:261),'r.')
hold on
plot(xx(:,262:522),yy(:,262:522), 'b.')
hold on
axis([0 27 0 27])

```

2. Program for tracking particle positions

```

%Constant
e = 1e-6;
td = 0;

%Define the step as 0.01 second
dt = 0.01;
tend = 160*td;
for i = 21:tend
    for h = 1:p

%Find the 3 nodes of the triangle element containing the point
for k = 1:totalelement
%Length of the three edges of an element
a1 = sqrt((X(nodes(k,1)) - X(nodes(k,2)))^2 + (Y(nodes(k,1)) - Y(nodes(k,2)))^2);
a2 = sqrt((X(nodes(k,2)) - X(nodes(k,3)))^2 + (Y(nodes(k,2)) - Y(nodes(k,3)))^2);
a3 = sqrt((X(nodes(k,3)) - X(nodes(k,1)))^2 + (Y(nodes(k,3)) - Y(nodes(k,1)))^2);
%Length of the point(xx,yy) to three nodes of an element
as1(h) = sqrt((X(nodes(k,1)) - xx(i-1,h))^2 + (Y(nodes(k,1)) - yy(i-1,h))^2);
as2(h) = sqrt((X(nodes(k,2)) - xx(i-1,h))^2 + (Y(nodes(k,2)) - yy(i-1,h))^2);
as3(h) = sqrt((X(nodes(k,3)) - xx(i-1,h))^2 + (Y(nodes(k,3)) - yy(i-1,h))^2);
sa = (a1+a2+a3)/2;
sas1(h) = (as1(h) + as2(h) + a1)/2;
sas2(h) = (as2(h) + as3(h) + a2)/2;
sas3(h) = (as3(h) + as1(h) + a3)/2;
Area = sqrt(sa*(sa - a1)*(sa - a2)*(sa - a3));
Areas1(h) = sqrt(sas1(h)*(sas1(h) - as1(h))*(sas1(h) - as2(h))*(sas1(h) - a1));
Areas2(h) = sqrt(sas2(h)*(sas2(h) - as2(h))*(sas2(h) - as3(h))*(sas2(h) - a2));
Areas3(h) = sqrt(sas3(h)*(sas3(h) - as3(h))*(sas3(h) - as1(h))*(sas3(h) - a3));
Areas(h) = Areas1(h) + Areas2(h) + Areas3(h);
if (abs(Area - Areas(h)) < e)
    n1(h) = nodes(k,1);
    n2(h) = nodes(k,2);
    n3(h) = nodes(k,3);
end
end
%End of finding the 3 nodes

% v(x,y)=Ax+By+C
AA=[X(n1(h)) Y(n1(h)) 1
    X(n2(h)) Y(n2(h)) 1
    X(n3(h)) Y(n3(h)) 1];
Bx=[uxx(n1(h))
    uxx(n2(h))
    uxx(n3(h))];
% A=C(1), B=C(2), C=C(3)
Cx=inv(AA)*Bx;
vx = [xx(i-1,h) yy(i-1,h) 1] * Cx;
By = [uyy(n1(h))
    uyy(n2(h))
    uyy(n3(h))];
Cy = inv(AA)*By;
vy = [xx(i-1,h) yy(i-1,h) 1] * Cy;
% vb(x,y)=Ax+By+C
Bxb = [uxxb(n1(h))

```



```

    uxxb(n2(h))
    uxxb(n3(h))];
Cxb = inv(AA)*Bxb;
vxb = [xx(i-1,h) yy(i-1,h) 1] * Cxb;
Byb = [uyyb(n1(h))
    uyyb(n2(h))
    uyyb(n3(h))];
Cyb = inv(AA)*Byb;
vyb = [xx(i-1,h) yy(i-1,h) 1] * Cyb;

%Periodic flow with T=0.2s
if (i <= 20-td)%left
xx(i,h) = xx(i-1,h) + dt*vxb;
yy(i,h) = yy(i-1,h) + dt*vyb;
elseif (i <= 40-td)%Top
xx(i,h) = xx(i-1,h) + dt*vx;
yy(i,h) = yy(i-1,h) + dt*vy;
elseif (i <= 60-td)%left
xx(i,h) = xx(i-1,h) + dt*vxb;
yy(i,h) = yy(i-1,h) + dt*vyb;
elseif (i <= 80-td)%Top
xx(i,h) = xx(i-1,h) + dt*vx;
yy(i,h) = yy(i-1,h) + dt*vy;
elseif (i <= 100-td)%left
xx(i,h) = xx(i-1,h) + dt*vxb;
yy(i,h) = yy(i-1,h) + dt*vyb;
elseif (i <= 120-td)%Top
xx(i,h) = xx(i-1,h) + dt*vx;
yy(i,h) = yy(i-1,h) + dt*vy;
elseif (i <= 140)%left
xx(i,h) = xx(i-1,h) + dt*vxb;
yy(i,h) = yy(i-1,h) + dt*vyb;
elseif (i <= 160)%Top
xx(i,h) = xx(i-1,h) + dt*vx;
yy(i,h) = yy(i-1,h) + dt*vy;
end
end
save xL54T75P20 xx;
save yL54T75P20 yy;
end
plot(xx(:,1:261), yy(:,1:261),'r')
hold on
plot(xx(:,262:522),yy(:,262:522), 'b.')
hold on
axis([0 27 0 27])

```

3. Program for calculating Entropy

```
clear all
clc

load xL54T75P20 xx
load yL54T75P20 yy

%Calculate for 10 points
m = [1 10 20 30 40 50 60 70 80 90 100 110 120 130 140 150 160];
for n = 1:length(m)
    x(m(n),:) = real(xx(m(n),:));
    y(m(n),:) = real(yy(m(n),:));
    e = 1e-10;
    Slocation(m(n)) = 0;
    %Define bin size
    binoneside = 27;
    M = binoneside*binoneside;
    Mx = sqrt(M);
    My = sqrt(M);
    for j = 1:M
        red(m,j) = 0;
        blue(m,j) = 0;
    end
    for i = 1:261 %Upper ball only
        j = 1;
        for jx = 1:Mx
            for jy = 1:My
                if (x(m(n),i) <= 27/Mx*jx & x(m(n),i) >= 27/Mx*(jx-1))
                    if (y(m(n),i) <= 27/My*jy & y(m(n),i) >= 27/My*(jy-1))
                        red(m(n),j) = red(m(n),j) + 1;
                    end
                end
                j = j + 1;
            end
        end
    end
end

for i = 262:length(xx) %Bottom ball only
    j = 1;
    for jx = 1:Mx
        for jy = 1:My
            if (x(m(n),i) <= 27/Mx*jx & x(m(n),i) >= 27/Mx*(jx-1))
                if (y(m(n),i) <= 27/My*jy & y(m(n),i) >= 27/My*(jy-1))
                    blue(m(n),j) = blue(m(n),j) + 1;
                end
            end
            j = j + 1;
        end
    end
end

Total(m(n),:) = blue(m(n),:) + red(m(n),:) + e;

for j = 1:M
    pcslashj(1,j) = red(m(n),j) / Total(m(n), j) + e;
```

```

    pslashj(2,j) = abs(1 - pslashj(1,j)) + e;
end

Sjspecies(m) = 0;
Slocationsspecies(m(n)) = 0;
Slocation(m) = 0;

for j = 1:M
    Sjspecies(m(n)) = 0;
    for c=1:2
        Sjspecies(m(n)) = Sjspecies(m(n)) - pslashj(c,j)*log(pslashj(c,j));
    end
    pj(j) = Total(m(n),j)/sum(Total(m(n),:));
    Slocationsspecies(m(n)) = Slocationsspecies(m(n)) + pj(j)*Sjspecies(m(n));
    ln pj(j) = log(pj(j));
    Slocations(m(n)) = Slocation(m(n)) - pj(j)*log(pj(j));
end

NormalizeSlocationsspecies(m(n)) = Slocationsspecies(m(n))/log(2);
S(m(n))=Slocationsspecies(m(n))+Slocations(m(n));
end

n = 1:1:17;

%P20
figure(1)
plot(m(n)/100, S(m(n)),'c-')
hold on
plot(m(n)/100, S(m(n)),'cv')
hold on
set(gca,'fontsize',12)
xlabel('Time (s)','fontsize',16)
ylabel('S','fontsize',16)
grid off
axis([0 1.6 2 5])

figure(2)
plot(m(n)/100, NormalizeSlocationsspecies(m(n)),'c-')
hold on
plot(m(n)/100, NormalizeSlocationsspecies(m(n)),'cv')
hold on
set(gca,'fontsize',12)
xlabel('Time (s)','fontsize',16)
ylabel('S_l_o_c_a_t_i_o_n_s(species)/ln(2)','fontsize',16)
grid off
axis([0 1.6 0 0.7])

figure(3)
plot(m(n)/100, Slocations(m(n)),'c-')
hold on
plot(m(n)/100, Slocations(m(n)),'cv')
hold on
set(gca,'fontsize',12)
xlabel('Time (s)','fontsize',16)
ylabel('S(locations)','fontsize',16)
grid off
axis([0 1.6 2 5])

```

4. Program for calculating stretching

```
clear all
clc

load xL54T75SP20 xx;
load yL54T75SP20 yy;

clear temp
real(xx);
real(yy);
for t = 1:1:160;
%Final distance
dx (t,:) = sqrt((xx(t, 263:524) - xx(t, 1:262)).^2 + (yy(t, 263:524) - yy(t, 1:262)).^2);
%Initial distance
dx0(t,:) = sqrt((xx(1, 263:524) - xx(1, 1:262)).^2 + (yy(1, 263:524) - yy(1, 1:262)).^2);
%Ratio of final to initial
rp(t,:) = real(dx(t,:)./dx0(t,:));
%Average ratio
mean(t) = sum(rp(t,:))/262;
meanlamda(t) = log10(mean(t));
end

figure(1)
%P20
t = 1:1:160;
plot(t/100, meanlamda(t), 'c-');
hold on

axis([0 1.6 -1 3])
xlabel("Time (s)",'fontsize',16)
ylabel("Mean Log(\lambda)",'fontsize',16)
title("",'fontsize',16)
set(gca,'fontsize',14)
grid off
```

References:

1. [Anderson 00] P. D. Anderson, 'Chaotic fluid mixing in non-quasi-static time-periodic cavity flows', *Int. J. Heat Fluid Flow*, 21, p176-185, 2000.
2. [Aref 84] H. Aref, 'Stirring by chaotic advection', *J. Fluid Mech.*, 143, 1984.
3. [Armstrong 92] R. J. Phillips and R. C. Armstrong, 'A constitutive equation for concentrated suspensions that accounts for shear-induced particle migration', *Phys. Fluids A* 4, 30-40, 1992.
4. [Avérous 98] Luc. Avérous, 'Determination of the microtexture of reinforced thermoplastics by image analysis', *Composites Science and Technology*, v.58, p377-387, 1998.
5. [Bae 00] Jong-Woo Bae, W. Kim, Suk-Hyeon Cho, Sang-Hyun Lee, 'Properties of AlN-filled epoxy molding compounds by the effects of filler size distribution', *Journal of Materials Science*, v35, 23, p 5907-5913, Dec, 2000.
6. [Baikerikar 00] Kiran K. Baikerikar, Alec B. Scranton, "Viscosity characterization of highly filled photopolymerizable liquid encapsulants for microelectronic devices," *Polymer Composites*, vol. 21, no. 2, pp 297-304, Apr. 2000.
7. [Bigg 74] D. Bigg and S. Middleman, "Laminar mixing of a pair of fluids in a rectangular cavity, *Ind. Eng. Chem. Fundam.* 13(3):184-190, 1974.
8. [Bigio 01] P. Elkouss, R. Mudalamane, Yue Huang, K. Broadwater, David Bigio, 'Impact Modification of Nylon 6,6 – An Experimental Study', *Antec* 2001
9. [Brady 94] P. R. Nott and J. F. Brady, 'Pressure-driven suspension flow: simulation

and theory', *J. Fluid Mech.* 275, p157-199, 1994.

10. [Brady 98] J. F. Morris and J. F. Brady, 'Pressure-driven flow of a suspension: buoyancy effects', *Int. J. Multiphase Flow*, V24, No. 1, p105-130, 1998.

11. [Brothman 45] A. Brothman, G. Wollan, and S. Feldman, *Chem. Metall. Eng.* 52: 102, 1945.

12. [Calce 03] Short course on introduction to electronic packaging, 2003.

13. [Conner 91] J. H. Conner, 'The application of a fundamental mixing theory', Master thesis, University of Maryland, College Park, 1991.

14. [Deanin 89] R. D. Deanin, C.F. Varnerin, C.-T. Lue, 'Effects of fillers on the coefficients of thermal expansion of polycarbonate', *ANTEC* 89, p 521-523, 1989.

15. [Dory 00] T. Dory, K. Takahashi, T. Kume, J. Kubota, S. Seki, T. Fujiyama, 'Simultaneous Chip-Join and Underfill Assembly Technology for Flip-Chip Packaging', *Intel technology Journal Q3*, 2000.

16. [Garrett 98] David W. Garrett, "Epoxy molding compounds for the encapsulation of electronic components," Technical Papers, Regional Technical Conference - Society of Plastics Engineers, *A Broader Meaning to Thermosets*, pp. 63-67, 1998.

17. [Han, 96] B. Han and Y. Guo, 'Determination of Effective Coefficient of Thermal Expansion of Electronic Packaging Components: A Whole-field Approach', *IEEE Transactions on Components, Packaging and Manufacturing Technology-Part A*, Vol. 19, pp. 240-247, 1996.

18. [Huang 03] Yue Huang, David Bigio, and Michael G. Pecht, "Investigation of packaging properties as a function of filler microstructure," Society of Plastics Engineers, *Antec*, May, 2003, pp. 1320-1324.

19. [Huang 04] Yue Huang, David Bigio, and Michael G. Pecht, "Fill pattern of underfill and particle distribution," *IEEE Trans. Comp., Packag., Technol.*, vol. 27, no. 3, pp. 493-498, Sep. 2004.
20. [Iwasaki 97] Shinichi Iwasaki, Shigehisa Ueda, "Development of Molding Compound for Non-Antimony and Non-Halogen," *Proc. Electronic Components and Technology Conf.*, pp. 1283-1288, 1997.
21. [Kwon 98] Y.W. Kwon, C. Kim, 'Micromechanical model for thermal analysis of particulate and fibrous composites', *Journal of Thermal Stresses*, v 21, n 1, Jan-Feb, p 21-39, 1998.
22. [Lantz 02] L. Lantz, S. Hwang, M. Pecht, 'Characterization of plastic encapsulant materials as a baseline for quality assessment and reliability testing', *Microelectronics Reliability*, v 42, p 1163-1170, 2002
23. [Lehmann 99] Y. Guo, G.L. Lehmann, T. Dricoll, E.J.Cotts, 'A model of the underfill flow process: Particle distribution effects', *1999 Electronic Components and Technology Conference*, p71-76, 1999.
24. [Leong 90] C. W. Leong, 'Chaotic mixing of viscous fluids in time-periodic cavity flows', Ph.D. dissertation, University of Massachusetts ,1990
25. [Lowry 2001] R.K. Lowry, K.L. Hanley, 'Assuring reliable PEMs by statistical monitoring of thermal and mechanical properties of molded plastic parts sampled from production', *Proceedings of the International Symposium and Exhibition on Advanced Packaging Materials Processes, Properties and Interfaces*, p 195-200, 2001.
26. [Manas 04] Ica Manas-Zloczower, et al, entropic mixing characterization in a single screw extruder, Antec 04.

27. [Manziona 90] L.T. Manziona, 'Plastic Packaging of Microelectronic Devices', Van Nostrand Reinhold, New York, 1990.
28. [Mead 01] A. Ramamoorthy, S. Pal, P. F. Mead, Z. Fathi, I. Ahmad, 'Variable Frequency Microwave Processing of Underfill Encapsulants for Flip-Chip Applications', 2001.
29. [Muzzio 94] F.J. Muzzio, Liu, M., 'Quantification of mixing in aperiodic chaotic flows', *Chaos, Solitons & Fractals*, v.4, No. 6, p869-893, 1994.
30. [Muzzio 94] F.J. Muzzio, Liu, M., 'Structure of the stretching field in chaotic cavity flows', *AIChE Journal*, v. 40, No. 8, p1273-1286, 1994.
31. [Nguyen 93] Luu T. Nguyen, K. L. Chen, "Molding compound trends in a denser packaging world: part iii - property optimization for minimum stress," American Society of Mechanical Engineers, EEP, v 6, *Electronic Packaging Reliability*, pp. 101-114, 1993.
32. [Nguyen 00] L. Nguyen, C. Quentin, P. Fine, B. Cobb, 'Flip Chip Underfill Flow Characteristics and Prediction', *IEEE Transactions On Components And Packaging Technologies*, Vol. 23, No. 3, September, 2000.
33. [Ostle 96] Bernard Ostle, Kenneth V. Turner, Charles R. Hicks, Gayle W. McElrath, *Engineering Statistics, The Industrial Experience*, Duxbury Press, 1996.
34. [Ottino 86] J. M. Ottino, 'Laminar mixing and chaotic mixing in several cavity flows'
35. [Ottino 89] J. M. Ottino, 'The kinematics of mixing: stretching, chaos and transport', Cambridge University Press, Cambridge, MA. 1989.
36. [Ottino 89] J. G. Franjione, C. W. Leong, J. M. Ottino, 'Symmetries within chaos: a route to effective mixing', *Phys. Fluids A1*, p1172-1783, 1989.
37. [Pecht 95] M. Pecht, *Plastic Encapsulated Microelectronics*, John Wiley & Sons,

New York, 1995.

38. [Rosler 89] R.K. Rosler Rigid, 'Epoxies'. *Electronic Materials Handbook, 1-Packaging*, ASM Intl. p810-816, 1989.

39. [Shannon 48] Shannon, C. E., A Mathematical Theory of Communication. *The Bell System Technical J.* **27**, 379-423 and 623-656, 1948.

40. [Shin 98] D. K. Shin, J. J. Lee, 'Effective material properties and thermal stress analysis of epoxy molding compound in electronic packaging', *IEEE Transactions on Components, Packaging, and Manufacturing Technology Part B: Advanced Packaging*, v 21, n 4, Nov, p 413-421, 1998.

41. [Spencer 51] T. Spencer, and R. Wiley, 'The mixing of very viscous liquids', *J. Colloid Sci.* 6:133, 1951.

42. [Tummala 88] Rao R. Tummala, Eugene J. Rymaszewski, Alan G. Klopfenstein, *Microelectronics Packaging Handbook*, Thomson Learning, 1988.

43. [Vo 01] H.T. Vo, M. Todd, F.G. Shi, A.A. Shapiro, M. Edwards, 'Towards model-based engineering of underfill materials: CTE modeling', *Microelectronics Journal*, v 32, n 4, p 331-338, 2001.

44. [Wang 01] Wang, W., Manas-Zloczower, I., Kaufman, M., *Intern. Polym. Process.*, 16, 1 (2001); *AIChE Journal*, 49, 1637, 2003.

45. [White 91] F.M. White, *Viscous Fluid Flow*, McGraw-Hill, 1991.

46. [Wong 01] L. fan, Z. Zhang, C. P. Wong, 'Effect of Filler Settling of Underfill Encapsulant on Reliability Performance', 2001.

47. [Wright 92] Ralph E. Wright, *Molded Thermosets: A Handbook for Plastics Engineers, Molders, and Designers*, Hanser Gardner Publications, 1992.

48. [Wu 85] S. Wu, 'Phase structure and adhesion in polymer blends: A criterion for rubber toughening', *Polymer* v.26, p1855-1863, 1985.

49. [Zerafati 94] M. Saeid Zerafati, 'Local and global mixing analysis of complex flow fields: a continuum kinematics approach to the mixing in a numerically simulated wavy channel flow', Ph.D. dissertation, University of Maryland, College Park, 1994.